Doctoral Dissertation
Doctoral Program in Materials Science and Technology - STM (37th Cycle)

Advanced Solid Polymer Electrolytes Based on Crosslinking and Concentrated Ionic Liquid

Mingjie Zhang
* * * * * *

Supervisor
Prof. Claudio Gerbaldi

Politecnico di Torino
October 31, 2024

I hereby declare that, the contents and organisation of this dissertation constitute my own original work and does not compromise in any way the rights of third parties, including those relating to the security of personal data.

MINGJIE ZHANG

…….....

Mingjie Zhang

Turin, October 31, 2024

Summary

The growing demand for energy storage, driven by advancements in renewable energy and electric vehicles (EVs), has led to the exploration of safer, more efficient, and sustainable alternatives to conventional lithium-ion batteries (LIBs). Solid-state lithium metal batteries (LMBs) have emerged as promising candidates, offering enhanced safety and higher energy density. However, critical challenges persist, particularly in the development of suitable, advanced electrolytes that can achieve high ionic conductivity and stability at ambient temperatures.

In such scenario, this thesis focuses on the design and development of advanced solid polymer electrolytes (SPEs) based on poly(ethylene oxide) (PEO) and highly concentrated ionic liquids (HCIL) for all-solid-state LMBs. Three major objectives are pursued: (1) the development of high-performance crosslinked PEO-based SPEs using UV-induced crosslinking strategies, (2) the study of the phase behaviour, ionic conductivity, and electrochemical performance of SPEs with varying ratios of PEO, N-propyl-N-methylpyrrolidinium bis(fluorosulfonyl) imide (C_3mpyrFSI) ionic liquid (IL) and lithium bis(fluorosulfonyl)imide (LiFSI) salt, and (3) the development of polymer-in-highly-concentrated ionic liquid (PiHCIL) SPEs with enhanced ion transport and electrochemical stability.

Key findings from this research include the achievement of combing UV-induced crosslinking and highly concentrated ionic liquids to synergistically reduce PEO crystallinity and improve electrochemical stability, and therefore leading to enhanced battery cell performance. Particularly, the crosslinked SPE achieved a promisingly high oxidative stability of 4.9 V vs. Li^+/Li and high ambient temperature ionic conductivity of 4×10^{-4} S cm^{-1}. Stable and reversible lithium plating/stripping was demonstrated over hundreds of hours. Laboratory-scale solid-state cells in which the crosslinked SPE was assembled with high loading lithium iron phosphate (LFP) or high loading, high voltage lithium manganese oxide (LMO) cathodes showed remarkable cycling performance. Another important

finding is the successful preparation of SPEs with a wide range of EO:Li:IL ratios, and the identification of an optimal ratio of 8:1:1 that achieved high ionic conductivity (5.6×10^{-4} S cm^{-1}) and a remarkable oxidative stability of 5.1 V vs. Li^+/Li. This novel electrolyte design enabled stable Li metal cell cycling over 100 cycles, suppressed dendrite formation, and supported all-solid-state LFP cell performance with over 99% capacity retention at C/5 rate for long-term cycling.

Advanced characterization techniques, including Fourier transform infrared (FTIR) spectroscopy, Raman spectroscopy, solid-state magic angle spinning (MAS) nuclear magnetic resonance (NMR), and electrochemical impedance spectroscopy (EIS), were employed to probe the ion mobility, ion interactions and the effect of ion coordination environment onto ion dynamics within the SPEs. Results reveal that crosslinking enhanced Li^+ solvation and more uniformly distributed ion clusters, thus accounting for the high ionic conductivity and the potential high electrochemical stability. In addition, increased HCIL content disrupted the crystallinity of PEO, enhanced chain mobility, and created interconnected ion-conducting networks that facilitated fast ion transport. Solid-state NMR further confirmed that the disordered ion environment in the PiHCIL-SPEs promoted superior ionic conductivity, which is key to the improved electrochemical performance of the LMBs.

Overall, this work contributes to the growing body of knowledge on solid-state batteries by proposing a novel approach to SPE design, addressing key challenges in achieving high-performance and safe all-solid-state LMBs. The findings open new pathways for future development of SPEs, bringing solid-state LMBs closer to commercialization for high-energy-density applications in EVs and beyond.

Acknowledgments

I would like to express my very great appreciation to my principal supervisor, Prof. Claudio Gerbaldi for providing the opportunity for me to pursue my education to PhD at the Politecnico di Torino. I appreciate his encouragement and support throughout the planning and development of this research. His positive attitude has inspired me and given me confidence. I consider myself lucky to have such a great supervisor who cared about my work and well-being. I would also like to thank my co-supervisor, A/Prof. Giuseppe A. Elia for his helpful suggestions and considerable support throughout my PhD.

I would like to offer my special thanks to Dr. Marisa Falco for her mentoring, training and help during my first year PhD and Dr. Giuseppina Meligrana for all her kind support at the Politecnico di Torino.

I would like to thank all the members of GAME lab group, without their support, it wouldn't be possible to complete this PhD.

I would like to sincerely thank Prof. Maria Forsyth for giving me the opportunity to conduct a research internship at the Deakin University and BatTRI-Hub. Her clear planning, insightful guidance, and unwavering support throughout the project were invaluable. Her encouragement and belief in my work gave me the confidence to push forward. Her willingness to give her time so generously has been very much appreciated. I feel very lucky to have worked with such a dedicated supervisor who always provide inspiring ideas and responds to my questions and concerns so promptly.

I would like to extend my gratitude to Dr. Urbi Pal and Dr. Faezeh Makhlooghiazad who mentored my internship projects. I am deeply grateful for their day-to-day help, guidance, advice, and enormous support throughout the entire internship. Their continue support afterward in reviewing manuscripts and handling the publications process are very much appreciated.

I wish to acknowledge the help provided by Dr. Luke O'Dell in NMR techniques. He kindly supported me and explained every basic concept of NMR patiently and clearly. Working with him was also an unrivalled experience.

I would like to offer my special thanks to Dr. Shinji Kondou for his valuable knowledge sharing in polymers and batteries and for the inspiring discussions on my results. He was always kindly available to answer my questions and gave me advice to improve my work.

A special thank you to my friend Łukasz Kufel for his valuable assistance in the lab during my experiments, the helpful discussions on my results, and his wonderful company during my time at Deakin.

I would also like to thank all the group members of the Electromaterials group at the IFM Deakin University, certainly without their support and collaboration I would have been unable to finish this thesis.

My special thanks to my friends Rui Sun and Jingyi Liu for their company and support during my time at Deakin.

I would also like to express my deep gratitude to my counselor, Jia ai, for her continuous support of my mental health throughout this PhD journey.

Last but not least, I would like to thank a very special friend in my life, Ms Hongyi Li. Words are not able to express my gratitude for all things you have done for me during this adventure. Thank you for your wholehearted support, encouragement, love and belief in me. I am deeply thankful for having you in my life.

Finally, I would like to acknowledge the institutions and funding bodies that supported my research work and allowed me to pursue my PhD path without any economic concerns. Particularly, the financial support of the European Union's Horizon 2020 research and innovation programme under the Marie Skłodowska-Curie grant agreement 860403, namely the POLYSTORAGE network, is here deeply acknowledged. I have been honored and lucky to have had the chance to advance my knowledge and career under such favorable conditions and in a network that strongly promotes international collaboration and provides support to early-stage researchers and students from all over the world.

List of Publications

1. Mingjie Zhang, Urbi Pal, Faezeh Makhlooghiazad, Luke A. O'Dell, Shinji Kondou, Giuseppe A. Elia, Claudio Gerbaldi, and Maria Forsyth. Advanced High-Voltage Electrolyte Design Using Poly(ethylene oxide) and High-Concentration Ionic Liquids for All-Solid-State Lithium Metal Batteries. *ACS Appl. Mater. Interfaces 2024, 16, 41, 56095–56105.*

2. Mingjie Zhang, Faezeh Makhlooghiazad, Urbi Pal, Mahin Maleki, Shinji Kondou, Giuseppe A. Elia, Claudio Gerbaldi, and Maria Forsyth. Synergistic Combination of Crosslinked Polymer and Concentrated Ionic Liquid for Electrolytes with High Stability in Solid-State Lithium Metal Batteries. *ACS Appl. Polym. Mater. 2024, 6, 23, 14469–14476*

3. Mingjie Zhang, Urbi Pal, Faezeh Makhlooghiazad, Luke A. O'Dell, Shinji Kondou, Giuseppe A. Elia, Claudio Gerbaldi, and Maria Forsyth. Design of Poly(ethylene oxide)-Based Polymer-in-High Concentrated Ionic Liquid Electrolyte for All-Solid-State Lithium Metal Batteries. Electrochemical Society Meeting Abstracts. 2024

4. Marisa Falco, Gabriele Lingua, Silvia Porporato, Ying Zhang, Mingjie Zhang, Matteo Gastaldi, Francesco Gambino, Elisa Maruccia, Sofia Saffirio, Matteo Milanesi, Hamideh Darjazi, Alessandro Piovano, Giuseppina Meligrana, Giuseppe Antonio Elia, Claudio Gerbaldi. Electrochemical Society Meeting Abstracts 244. 2023

To my dearest friends:
Hongyi, Xi, Luyan,
Łukasz, *and* ***Meng*** *who love me and encourage me to work hard for the things I aspire to achieve.*

Contents

List of Tables

List of Figures

Acronyms

AC	*Alternating Current*
CIL	*Concentrated Ionic liquid*
DSC	*Differential Scanning Calorimetry*
HOMO	*Highest Occupied Molecular Orbital*
EIS	*Electrochemical Impedance Spectroscope*
EV	*Electric Vehicle*
FTIR	*Fourier Transform Infrared*
IL	*Ionic liquid*
LFP	*Lithium Iron Phosphate*
LIB	*Lithium Ion Battery*
LIFSI	*Lithium bis(fluorosulfonyl)imide*
LMB	*Lithium Metal Battery*
LMO	*Lithium Manganese Oxide*
LUMO	*Lowest Un-occupied Molecular Orbital*
LSV	*Linear Sweep Voltammetry*
MAS	*Magic Angle Spinning*
MD	*Molecular Dynamics*
MOF	*Metal Organic Framework*
NMC	*Lithium Nickel Manganese Cobalt Oxide*
NMR	*Nuclear magnetic Resonance*
PMMA	*Poly(methyl methacrylate)*
PVDF	*Poly(vinylidene fluoride)*
RT	*Room Temperature*
SEM	*Scanning Electron Microscopy*
SPE	*Solid Polymer Electrolyte*
SS	*Stainless Steel*
SSB	*Solid State Battery*
SSE	*Solid State Electrolyte*
SSLMB	*Solid State Lithium Metal Battery*
T_g	*Glass Transition Temperature*
TGA	*Thermogravimetric Analysis*
UV	*Ultraviolet*

Chapter 1

Introduction

1.1 General Overview

The global demand for energy storage has increased dramatically in recent years, driven by the fast progress in development of renewable energy and the increasing demand of electric vehicles (EVs). Batteries, particularly lithium-ion batteries (LIBs), have been at the forefront of this transformation, offering a versatile and efficient solution for energy storage across various applications[1]. However, as the deployment of LIBs expands, several challenges related to technology, environment, and economy have emerged.

Technologically, the limitations of LIBs, including safety concerns, limited energy density, and cost, have prompted the exploration of alternative energy storage systems such as flow batteries, sodium batteries and solid state batteries.[2] Environmental issues, such as the mining and processing of lithium and cobalt, have raised significant concerns about the sustainability of LIBs. These processes are energy-intensive, contribute to greenhouse gas emissions, and often involve ethical issues such as child labor.[3] Economically, the reliance on geographically concentrated raw materials has led to fluctuating market prices and vulnerable supply chains.[4]

In response to these challenges, solid-state batteries (SSBs) have gained increased attention. SSBs promise enhanced safety, higher energy density, and the potential to use more sustainable materials, making them a promising alternative to traditional LIBs.[5] This shift towards solid-state technology represents a critical step in meeting the growing global demand for safer, more efficient, and more sustainable energy storage solutions.

1.2 Solid-State Batteries vs. Lithium-Ion Batteries

Solid-state batteries differ from conventional LIBs primarily in their use of a solid or polymer electrolyte instead of a liquid one (Figure 1-1). This fundamental difference brings both advantages and challenges.[6]

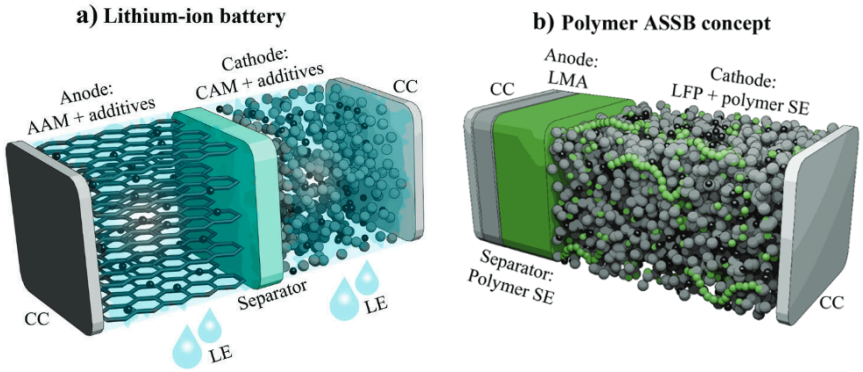

Figure 1 - 1. Schematic illustrations of a) A liquid electrolyte (LE) based lithium-ion battery and b) A polymer electrolyte based all-solid–state battery with lithium metal anode (LMA). Adapted from Ref. 6, with permission from Advanced Energy Material. Copyright 2023.

Advantages:

- **Safety:** One of the most significant benefits of SSBs is their improved safety profile. Unlike conventional LIBs, SSBs do not contain liquids, which can cause leakage, overheating, fire, and explosion. SSBs do not experience these detrimental conditions and perform better in extreme environments than standard LIBs. Safety is particularly crucial for EV and aviation applications, where battery stability is vital during operation and in the event of accidents.[7]
- **Energy/Power Density:** SSBs can store more energy and achieve higher energy densities. This is partly because solid electrolytes allow using lithium metal as anode, which has a much higher theoretical capacity compared to graphite anodes used in LIBs (Figure 1-2).[5] This increased energy capacity enables longer driving ranges for EVs between charges, addressing a key concern for consumers. Although slow kinetics is often considered in solid-state systems, studies show that SSBs may provide higher specific power than conventional LIB cells[8].

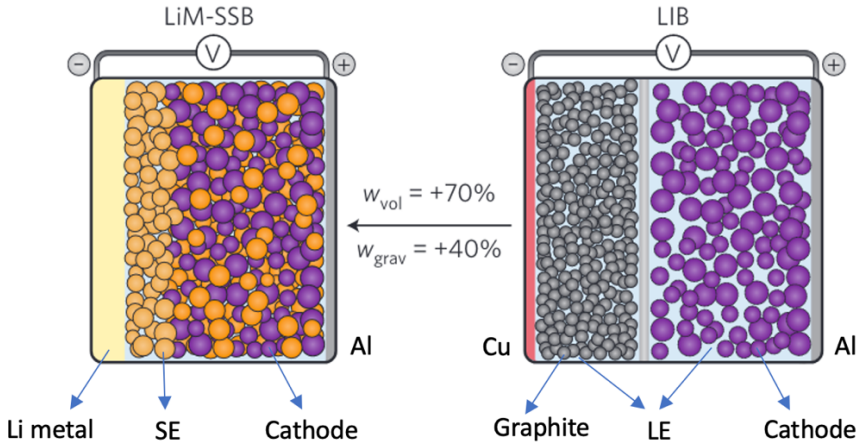

Figure 1 - 2. Schematic illustration of architectures of LIB and lithium metal SSB. Energy density changes are estimated based on the density increase when replacing liquid with solid, considering the complete change of graphite and anode electrolyte with Li metal. W_{vol} and W_{grav} are the volumetric and gravimetric energy densities, respectively. Adapted from Ref. 5, with permission from Nature Energy. Copyright 2016.

- **Stability:** Solid electrolytes are typically more thermally and chemically stable than liquid electrolytes, leading to longer battery lifespans and better performance under a wide range of temperatures[9]. Stability is essential for applications requiring consistent high performance, such as in EVs.
- **Faster charge:** The fast-charging ability of SSBs is another significant advantage. Theoretically, these batteries could achieve charging rates up to 6 times faster than current LIBs, allowing users to charge to 80% in 10 minutes[10]. This could dramatically enhance the convenience of using EVs, making long-distance travel more feasible without lengthy charging stops.
- **Environmental benefits:** From an environmental perspective, SSBs are advantageous as they contain no flammable components, thereby reducing risks associated with disposal and recycling. Their longer lifespan also means fewer batteries end up in landfills, contributing to a more sustainable battery technology[3].
- **Versatility and applications:** The potential applications of SSBs extend beyond EVs. Thin-film solid-state batteries, for example, offer exceptional flexibility and low weight which makes them suitable for a wide range of devices, including medical equipment and military gear[11]. As the technology matures, its versatility may lead to widespread adoption across various sectors.

Challenges:

- **Ionic conductivity:** Despite their benefits, solid electrolytes, in particular solid polymer electrolytes generally exhibit lower room temperature (RT) ionic conductivity compared to their liquid counterpart. This can cause

concentration gradient and limit the cycling and power performance of SSBs[12]. Nevertheless, today, there are some solid electrolytes reach ionic conductivities of 10 mS cm^{-1} at RT which are comparable to liquid electrolyte for practical use[13].

- **Interface issues:** One of the primary challenges in SSBs is the compatibility of solid electrolytes (SEs) with electrode materials. The limited contact areas between SE and electrodes can lead to high interfacial resistance, which impedes Li ion transport. When Li metal anode is used, the SE must remain stable in contact with lithium metal to minimize interface resistance, polarization and formation of Li dendrites (Figure 1-3). Techniques such as electrochemical impedance spectroscopy (EIS) can be employed to measure compatibility over extended periods. Additionally, volume changes in electrodes during cycling can lead to a loss of contact between SE and electrodes, increasing resistances. Strategies such as atomic layer deposition (ALD) coatings have shown promise in improving interface contact and reducing interfacial resistance[13].

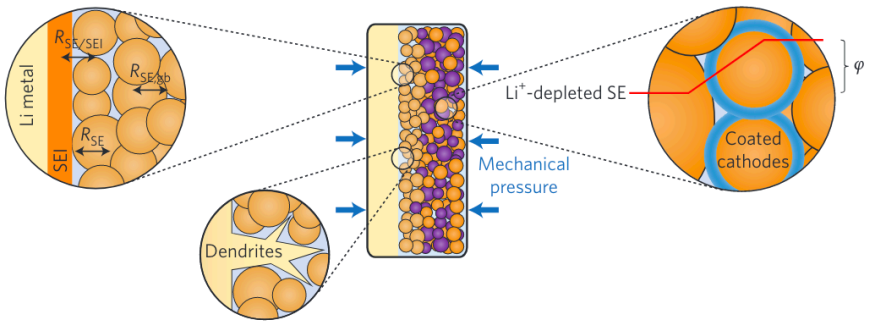

Figure 1 - 3. Major interface issues in LiM-SSBs. On the anode side, a resistive SEI ($R_{SE/SEI}$) layer is formed at the anode/SE interface. The grain and grain boundary resistances are presented by R_{SE} and $R_{SE,gb}$ respectively. Li dendrites are formed due to inhomogeneous Li deposition which can cause detrimental short-circuit. On the cathode side, most solid electrolytes react with cathode materials and need to be protected with a coating. Proper coating can also help prevent Li depletion (due to a drop in electric potential across the space charge). Adapted from Ref. 5, with permission from Nature Energy. Copyright 2016.

- **Manufacturing complexity:** The fabrication of SSBs is more complex and costly than current LIBs.[6] Ceramic electrolytes, while offering superior ionic conductivity and thermal stability compared to polymers, have the brittle nature which makes them more susceptible to cracking under mechanical stress[9].The need for thin, uniform solid electrolyte layers and the challenges associated with the interface between the SE and electrodes require advanced manufacturing techniques such as mechanical mixing, advanced coating and film formation[14].
- **Economic viability:** The economic viability of SSB production is another challenge, particularly when compared to well-established LIB

technologies. It is difficult to scale up SSBs economically without significant investment and innovation in production methods. Innovative manufacturing approaches, such as roll-to-roll production and inkjet printing, are being explored to streamline processes and reduce costs, but achieving a balance between production efficiency and cost-effectiveness remains a big challenge[15].

Given these factors, ongoing research is focused on improving the properties of SEs while optimizing the manufacturing processes to make SSBs more economically viable. There is still a long way to go to make SSBs a competitive alternative to current LIBs.

1.3 Solid State Electrolytes

Solid-state electrolytes (SSEs) are essential to the development of advanced SSBs. There are mainly three types of SSEs, inorganic solid electrolyte, solid polymer electrolyte and hybrid electrolyte, each with unique properties. Figure 1-4 illustrates the ionic conductivities and suitable voltage windows of different electrolytes.[16]

Inorganic Solid Electrolytes*:*

- Oxides: Known for high stability with lithium metal and good mechanical properties, effectively mitigating dendrite growth.
- Sulfides: High ionic conductivity at room temperature but prone to moisture sensitivity and degradation.
- Halides: Moderate ionic conductivity and stability; recent research focuses on lowering the cost and improving stability.
- *Advantages*: Generally non-flammable and capable of blocking dendrites. They offer structural rigidity, making them safer and potentially enabling higher energy density applications.
- *Disadvantages*: Some are brittle and challenging to process, with sensitivity to air/moisture (sulfides), high cost (oxides), or compatibility issues with lithium metal (halides).

Solid Polymer Electrolytes (SPEs)*:*

- Use polymer matrices like poly(ethylene oxide) (PEO) or poly(methyl methacrylate) (PMMA), typically combined with lithium salts.
- *Advantages*: Flexible and processable into thin films, often enhancing contact with electrodes. Less rigid than inorganic SSEs, offering mechanical flexibility. Low flammability compared to liquid electrolytes.
- *Disadvantages*: Lower ionic conductivity (~10^{-5} to 10^{-6} S cm^{-1} at room temperature), which limits performance at ambient temperatures. Require

heating to around 60–80°C to reach higher conductivity, constraining their applications to low-temperature environments or high-rate devices.

***Hybrid Solid Electrolytes**:*

- Hybrid solid electrolytes combine the benefits of both solid and polymer electrolytes. These hybrids integrate SPEs with inorganic fillers such as oxides (e.g., Al_2O_3, SiO_2).
- *Advantages*: Enhance the mechanical properties and thermal stability of the polymer matrix, reduce polymer crystallinity and, thus, enhancing ionic conductivity while also sometimes serving as additional pathways for ion conduction.
- *Disadvantages*: Some inorganic fillers are sensitive to moisture, which can compromise stability and performance. Additionally, producing uniform composites with consistent filler distribution can be complex and costly, especially at scale.

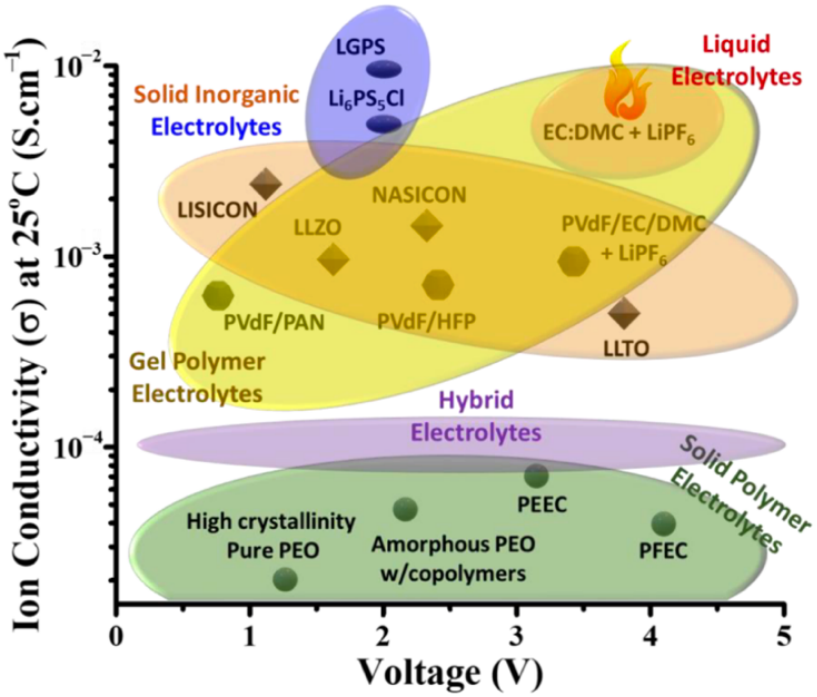

Figure 1 - 4. Ionic conductivities and suitable voltage windows of different electrolytes.[16] Adapted from Ref. 16, with permission from Batteries. Copyright 2024.

1.4 Solid Polymer Electrolytes in Lithium Batteries

SPEs are promising for solid-state lithium batteries (SSLBs) with their benefits in flexibility, ease of processing, and potential for safer, more stable battery operation. SPEs generally consist of a polymer matrix, such as PEO, which can

dissolve lithium salts and facilitate ion transport[16]. The structures of several common polymers capable of being used as SPEs are shown in Figure 1-5.[17]

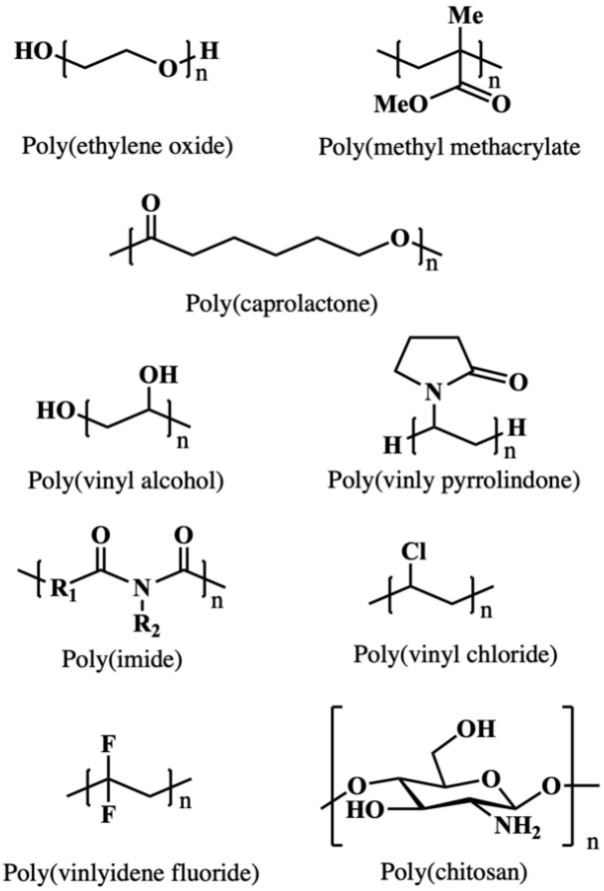

Figure 1 - 5. Structures of common polymers used as SPEs.

The mechanical strength of the SPE is crucial for its operational stability and dendrite suppression ability. In theory, SPEs with a shear modulus twice that of metallic lithium should physically block the growth of lithium dendrites. However, polymers with higher shear moduli have lower ionic conductivity because their stiffness limits chain movement and ion transport. This conflict between strength and conductivity has led to research on plasticized and composite polymer electrolytes.[17]

Types of Solid Polymer Electrolytes:

- **Linear SPEs:** These are the simplest form of SPEs, where the polymer chains are linear, allowing straightforward pathways for ion conduction. However, their ionic conductivity is often hindered by the semi-crystalline nature of the polymer, as ion transport happens primarily in the amorphous region of the polymer matrices[19].
- **Crosslinked SPEs:** Introducing crosslinking into the polymer matrix reduces crystallinity, leading to higher ionic conductivity and better

mechanical properties[20]. Crosslinked SPEs also show increased electrochemical stability, and therefore are believed to be more versatile for high energy density applications[21].

- **Plasticized SPEs:** Plasticized polymer electrolytes incorporate plasticizers such as ionic liquids, to improve ion conductivity by reducing the strength of interactions between the polymer chains. This allows for better ion-polymer interactions. Adding plasticizers also lowers the polymer's glass transition temperature (Tg) and increase the dissociation of Li salts in the polymer, enhancing ion transport[13]. However, reduction in crystallinity weakens the mechanical strength of the polymer at room temperature[17]. Plasticizers can also affect other SPE properties such as electrochemical stability and discharge time[22].
- **Composite SPEs:** These SPEs are reinforced with inorganic fillers, to enhance ionic conductivity, chemical stability, and mechanical integrity. Composite SPEs offer a balance between flexibility and performance, making them a hot area of current research[23].

Recent advancements in SPE research have focused on the improvement of RT ionic conductivity, interfacial stability, and developing SPEs that can support high-voltage operations required for next-generation lithium batteries[24]. Future SPE research will likely focus on developing hybrid materials that combine the benefits of both organic and inorganic components, as well as exploring new polymer systems that can decouple ion transport and segmental motion of the polymer, single-ion SPEs, and cathodes property-matched SPE. Additionally, there is growing interest in designing SPEs that are compatible with more sustainable and abundant materials to further reduce the environmental impact of lithium batteries[16].

1.5 Electrode Materials in Lithium Batteries

In lithium-based batteries, electrode materials play a critical role in determining the energy density, cycle life, and safety of the cell. Cathode materials, such as $LiFePO_4$ (LFP) and high-voltage options like $LiCoO_2$ (LCO), the $LiNi_xMn_yCo_zO_2$ (NMC) family and $LiMn_2O_4$ (LMO) present specific performance characteristics that make them suitable for different applications. For the anode, lithium metal offers superior energy density but brings unique challenges, especially in solid-state systems.

LFP Cathode

LFP cathode is known for its excellent thermal stability, safety, and long cycle life. As a low-voltage cathode (ca. 3.45 V vs. Li/Li^+), LFP sacrifices some energy density compared to high-voltage materials but compensates with high structural stability and resistance to thermal runaway[25]. This stability makes it ideal for applications where safety is paramount, such as electric buses, stationary energy

storage, and other high-cycle applications. Despite its lower energy density, LFP's reliability and lower cost make it highly attractive for large-scale implementations.

High-Voltage Cathodes

High-voltage cathodes like LMO operate at a higher voltage (above 4.0 V vs. Li^+/Li), increasing energy density but also presenting challenges in thermal stability and electrolyte compatibility. LMO's spinel structure provides a three-dimensional lithium ion diffusion pathway, enabling high rate capability, making it suitable for applications that require high-power output, like power tools and electric vehicles. However, LMO is prone to degradation at high temperatures and in the presence of liquid electrolytes, where it can undergo electrolyte decomposition, accelerating capacity loss[26]. This has driven research into solid and hybrid electrolytes, which are more compatible with high-voltage operation, to maintain LMO's stability and improve the safety of high-energy applications. Innovations like doping and surface coating have also helped stabilize LMO, enabling it to achieve longer cycle life and maintain performance in more demanding environments.

Layered oxide cathodes, such as $LiCoO_2$ and the mixed derivatives of the NMC family, are widely used in LIBs due to their high energy density and good cycling performance. $LiCoO_2$, the first commercialized layered cathode, features a well-ordered structure that facilitates two-dimensional lithium-ion diffusion. However, its practical capacity is limited to about 140 mAh g^{-1} due to structural instability and oxygen loss at high states of charge. To overcome these limitations, NMC materials have been developed by substituting cobalt with nickel and manganese, offering a balance between energy density, thermal stability, and cost-effectiveness. Among these, NMC 811 (80% Ni, 10% Mn, 10% Co) achieves higher capacity and energy density by increasing nickel content, though at the expense of reduced thermal stability, safety and sustainability. Advances in doping strategies, particle morphology optimization, and surface coatings are ongoing to mitigate these trade-offs and further enhance the performance and safety of layered oxides in next-generation lithium-ion batteries.

Lithium Metal Anode

Lithium metal is considered the "holy grail" of anodes due to its exceptional theoretical capacity (~3860 mAh g^{-1}) and low density, enabling batteries with significantly higher energy densities than those using graphite or silicon-based anodes. However, lithium metal is also highly reactive, forming dendrites upon repeated cycling that can lead to short circuits and potential safety hazards. This issue is particularly critical in liquid electrolytes, which may lead to uncontrollable dendrite growth and increased risk of thermal runaway[27]. In solid-state and hybrid systems, the interface between lithium metal and the electrolyte plays a crucial role. SSEs, especially those with high mechanical strength, can suppress dendrite formation by physically blocking dendrite propagation, enabling safer lithium metal cycling. Additionally, SPEs or hybrid electrolytes with flexible polymer matrices

can improve interfacial contact and minimize resistance, enhancing the feasibility of lithium metal in real-world applications. The development of SSE formulations that provide stable interfaces and limit side reactions with lithium metal is crucial.

1.6 Research Aim

The goal of this thesis is to develop highly conductive, stable, safe and sustainable high-performing SPEs for solid-state lithium metal batteries (SSLMBs). By leveraging advanced polymer chemistry and incorporating innovative crosslinking strategies, this research aims to overcome the current limitations of PEO-based SPEs, particularly in terms of ionic conductivity and oxidative stability. The ultimate goal is to create SPEs that can enable the practical application of SSLMBs in high-energy storage systems, contributing to a greener and more sustainable future.

Specific aims of the thesis:

Aim 1: conduct a comprehensive literature review on the crosslinking strategy as a powerful tool for developing high-performance SPEs for advanced lithium batteries (Chapter 2).

Aim 2: develop high-performing SPEs by combining a UV-crosslinked polymer matrix with a concentrated ionic liquid (CIL), addressing the key limitations such as low RT ionic conductivity and limited electrochemical window of traditional PEO-based SPEs. This aim included understanding the phase behavior and its effects on local structure and ion dynamics in the designed SPE, and relating these structural changes to ionic conductivity, electrochemical stability, and cycling performance in laboratory-scale battery cells with various cathodes and Li metal (Chapter 4).

Aim 3: Optimizing PEO-in-highly-concentrated ionic liquid (HCIL) SPEs by varying the HCIL concentration. Study the effect of HCIL concentration on the physicochemical and electrochemical properties of the designed electrolyte. This included understanding the phase behavior and ion interactions and their relationship with the Li^+ ion coordination environment, and relating these changes to ionic conductivity, electrochemical stability, lithium metal compatibility, and battery performance (Chapter 5).

1.7 PhD Thesis Structure

The outcome of this work is organized into six chapters, beginning with an introductory section and concluding with final remarks. **Chapter 1** provides a general introduction to Li-based batteries and materials, with a particular focus on solid-state technologies and related electrolytes. This chapter also outlines the research aim and thesis structure, guiding the reader through the study's scope. **Chapter 2** presents an in-depth literature review of crosslinking strategies, establishing a foundation for the subsequent experimental work. **Chapter 3** covers

the fundamentals of the experimental techniques and specific settings employed in this research. Moving into the core of the work, **Chapter 4** details the design of high-performance SPEs achieved by combining crosslinking with concentrated ionic liquid. This chapter examines how crosslinking influences the phase behavior, ionic conductivity, electrochemical characteristics, and cycling performance of the SPEs. In **Chapter 5**, advanced PEO-based SPEs are developed with high-concentration ionic liquids, aiming to optimize their use in solid-state lithium-metal batteries (SSLMBs). Here, the focus is on understanding the effects of high-concentration ionic liquid (HCIL) on phase behavior, coordination environment, and the resulting relationships with ionic conductivity, electrochemical stability, Li-metal compatibility, and overall battery performance. Finally, **Chapter 6** offers a synthesis of conclusions and suggestions for future work, underscoring the advancements made and potential directions for continued exploration.

1.8 References

1. Goodenough, J. B. & Park, K.-S. The Li-Ion Rechargeable Battery: A Perspective. *J. Am. Chem. Soc.* **135**, 1167–1176 (2013).
2. Manthiram, A. An Outlook on Lithium Ion Battery Technology. *ACS Cent. Sci.* **3**, 1063–1069 (2017).
3. Swain, B. Recovery and recycling of lithium: A review. *Sep. Purif. Technol.* **172**, 388–403 (2017).
4. Vikström, H., Davidsson, S. & Höök, M. Lithium availability and future production outlooks. *Appl. Energy* **110**, 252–266 (2013).
5. Janek, J. & Zeier, W. G. A solid future for battery development. *Nat. Energy* **1**, 16141 (2016).
6. Schmaltz, T. *et al.* A Roadmap for Solid-State Batteries. *Adv. Energy Mater.* 2301886 (2023) doi:10.1002/aenm.202301886.
7. Tarascon, J.-M. & Armand, M. Issues and challenges facing rechargeable lithium batteries. *Nature* **414**, 359–367 (2001).
8. Kato, Y. *et al.* High-power all-solid-state batteries using sulfide superionic conductors. *Nat. Energy* **1**, 16030 (2016).
9. Fergus, J. W. Ceramic and polymeric solid electrolytes for lithium-ion batteries. *J. Power Sources* **195**, 4554–4569 (2010).
10. Ye, L., Lu, Y., Wang, Y., Li, J. & Li, X. Fast cycling of lithium metal in solid-state batteries by constriction-susceptible anode materials. *Nat. Mater.* **23**, 244–251 (2024).
11. Kim, J. G. *et al.* A review of lithium and non-lithium based solid state batteries. *J. Power Sources* **282**, 299–322 (2015).
12. Zhao, Y. *et al.* Solid Polymer Electrolytes with High Conductivity and Transference Number of Li Ions for Li-Based Rechargeable Batteries. *Adv. Sci.* **8**, 2003675 (2021).
13. Janek, J. & Zeier, W. G. Challenges in speeding up solid-state battery development. *Nat. Energy* **8**, 230–240 (2023).
14. Duffner, F. *et al.* Post-lithium-ion battery cell production and its compatibility with lithium-ion cell production infrastructure. *Nat. Energy* **6**, 123–134 (2021).
15. Hatzell, K. B. & Zheng, Y. Prospects on large-scale manufacturing of solid state batteries. *MRS Energy Sustain.* **8**, 33–39 (2021).
16. Karkar, Z., Houache, M. S. E., Yim, C.-H. & Abu-Lebdeh, Y. An Industrial Perspective and Intellectual Property Landscape on Solid-State Battery Technology with a Focus on Solid-State Electrolyte Chemistries. *Batteries* **10**, 24 (2024).
17. An, Y. *et al.* Progress in Solid Polymer Electrolytes for Lithium-Ion Batteries and Beyond. *Small* **18**, 2103617 (2022).
18. Aziz, S. B., Woo, T. J., Kadir, M. F. Z. & Ahmed, H. M. A conceptual review on polymer electrolytes and ion transport models. *J. Sci. Adv. Mater. Devices* **3**, 1–17 (2018).

19. Armand, M. Polymer solid electrolytes - an overview. *Solid State Ion.* **9–10**, 745–754 (1983).
20. Watanabe, M., Nagano, S., Sanui, K. & Ogata, N. Ionic Conductivity of Network Polymers from Poly(ethylene oxide) Containing Lithium Perchlorate. *Polym. J.* **18**, 809–817 (1986).
21. Falco, M. *et al.* Understanding the Effect of UV-Induced Cross-Linking on the Physicochemical Properties of Highly Performing PEO/LiTFSI-Based Polymer Electrolytes. *Langmuir*. 2019, 35, 25, 8210–8219 (2019)
22. Hirankumar, G. & Mehta, N. Effect of incorporation of different plasticizers on structural and ion transport properties of PVA-LiClO4 based electrolytes. *Heliyon* **4**, e00992 (2018).
23. Famprikis, T., Canepa, P., Dawson, J. A., Islam, M. S. & Masquelier, C. Fundamentals of inorganic solid-state electrolytes for batteries. *Nat. Mater.* **18**, 1278–1291 (2019).
24. Song, Z. *et al.* A reflection on polymer electrolytes for solid-state lithium metal batteries. *Nat. Commun.* **14**, 4884 (2023).
25. Zhang, W.-J. Structure and performance of LiFePO4 cathode materials: A review. *J. Power Sources* **196**, 2962–2970 (2011).
26. Ammundsen, B. & Paulsen, J. Novel Lithium-Ion Cathode Materials Based on Layered Manganese Oxides. *Adv. Mater.* **13**, 943–956 (2001).
27. Wang, L., Chen, B., Ma, J., Cui, G. & Chen, L. Reviving lithium cobalt oxide-based lithium secondary batteries-toward a higher energy density. *Chem. Soc. Rev.* **47**, 6505–6602 (2018).
28. Li, W., Erickson, E. M. & Manthiram, A. High-nickel layered oxide cathodes for lithium-based automotive batteries. *Nat. Energy* **5**, 26–34 (2020).
29. Li, S. *et al.* Developing High-Performance Lithium Metal Anode in Liquid Electrolytes: Challenges and Progress. *Adv. Mater.* **30**, 1706375 (2018).

Chapter 2

Crosslinking: a powerful tool for developing high-performance solid polymer electrolytes

This chapter reviews the development of crosslinking methods for solid polymer electrolytes (SPEs), emphasizing their role in advancing solid-state battery performance. Crosslinking techniques, including UV-induced, chemical, thermal, and in-situ methods, are explored for their ability to enhance the mechanical stability, thermal resilience, and electrochemical properties of SPEs. UV-induced crosslinking is highlighted for its rapid processing and minimal thermal impact, while chemical and thermal methods provide robust, stable networks. In-situ crosslinking, which improves electrolyte integration with electrodes, is also discussed as a promising approach for practical battery applications. Key challenges, such as optimizing crosslink density to balance ionic conductivity and mechanical strength, are addressed, along with future directions for sustainable, high-performance SPE development. This chapter provides a comprehensive overview of crosslinking methods, their benefits, limitations, and potential for facilitating safer, more efficient energy storage solutions.

2.1 Introduction

2.1.1 Background

Developing high-performance SPEs holds great potential for the advancement of solid-state batteries (SSBs). While liquid electrolytes are commonly used, they bring several challenges, such as leakage, flammability, and limited electrochemical stability. These challenges not only raise safety concerns but also restrict the lifespan and efficiency of batteries. In contrast, SPEs hold great promise as they have the potential to enhance safety and improve overall performance metrics. Their high flexibility, ease of processing, low cost, and ability to work with

Li metal make them an attractive choice for the development of high-performance SSBs as the power source for practical high-energy applications such as EV and grid energy storage[1–3].

Despite their benefits, SPEs faces challenges such as lower ionic conductivity compared to their liquid counterpart and poor mechanical integrity compared to ceramic electrolytes[4]. Addressing these limitations is crucial for the broader adoption of SPEs in commercial applications. One of the promising strategies to enhance the robustness of SPEs is crosslinking. Crosslinking is a transformative technique in polymer chemistry that has emerged as a powerful tool for the development of high-performance SPEs. By interlinking polymer chains through covalent or ionic bonds, crosslinking significantly enhances the mechanical stability, ionic conductivity, and overall performance of SPEs, making them integral to advanced energy storage solutions, such as lithium-ion and lithium-metal batteries[5–7]. The pioneering work of Wright and Armand in the 1970s initially sparked interest in polymer electrolytes for rechargeable batteries[1,8]. Later, researchers such as Watanabe et al. explored crosslinked SPE systems, showing how crosslinking could reduce crystallinity and enhance the ionic conductivity and mechanical integrity of SPEs, thereby paving the way for their use in advanced energy storage applications[9].

Subsequent studies have further optimized the properties of polymer electrolytes by exploring various crosslinking techniques. Key studies have demonstrated the effectiveness of crosslinking in SPEs (Figure 2-1). For instance, Nair et al. reported novel UV-cured methacrylic based polymer electrolytes with high values of ionic conductivity[10]. The results show that using UV-induced crosslinking is an easy way to create polymer membranes for lithium batteries. Kim et al. further studied UV-crosslinked PEO systems that use C4mpyrTFSI ionic liquids with LiTFSI (33 mol%) to enhance ionic conductivity and mechanical stability (Figure 2-1)[11]. The UV crosslinking process creates a stable network that boosts the mechanical strength of the SPE while still allowing the ionic liquids to provide their benefits. Khurana and colleagues were pioneers in utilizing crosslinking to introduce a high-strength species into the polymer electrolyte, aimed at suppressing dendrite growth[12]. Porcarelli et al. were among the earliest to exploit rapid, solvent-free, scalable UV-induced (co)polymerization, demonstrating that efficient interlinking between PEO chains and plasticizing with tetraglyme lead to improved mechanical strength, high flexibility, and high amorphicity (Figure 2-2)[13]. Li et al. described a highly conductive and stable dual-salt SPE, which represents one of the initial uses of crosslinked polymers to infiltrate the active material in cathode, creating continuous pathways for ion transport under high voltages (Figure 2-3)[14]. Choudhury et al. employed straightforward light-initiated crosslinking to form a thin SPE layer directly on lithium metal anodes, targeting high-performance lithium metal batteries[15]. Falco et al. examined the impact of UV-induced crosslinking on the structure and transport properties of PEO/LiTFSI-based SPEs (Figure 2-4)[16]. The resulting crosslinked SPE showed high ionic conductivity at RT, broad electrochemical stability window, and enhanced interfacial stability

with lithium metal. These advancements demonstrate the important role of crosslinking in the development of SPEs.

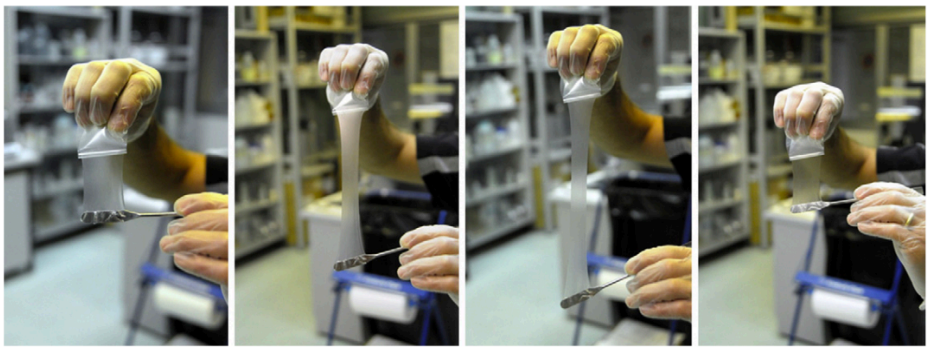

Figure 2 - 1. UV-crosslinked PEO–LiTFSI–C4mpyrTFSI ternary SPE subjected to manual elongation. Adapted from Ref. 11, with permission from Journal of Power Sources. Copyright 2010.

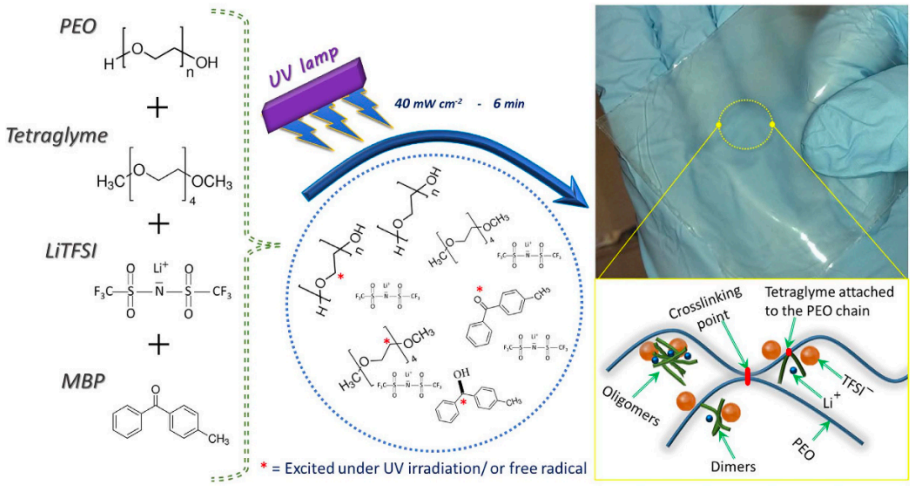

Figure 2 - 2. Scheme of SPE preparation and illustration of crosslinked PEO chains. Adapted from Ref. 13, with permission from Science Report. Copyright 2016.

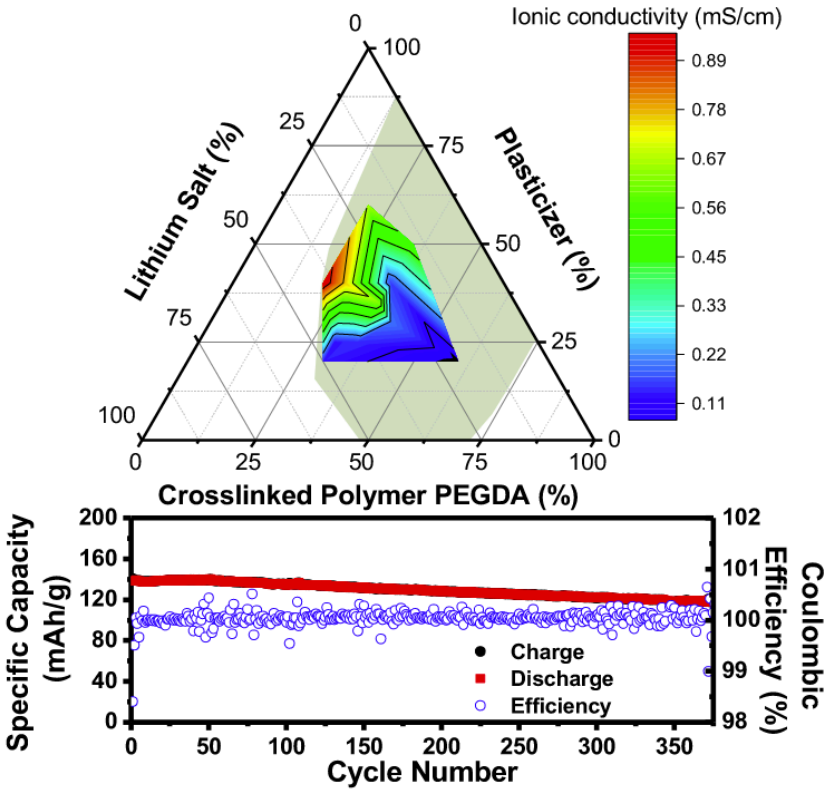

Figure 2 - 3. A ternary phase diagrams for searching polymer composites with high ionic conductivity. The optimized ionic conductivity (1.0 mS cm^{-1} at RT) was found in the isotropic phase of the dual-salt SPE. Adapted from Ref. 14, with permission from Joule. Copyright 2018.

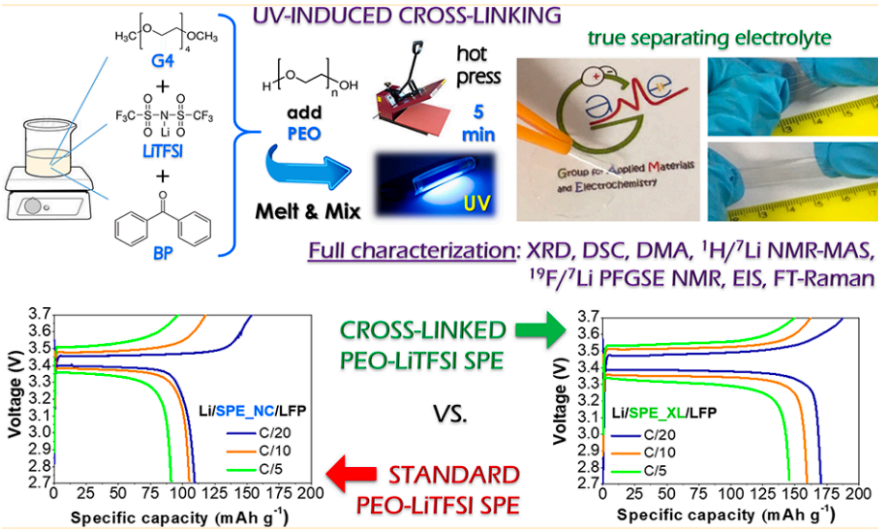

Figure 2 - 4. Schematic illustration of UV-induced crosslinking for SPE preparation (top). Comparison of voltage profile vs. specific capacity of crosslinked and non-crosslinked Li//LFP cell under different C-rates, showing the advantages of UV-crosslinked SPE in cell performance (bottom). Adapted from Ref. 16, with permission from Langmuir. Copyright 2019.

Crosslinking can be facilitated by various methods, such as UV-irradiation and thermal conditions. The choice of method and optimization of crosslinking conditions play an important role in determining the network properties and crosslink density of the resulting polymer. UV-induced crosslinking is recognized for its rapid, and facile operation, and it has been extensively used in SPE research. For example, Ahmed et al. used this method to create SPEs with better safety features and performance, showing its potential in practical applications[17]. Chemical crosslinking in SPEs usually use crosslinkers to polymerize multifunctional monomers to form a crosslinked network. Xue et al. reviewed different ways of crosslinking and crosslinkers used in PEO-based electrolytes[18]. The study found that chemical crosslinking is very effective in enhancing ionic conductivity and mechanical properties.

Thermal crosslinking is another widely used technique to enhance the properties of SPEs. The crosslinking process is initiated by the thermal treatment using a thermal initiator. Xin et al. reported a thermally crosslinked PEO-based SPE with polyaryl polymethylene isocyanate (PAPI) as the crosslinker[19]. Crosslinking improves the mechanical property, inhibits Li dendrite, and extends battery life. They also found that an optimal PAPI amount of 0.4 mL best balanced the mechanical and electrochemical properties of the SPEs. In situ crosslinking has gained great interest in recent years. It forms crosslinked networks directly within the battery during assembly, so that interface stability and cell performance can be significantly improved. Nair et al. reviewed in situ polymerization processes for lithium polymer batteries (LPBs) and highlighted its advantage in SPE integration and potential for large-scale production[20]. Different crosslinking methods may improve the properties of SPEs in different ways. Understanding the trade-offs and synergies among these properties is important for designing high performance SPEs.

2.1.2 Research Gaps

Despite the progress in various crosslinking methods, there are still challenges in developing high performance crosslinked SPEs. One main challenge is the trade-off between crosslinking density and ionic conductivity. Increasing crosslinking density can improve mechanical strength but might hinder ion mobility, reducing the overall ionic conductivity of the SPE. Homann et al. discussed the need to find the right balance between crosslinking density and ionic conductivity to achieve the desired performance[21]. Another concern is the scalability of crosslinking techniques for large-scale production. While lab-scale studies have shown promising results, more research are needed to apply these findings on an industrial scale. Additionally, the environmental impact and sustainability of materials and crosslinking processes must be considered to meet the zero-emission target.

2.1.3 Research Contributions

This review aims to provide a comprehensive overview of different crosslinking strategies and discuss their impact on the properties and performance

of SPEs. The study supplements existing research by addressing several key gaps. Firstly, it provides a comprehensive analysis of various crosslinking techniques used in SPEs such as UV-induced crosslinking, thermal crosslinking, chemical crosslinking, and in situ crosslinking, discussing their advantages and limitations. Secondly, it examines how crosslinking affects the physical and electrochemical properties of SPEs, such as ionic conductivity, mechanical strength, thermal stability, and electrochemical stability. Thirdly, it explores real-world applications of crosslinking employed by automobile industries and battery technology companies. Studies by Song et al. and Nair et al. have laid the groundwork of showing the benefits of crosslinking polymer electrolytes[20,22]. However, more research is required to understand the relationship among crosslinking density, ion dynamics, and long-term performance under practical conditions. By addressing these gaps, we aim to provide a deeper understanding of the potential and limitations of crosslinking in SPE development.

In the next sections, we cover the current research directions, including crosslinking methods, effects of crosslinking on SPE properties, and critical viewpoints. Then, applications of crosslinking in advanced lithium batteries and future research directions are explored, followed by a conclusion summarizing key findings and significance.

2.2 Current Research Directions

Various crosslinking techniques have been explored in SPE development, including UV-induced crosslinking, chemical crosslinking, thermal crosslinking, and in situ crosslinking. Each technique has its unique advantages and limitations for enhancing the properties and performance of SPEs.

2.2.1 Crosslinking Methods

UV-Induced Crosslinking

Crosslinking is known as an effective approach to improve the mechanical properties of SPEs, particularly in PEO-based SPE systems[12,23]. For linear PEO, mechanical strength depends on the crystalline phase and molecular weight. It loses mechanical stability above its melting temperature around 60 °C, posing significant risks to short circuiting. Various strategies have been explored to increase the mechanical strength of PEO-based SPE, and one effective method is UV-induced crosslinking[13]. This technique requires precise control of the curing process such as exposure time and UV power density. It is a simple and efficient technique, but extra UV exposure may cause polymer degradation and UV light might not be compatible with certain additives/plasticizers which used to enhance SPE properties[24].

Research by C. Decker et al. reviewed and highlighted the benefits of photoinitiated crosslinking polymerization, emphasizing its efficiency and control over the crosslinking process[25]. Exceptionally high polymerization rates are achievable under intense illumination. This rapid reaction enables phase or

structural changes to occur in fractions of a second. Additionally, a unique characteristic of radiation-induced reactions is their spatial selectivity, as polymerization takes place exclusively in the illuminated regions which allows a precise control of the relief patterns after crosslinking. It is well known that radiation causes chain fragmentation and crosslinking, and the final outcomes are influenced by the polymer's physical state and temperature[26]. Typically, chain fragmentation predominates, reducing PEO's molar mass. However, photochemical crosslinking is possible using a photoinitiator such as benzophenone (BP)[27]. It initiates hydrogen abstraction from PEO under UV, forming a network through recombination as depicted in Figure 2-5. Studies with thin PEO films with 5 wt% BP demonstrated 80% gel fraction by photo-crosslinking at 70°C[28].

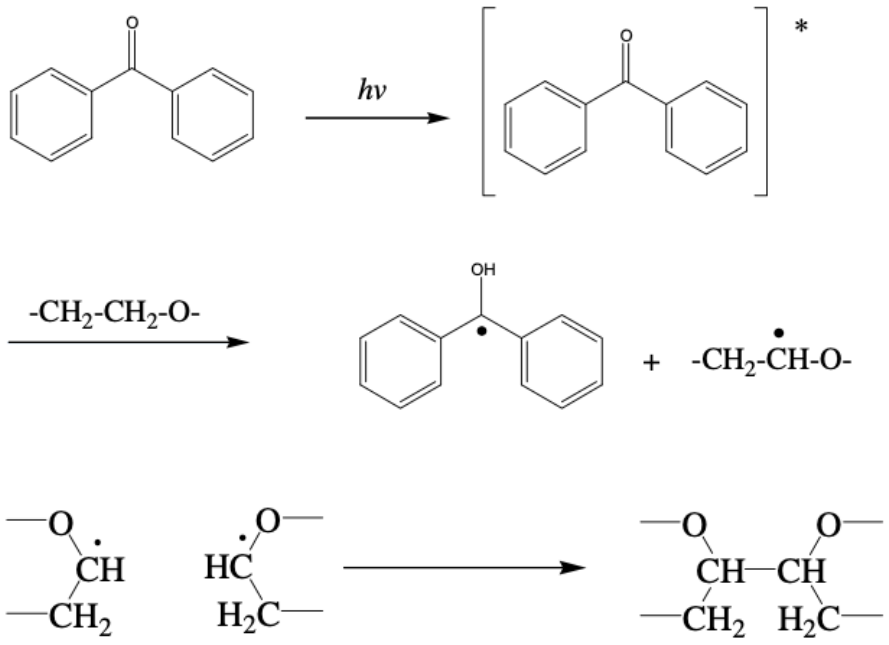

Figure 2 - 5. Crosslinking of PEO by photo-irradiation using benzophenone as photoinitiator. Adapted from Ref. 28, with permission from European Polymer Journal. Copyright 2008.

Among photo-irradiation methods, UV-curing is a well-known polymerization technique that is performed at room temperature under ultraviolet (~ 100 – 400 nm) light. This process involves a poly-functional monomer with a suitable photoinitiator, which, upon UV irradiation, forms a highly crosslinked solid film. Typically, the formulation is solvent-free, containing multiple monomers and oligomers, and requires only a few seconds to minutes of UV exposure. This method is considered fast, energy-efficient, and environmentally friendly, with no emission of volatile organic compounds. UV-curing is widely used in various industries like protective coatings, printing inks, adhesives, photolithography, and biomedical applications. Recently, UV-induced crosslinking has also become a

highly effective method for improving the properties of solid polymer electrolytes (SPEs) for advanced lithium batteries. Nair et al. showed that UV-induced photopolymerization is a fast and easy way to prepare SPEs[20]. The resulting SPEs have high mechanical and thermal stability without losing ionic conductivity due to the crosslinked polymer network. Falco et al. further explored this method[16]. A uniform PEO/LiTFSI-based network is formed by UV-crosslinking with significant enhancement in both mechanical strength and ionic conductivity.

Ionic liquids (ILs) have received increased interest due to their negligible vapor pressure, nonflammability, and outstanding thermal and chemical stability[29]. However, adding ILs often comes with a reduction of mechanical strength. Rupp et al. proposed using UV-induced crosslinking with BP as the photoinitiator to solve this dilemma[28]. They studied a ternary SPE system based on PEO, $PYR_{14}TFSI$ ionic liquid, and LiTFSI salt, showing that UV-crosslinking increased the mechanical strength of the crosslinked SPE without compromising ionic conductivity. Moreover, the crosslinking process decreased the degree of PEO crystallinity that leads to an improvement in ionic conductivity. Wetjen et al. further investigated the impact of temperature on the electrochemical performance of this crosslinked SPE system[30]. The study demonstrated that higher operating temperatures enhanced ionic conductivity and rate capability without significantly degrading electrochemical stability. The obtained SPEs exhibit exceptional capacities, particularly at higher discharge rates and temperatures, making them promising for advanced lithium metal batteries (LMBs).

Crosslinked SPEs have also been shown to suppress Li dendrites growth. Khurana et al. reported a UV crosslinked PE/PEO SPE with high room temperature ionic conductivity and excellent ability to suppress Li dendrite growth[12]. Similarly, Homann et al. demonstrated that a PEO-based semi interpenetrating network developed by UV-crosslinking can effectively suppress Li dendrite penetration due to improved mechanical robustness and result in a voltage-noise-free cell cycling[21]. Ha et al. also reported a facile UV crosslinked semi-interpenetrating polymer network plasticized by plastic crystal[31]. The result SPE shows high thermal stability, nonflammability, and exhibits exceptional bendability, holding great promise for use in flexible all-solid-state LIBs. Stalin et al. further explored the development of crosslinked PEO-based electrolytes to enhance the uniformity of lithium electrodeposition in lithium metal batteries[32]. The study demonstrates that the crosslinked structure mitigates dendrite formation, leading to improved cycling stability and battery performance.

Additionally, other polymer forms and structures are also benefit from utilizing UV-induced crosslinking. Xu et al. report on a UV-induced double crosslinked PEO-based polymer electrolyte using C-S-C groups and metal-organic frameworks, achieving high energy and stability in solid-state lithium batteries[33]. Mackanic et al. reported a UV-crosslinked poly(tetrahydrofuran) network[34]. The obtained SPE showed improve ionic conductivity while maintaining high electrochemical stability. He et al. reported a UV-crosslinked block copolymer SPE that has both ion-solvating sites and crosslinking sites[35]. The resulting SPE showed high ionic conductivity and enhanced mechanical stability simultaneously. The effectiveness

and flexibility of UV-crosslinking has also been validated by other researchers in the past decade[36–40].

In summary, UV-crosslinking is a simple and efficient polymerization method. It forms crosslinked SPE networks with improved properties and performances, making it suitable for large-scale SPE production.

Chemical Crosslinking

Chemical crosslinking creates covalent bonds between polymer chains via specific chemical reactions, usually at room temperature. These bonds are highly stable and provide mechanical strength and thermal stability to the polymer. Typically, chemical crosslinking is irreversible, causing the thermosetting material to degrade or combust when heated, rather than melt. In the development of SPEs, various crosslinking agents and reactions can be used, for example, Xue et al. designed a crosslinked SPE based on reactions between amine-functionalized polymers and aldehyde groups[41]. The obtained SPE achieved high ionic conductivity and stability due to the dynamic bonds formed within the crosslinked network. Lee et al. developed a poly(ethylene glycol) (PEG)-based crosslinked SPE[42]. The study shows that adding non-volatile plasticizers and crosslinking agents significantly improves the ion conductivity of the SPE. In another study by the same group, a new crosslinking agent, poly(ethylene glycol) borate acrylate (PEGBA), was developed to further enhance the ionic conductivity and stability of the SPE[43]. Lin et al. introduced "mobile crosslinks" by crosslinking α-cyclodextrins (CDs) in a PEG-based polyrotaxane (Figure 2-6)[44]. The PEG facilitates the ion transport, and the crosslinked CDs suppress PEG crystallization, ensuring its segmental mobility. Bao et al. developed a new crosslinking strategy using metal alkoxy-terminated polymers and plasticizers[45]. The obtained SPEs showed superior mechanical properties and ionic conductivity. Combining chemical crosslinking with UV-induced crosslinking can further enhance the crosslinking effectiveness. Sakakibara et al. combined both methods to develop a hybrid SPE which showed excellent mechanical strength, thermal stability, and ionic conductivity[46].

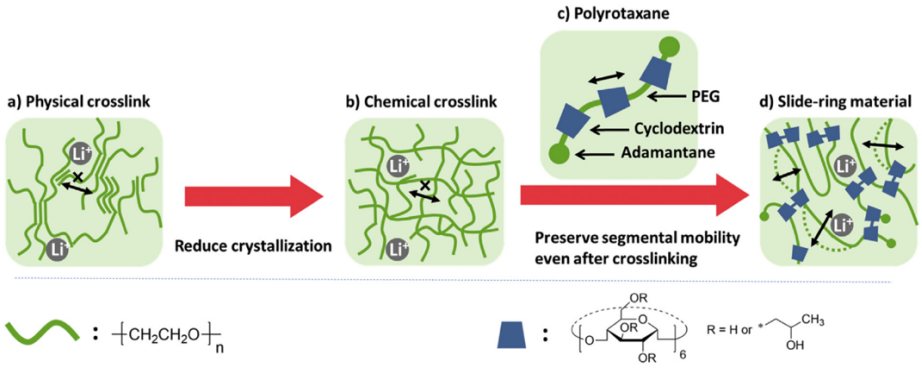

Figure 2 - 6. (a) PEG-based SPEs are prone to crystallization and can easily form physical crosslinks. (b) Crosslinking reduces the crystallinity of PEG-based SPEs, showing good mechanical strength with a compromise in chain mobility. (c) Illustration of a polyrotaxane.

(d) The slide-ring material has good PEG mobility while provide good mechanical strength. Adapted from Ref. 44, with permission from Polymer. Copyright 2018.

In summary, chemical crosslinking is an important technique to increase the mechanical strength and electrochemical stability of SPEs. It is useful for many applications, including advanced lithium batteries.

Thermal Crosslinking

Thermal-induced polymerization is another effective method for crosslinking. This process involves heating the monomer precursor at temperatures below their decomposition threshold. In thermal crosslinking, a thermal initiator such as 2,2'-azobis(2-methylpropionitrile) (AIBN) is often used. The applied heat initiates the crosslinking process and forms a 3D polymer network structure. The advantage of thermal crosslinking is that it allows the precise control of the crosslink density by adjusting the polymer chain length. It is also efficient and easy to control, and therefore highly suitable for large-scale SPE fabrication.

Many research works have explored the use of thermal crosslinking to create high-performance of SPEs. For example, the early study by Sylla et al. compared the electrochemical properties of linear and thermally crosslinked PEO-based polymer electrolytes[47]. The crosslinked SPEs exhibit enhanced ionic conductivity, mechanical strength and better overall battery performance compared to their linear counterparts. Motaba et al. further investigated the ionic conductivity and mechanical properties of PEO-based SPEs, using crosslinking to prevent PEO crystallization[48]. The study shows that it is crucial to control the crosslinking when designing SPEs for practical use. Later, Lee et al. explores a series of thermally crosslinked SPEs based on polyethylene glycol dimethacrylate (PEGDMA) and different alkyl methacrylate monomers[49]. The study shows that the crosslinked SPEs exhibit improved ionic conductivity, mechanical properties, and electrochemical stability, making them suitable for rechargeable lithium polymer batteries. Pan et al. developed thermally crosslinked PEO-polyhedral oligomeric silsesquioxane (POSS) hybrid electrolytes with controlled network (Figure 2-7)[50]. The hybrid network demonstrated superior ionic conductivity, mechanical integrity, and electrochemical stability, resulting in enhanced battery performance. Similarly, Li et al. designed comb-chain SPEs for all-solid-state LMBs, using POSS as crosslinkers to crosslink PEG in a single-step polymerization process[51]. These SPEs exhibited high ionic conductivity, excellent mechanical strength, and enhanced performance in LMBs without the need for additives. Zheng et al. reported an interpenetrating network (IPN) based on PEO and poly(propylene carbonate), showing improved ionic conductivity and Li transference number (t_{Li+})[52]. Similarly, Lehmann et al. introduced a one-step process to produce crosslinked SPEs composed of branched PEI and PEO[53]. The amine functional groups in the crosslinked matrix enhance lithium salt dissolution, leading to a high t_{Li+}.

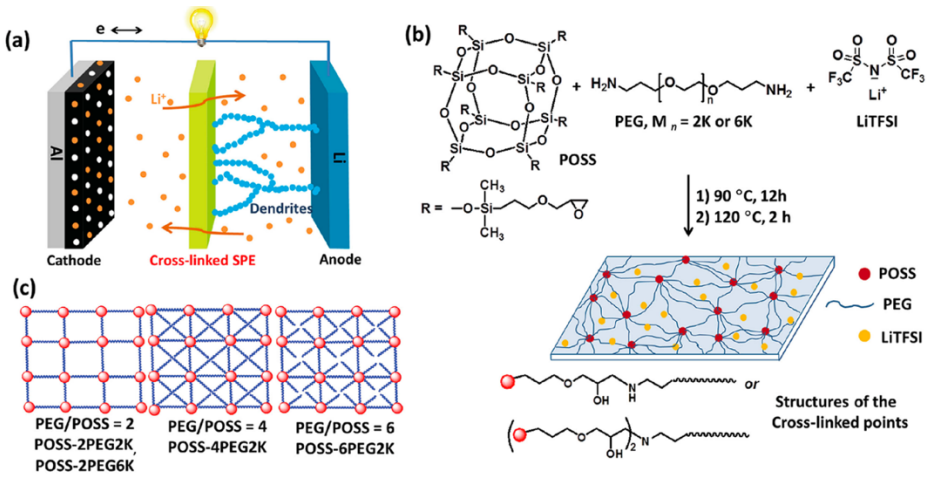

Figure 2 - 7. (a) Illustration of lithium dendrites blocking by the crosslinked SPE. b) Preparation of POSS-PEO SPEs. c) Structures of the ideal crosslinked networks. Adapted from Ref. 50, with permission from Advanced Materials. Copyright 2015.

Other polymer systems and hybrid structures also benefit from thermal crosslinking. For example, Rymarczyk et al. developed a thermally crosslinked SPE based on poly(urethane acrylate) (PUA), LiTFSI, and $PYR_{14}TFSI$ ionic liquid[54]. The designed SPE showed high room temperature ionic conductivity of 0.1 mS cm^{-1} with 40 wt% of ionic liquid. Whiteley et al. developed a thermally crosslinked self-healing polyimides matrix to address the mechanical and durability issues[55]. This crosslinked SPE is an ultra-thin and flexible membrane with high ionic conductivity, high mechanical strength, and self-healing abilities. This significantly enhances the battery performance and longevity. Chaudoy et al. used a solvent-free thermal crosslinking approach with methacrylate-based oligomers and AIBN thermal initiator[24]. The crosslinked structure provided enhanced mechanical stability and ionic conductivity for high-performance lithium batteries. Lopez et al. introduced a dual-crosslinking design of PPO elastomer through thermal crosslinking[56]. The combination of both ionic and covalent crosslinking results in a highly resilient structure that can withstand mechanical stresses while maintaining high ionic conductivity.

Researchers have also explored the influence of temperature and heating time on the crosslinking efficiency and ion conductivity of SPEs. Increasing temperature generally increases the crosslinking efficiency by promoting more chemical reactions between the polymer chains and crosslinking agents. For instance, Zhang et al. found that thermally crosslinked sulfonated poly(phenylene sulfone) membranes exhibited improved mechanical and thermal stability, with the highest conductivity observed at 120 °C[57]. Di Vona et al. discussed that increased heating time improves the mechanical strength and hydrolytic stability of SPE membranes by enhancing the degree of crosslinking[58].

While longer heating time allows for more thorough crosslinking, excessive heating can lead to degradation. Therefore, it is crucial to optimize the thermal crosslinking parameters to fully realise the potential of this technique. Overall,

thermal crosslinking is a valuable technique for creating SPEs with improved characteristics. It is suitable for large-scale applications in lithium batteries and other energy storage devices.

In situ Crosslinking

The in situ crosslinking technique involves forming crosslinked networks directly in the battery during assembly. This process can significantly improve the integration of SPEs with electrodes, leading to improved interfacial stability, ion transfer, and electrochemical performance of SPEs. Recently, in situ crosslinking has become a smart tool to address challenges related to SPE integration. Choudhury et al. reported SPEs based on crosslinked PEO and LiTFSI for room temperature LMBs[15]. These crosslinked solid polymer electrolytes (SPEs) offer liquid-like characteristics that promote ion transport while providing solid-like mechanical strength at the lithium metal anode. The effectiveness of in situ crosslinking has also been confirmed by other researchers. Niu et al. emphasized the potential of in situ crosslinking for advanced SPEs, highlighting their ability to enhance both mechanical strength and ionic conductivity[59]. Lim et al. developed an innovative bicontinuous crosslinked structure through an in situ, solvent-free ring-opening polymerization[60]. The crosslinked SPE shows both high ionic conductivity and high mechanical strength simultaneously. Furthermore, the advantages and advancements of in situ polymerization are thoroughly reviewed by Liu et al. and Vijayakumar et al[61,62].

In situ crosslinking is often combined with other crosslinking strategies to maximize the synergistic benefits. Choi et al. reported in situ thermally crosslinked ethylene oxide/propylene oxide (EO/PO) copolymer electrolytes for lithium polymer batteries (Figure 2-8)[63]. The crosslinked SPEs demonstrated excellent electrochemical stability and ionic conductivity. Nair et al. developed truly solid membranes by in situ thermal-induced crosslinking[64]. A semi-inter penetration network (IPN) structure is formed by crosslinking dimethacrylate oligomer with PEO. The obtained SPE is freestanding, flexible and non-tacky. Wang et al. developed a high-strength thin SPE for all solid state LMBs using in situ thermal crosslinking[65]. The resulting electrolyte displayed excellent mechanical strength, interface compatibility, and high ionic conductivity. Z. Wang et al. develops a 3D PEG thin SPE supported by porous poly(vinylidene fluoride) (PVDF) via an in situ thermal curing method for flexible and high-temperature LMBs (Figure 2-9). The crosslinked PEG electrolyte shows excellent thermal stability, mechanical flexibility, and high ionic conductivity (Figure 2-5)[66]. Duan et al. reported a thermal-crosslinked double-network structure via an in situ approach[67]. The crosslinked electrolyte showed significantly improved ionic conductivity, flexibility, interfacial stability, and thermal stability.

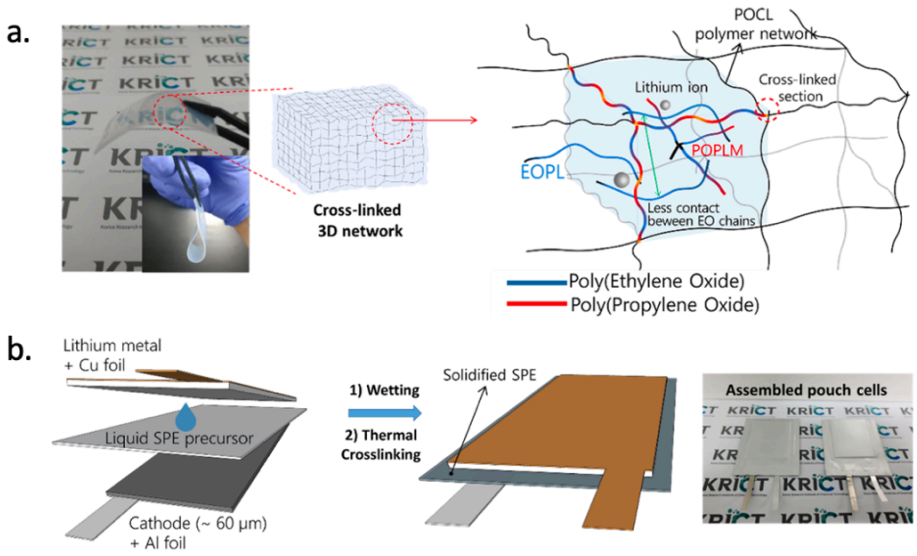

Figure 2 - 8. a) Schematic and picture of the thermally crosslinked SPE. b) Schematic illustration of pouch cell fabrication by precursor wetting and then in situ crosslinking. Adapted from Ref. 63. with permission from ACS Applied Materials and Interfaces. Copyright 2021.

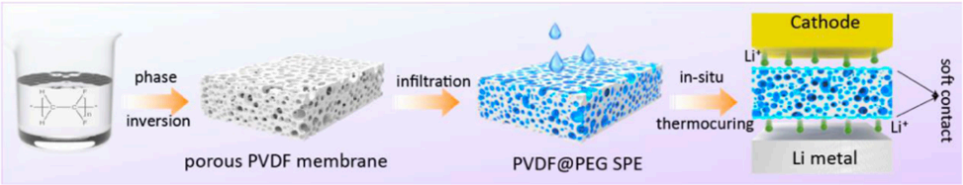

Figure 2 - 9. Preparation of PVDF@PEG electrolyte. Adapted from Ref. 66, with permission from Chemical Engineering Journal. Copyright 2022.

In situ crosslinking is also commonly combined with UV-induce crosslinking. Kim et al. prepared a highly conductive SPE by in situ UV-crosslinking PEO with LiTFSI salt and the pyrrolidinium ionic liquid[11]. The crosslinked SPE showed high room temperature ionic conductivity of nearly 1.0 mS cm^{-1} due to the reduced crystallinity of the ternary SPE and superior mechanical properties compared to non-crosslinked SPEs. Similarly, Porcarelli et al. reported a flexible and robust PEO-based network prepared by UV-induced in situ crosslinking. This SPE exhibited enhanced room temperature ionic conductivity and electrochemical stability while maintaining mechanical robustness[13]. The benefits of in situ UV-crosslinking have been confirmed by other researchers[16,68–70].

Recently, in situ crosslinking has gained interest for developing ultra-thin SPEs. Chen et al. introduced an ultra-thin (8 μm) in situ crosslinked carbonate-ester-based electrolyte for high-voltage (24 V) bipolar LMBs[71]. This SPE showed excellent electrochemical stability, high ionic conductivity, and Li metal compatibility. Wen et al. reported an ultra-thin crosslinked SPE prepared by a single-step in situ crosslinking based on DOL and trimethylol-propane triglycidyl ether(TTE)[72]. The obtained SPE showed high room temperature ionic conductivity,

high mechanical strength, and rapid charge transfer across interfaces. It offers a promising pathway for highly flexible all-solid-state batteries. Additionally, initiator-free and self-catalysing are desirable for cost-effective and scalable SPE preparation. Cui et al. reported an initiator-free strategy toward the preparation of crosslinked SPE based on poly(ethylene glycol) diglycidyl ether[73]. The obtained SPE showed a wide electrochemical stability window (ESW) up to 4.5 V and deliver stable charge/discharge profiles in LFP cells, making it an effective method for developing advanced SPEs.

In summary, the in situ crosslinking technique simplifies the preparation process and enhances battery performance by forming integrated interfaces. It improves interfacial compatibility, inhibits transition metal dissolution, suppresses lithium dendrite growth, and enhances the cycle performance.

2.2.2 Effects of Crosslinking

Impact on Ionic Conductivity

Understanding how crosslinking affects the ionic conductivity of SPEs is a key research focus. Ionic conductivity measures how effectively ions move through the electrolyte and its interfaces. Research has demonstrated that crosslinking can enhance the ionic conductivity of SPEs at RT by altering the polymer network structure and its mobility.

Nest et al. first studied how ions move in crosslinked polyether-based networks, highlighting two key needs for high ionic conductivity in SPEs: good Li salt dissociation and low glass transition temperature (T_g)[74]. Zhang et al. explored the ion transport of crosslinked polysiloxane-based SPEs (Figure 2-10)[75]. The study found significant improvements in room temperature ionic conductivity, ranging from 2.5×10^{-5} to 1.6×10^{-4} S cm^{-1}, depending on crosslinking density. Falco et al. explored at how UV-induced crosslinking affects PEO-based SPEs. They found that crosslinking lead to high room temperature ionic conductivity and better stability with Li metal[16]. Liang et al. demonstrated a superionic conductive SPE with crosslinked networks that showed excellent room temperature ionic conductivity (> 1.76 mS cm^{-1}) and long cycle life (1000 cycles)[39].

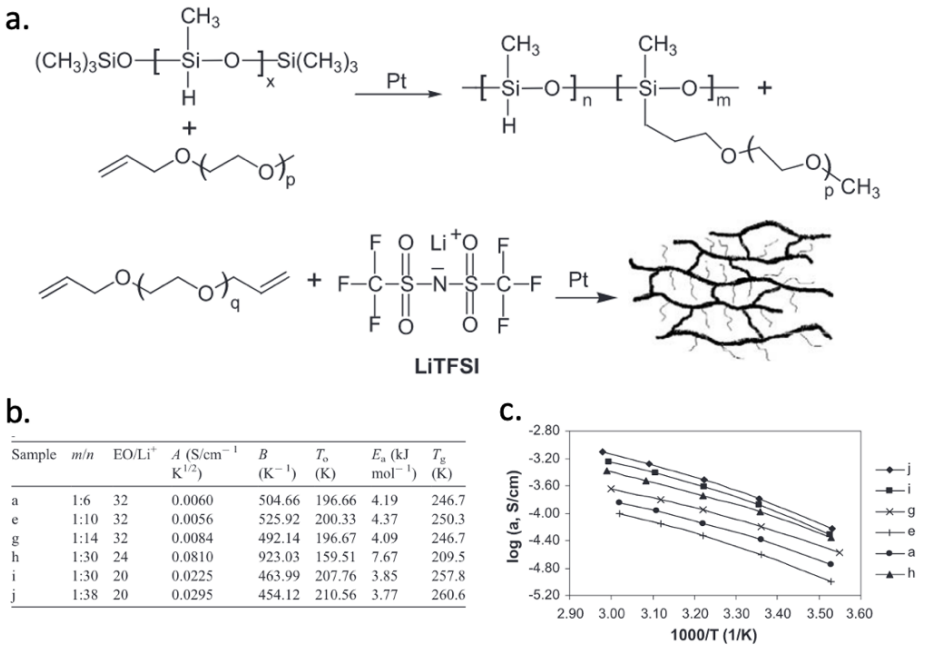

Sample	*m*/*n*	EO/Li$^+$	*A* (S/cm^{-1} K$^{1/2}$)	*B* (K^{-1})	T_o (K)	E_a (kJ mol^{-1})	T_g (K)
a	1:6	32	0.0060	504.66	196.66	4.19	246.7
e	1:10	32	0.0056	525.92	200.33	4.37	250.3
g	1:14	32	0.0084	492.14	196.67	4.09	246.7
h	1:30	24	0.0810	923.03	159.51	7.67	209.5
i	1:30	20	0.0225	463.99	207.76	3.85	257.8
j	1:38	20	0.0295	454.12	210.56	3.77	260.6

Figure 2 - 10. a) Synthesis of precursors and crosslinked polysiloxane network SPE. b) Various parameters for the polymer/LiTFSI complexes. c) Li^+ conductivity vs. temperature. Adapted from Ref. 75, with permission from Solid State Ionics. Copyright 2004.

However, the relationship between crosslinking density and ionic conductivity is complex. More crosslinking can improve mechanical strength but may also limit ion mobility by restricting chain movement. Thiama et al. studied how crosslinking density affects the ionic conductivity and mechanical properties of SPEs[76]. They found that adjusting the crosslink density significantly impacts ionic conductivity and mechanical properties. By manipulating crosslinking density, they achieved a large improvement in RT ionic conductivity compared to linear PEO electrolytes.

In summary, crosslinking can have mixed effects on ionic conductivity. On one hand, it can inhibit chain motion, reducing ionic conductivity. On the other hand, it can create defined ion transport pathways. By using plasticizers like ionic liquids and optimizing crosslinking density, it is possible to solve this dilemma. The key is to balance the rigidity from crosslinking with enough segmental motion to achieve optimal ionic conductivity.

Impact on Thermal Stability

Crosslinking improves the thermal stability of SPEs by creating a robust polymer network that resists thermal degradation. This is important for maintaining battery performance and safety during operation, especially to prevent safety risks such as thermal runaway, a situation when a battery overheats and catch fire. Wang et al. demonstrated that crosslinked polymer electrolytes have high thermal stability and can maintain their properties even at 100ºC, which greatly enhances battery safety and reliability[66]. Cui et al. developed a fireproof lightweight SPE using a self-catalyzed crosslinking method. The crosslinked SPE showed excellent thermal stability and mechanical strength[77]. Similarly, Chen et al. developed a crosslinked

network with H bonds and dynamic disulfide bonds, which demonstrated excellent self-healing abilities and non-flammability (Figure 2-11)[78]. Oh et al. reported a comb-type crosslinked SPE[79]. These SPEs exhibited ionic conductivity of nearly 10^{-4} S cm^{-1} at RT and remarkable thermal stability, withstanding temperatures up to 500 °C.

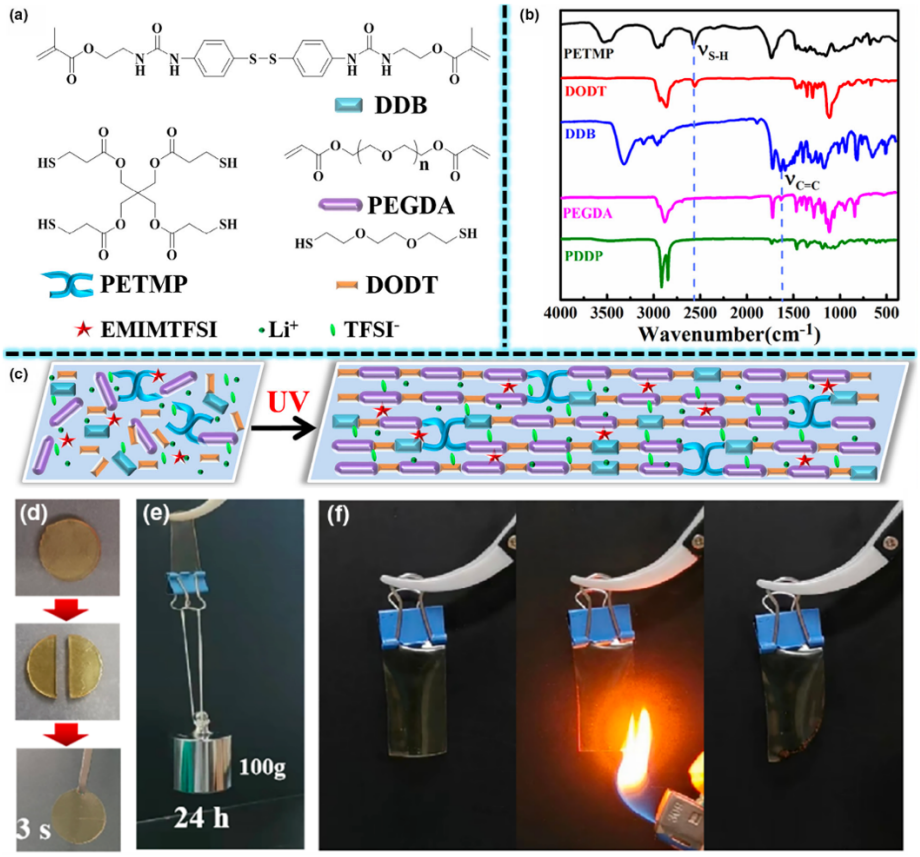

Figure 2 - 11. a) Chemical structures of the precursors b) FTIR spectra of the precursors and the UV-crosslinked PDDP SPE. c) Illustration of SPE preparation by UV-crosslinking. d) Photos of self-healing of PDDP-5. e) Mechanical integrity test of the healed PDDP-5. f) Flammability test of PDDP-5. Adapted from Ref. 78, with permission from Energy Environmental Materials. Copyright 2023.

In summary, crosslinking is an effective way to prevent thermal risks and polymer degradation of SPEs. The crosslinked SPEs are more heat resistant due to limited chain movements. This improved thermal stability is important to maintain SPE performance at high temperatures, contributing to the longevity and safety of the battery.

Impact on Mechanical Strength

Crosslinking is one of the most widely used method for improving the mechanical properties of SPEs. Crosslinking typically increases the tensile strength and toughness by creating a 3D network that resists deformation under stress. This network structure boosts the modulus or stiffness of the polymer, providing greater

structural integrity compared to non-crosslinked counterparts. Consequently, crosslinked SPEs are stronger, more elastic, and more resistant to deformation compared to non-crosslinked SPEs. The crosslinked network that can sustain mechanical stresses and strains, inhibit the growth of lithium dendrites during cycling, and prevent potential battery short-circuit.

Generally, mechanical metrics such as Young's modulus, tensile strength, and toughness improve with polymer molecular weight[5]. Sung et al. discussed the effect of molecular weight on the photocycloaddition reaction of PEG oligomers, showing enhanced mechanical stability by crosslinking[80]. Reducing chain activity usually enhances its mechanical strength, and therefore crosslinking the polymer chains is an effective way to increase mechanical stability. Khurana et al. developed a novel electrolyte system that combines the mechanical robustness with the ionic conductivity of PEO[12]. The crosslinked structure effectively prevents dendrites formation, leading to enhanced safety and prolonged cycle life in LMBs. Similarly, Zheng et al. reported a crosslinked PE-PEO-based SPE with high room temperature ionic conductivity (close to 1 x 10^{-3} S cm^{-1}) and excellent dendrite suppression[81]. Their study found that crystallinity affects the size and shape of lithium dendrites. Crosslinking also enhances mechanical properties by creating a more cohesive and elastic polymer matrix. Lopetz et al. reported an elastic crosslinked SPE consisting of both covalent and hydrogen bonding (Figure 2-12)[56]. The obtained SPE exhibited high mechanical resilience without sacrificing ionic conductivity. The SPE can still operate even after intense mechanical impact testing. Kang et al. developed a cyanoethyl polyvinyl alcohol (PVA-CN) based crosslinked network through in situ polymerization[82]. The obtained SPE showed significantly improved mechanical properties even above the melting temperature.

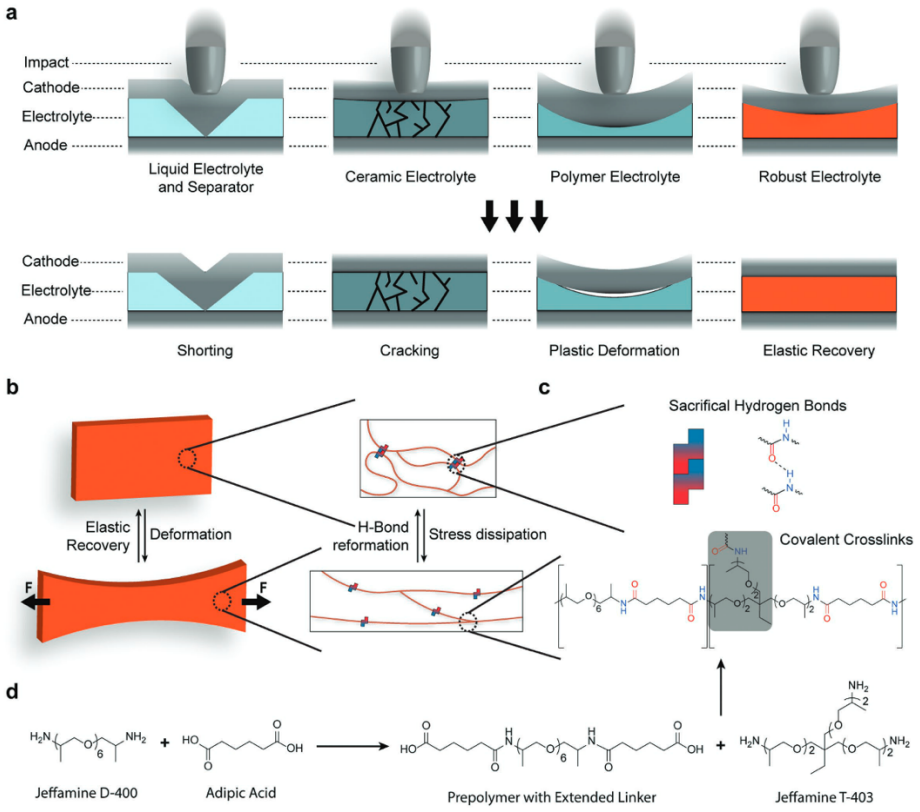

Figure 2 - 12. a) Schematic of impact response of various electrolytes. b) Deformation recovery aid by H-bond reformation. c) Chemical structure of covalent crosslinks and sacrificial H bonds on ePPO elastomer. d) Synthesis of dual crosslinked ePPO elastomer. Adapted from Ref. 56, with permission from Advanced Materials. Copyright 2018.

In summary, the enhanced mechanical stability by crosslinking reduces the risk of dendrite formation and short circuits. It also ensures that the SPE can withstand the mechanical stresses during battery assembly and operation. However, reducing polymer chain mobility can lead to a lower ionic conductivity. Thus, it is crucial to find a careful balance during the design of SPEs.

Impact on Electrochemical Properties

The electrochemical stability of SPEs can also be influenced by crosslinking. A stable electrolyte/electrode interface is essential to ensure fast ion transfer and prevent side reactions. Crosslinked SPEs often show better compatibility with electrodes, leading to more stable interfaces. Moreover, the improved mechanical properties of the crosslinked SPEs can help maintain this stable interface over prolonged charge/discharge cycles. By preventing the electrolyte degradation and harmful by-products formation at the interface, crosslinked SPEs facilitate longer cycle life and consistent performance of the battery.

Zhang et al. recently compared the electrochemical properties of linear and crosslinked PEO-based SPEs (Figure 2-13. a and b)[83]. The result demonstrated that crosslinked SPEs exhibit high oxidative stability of up to 4.9 V vs Li^+/Li compared to linear SPE which started oxidizing above 4V vs Li^+/Li. Additionally, the

crosslinked SPE showed high compatibility with Li metal electrode, maintaining an overpotential of 60 mV over 260 hours during Li plating/striping test. Tang et al. introduced a polyfluorinated crosslinker to improve the oxidative stability of SPEs (Figure 2-13. c and d)[84]. The resulting SPE showed wide ESW due to electron-withdrawing inductive effect. The Li||NMC cell, with a cut-off voltage of 4.5 V, achieves high discharge capacity and a 90% capacity retention after 200 cycles. Mu et al. introduced an in situ crosslinked SPE, which showed high ionic conductivity of 2.2×10^{-3} S cm^{-1} at 30 °C, an exceptionally high lithium transference number of 0.88, and a wide ESW of 5.2 V[85]. The solid-state LMBs using this SPE demonstrated outstanding long-cycle performance and capacity retention. Khan et al. designed a PEO-based SPE with excellent electrochemical performance for advanced LMBs[86]. This SPE achieved a maximum ionic conductivity of 1.9×10^{-4} S cm^{-1} at 40°C and maintained stability over 2000. The Li||LFP battery delivered 159.2 mA h g^{-1} capacity at 1 C and 95.2% capacity retention after 400 cycles. Xu et al. developed a double crosslinked PEO-based SPE with functionalized metal organic frameworks (MOFs), with increased ionic conductivity and improved mechanical, electrochemical, and thermal stability[87]. Nevertheless, Cabañero Martínez et al. pointed out the need for more detailed investigations into the long-term performance and degradation behavior of crosslinked SPEs to ensure their reliability and durability in real-world applications[88].

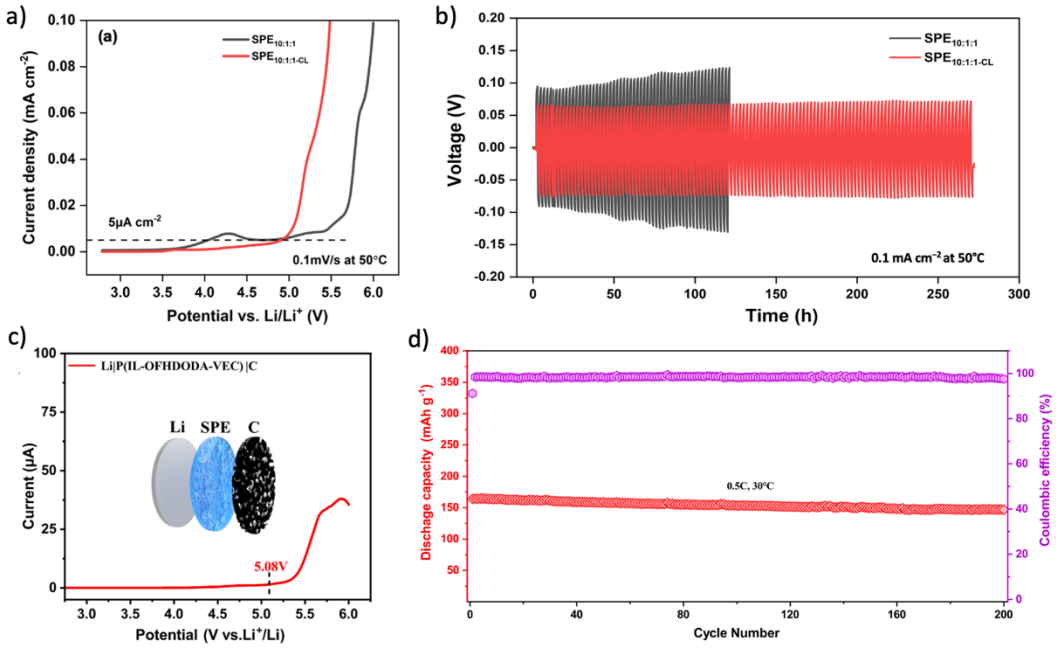

Figure 2 - 13. a) Electrochemical stability of linear and crosslinked SPEs. b) Voltage profiles of linear and crosslinked SPEs during Li plating-striping test. Adapted from Ref. 83, with permission from ACS Applied Materials and Interfaces. Copyright 2024. c) Linear sweep voltammetry curve of the designed SPE. d) Cycling performance of Li||NCM523 cycling performance at 0.5 C. Adapted from Ref. 84, with permission from Nature Communications. Copyright 2023.

2.2.3 Critical Viewpoints

While crosslinking is straightforward and beneficial, opinions on its effectiveness in enhancing SPE properties vary. Some researchers believe that crosslinking can significantly improve mechanical strength without reducing ionic conductivity[11,13]. However, others point out potential drawbacks, such as increased rigidity leading to reduced ionic mobility, which might lower the overall performance of the electrolyte[48,89].There is ongoing debate regarding its beneficial impact on the property and sustainability of the development of SPEs. Zhang et al. studied crosslinked on gel polymer electrolytes based on multiple epoxy groups[90]. They found that while crosslinking improved ionic conductivity and interfacial stability, it also introduces challenges in achieving consistent mechanical properties across different batches. Xu et al. discussed the effect of crosslinking on polyaniline cathode materials[87]. The study emphasized the need for a balance between crosslinking degree and flexibility. Tang et al. reported polyfluorinated crosslinker-based SPEs with improved oxidation resistance and electrochemical stability. However, they raised concerns about the increased complexity of synthesis and potential material costs[84].

To address these concerns, various strategies have been studied. Thiam et al. explored the use of flexible crosslinking agents to create soft polymer networks[76]. The designed SPE showed high ionic conductivity without sacrifice mechanical strength. Kang et al. developed a novel crosslinker from EO grafted polysiloxane with acrylate groups[82]. They found that the ionic conductivity of the crosslinked SPE increases with the main chain length. This enhancement was attributed to increased chain flexibility. Baroncini et al. investigated the ionic conductivity and Li ion transport in crosslinked thiol-based SPEs by analysing the structure-property relationships[91]. The study indicated that there is an ideal range for Tg, crosslinking density, and dielectric constant of the polymer to achieve high Li^+ transport in SPEs, and extreme values of these parameters may not be advantageous. Similarly, Stalin et al. developed crosslinked PEO-based SPEs via thiolene chemistry to examine lithium electrodeposition in crosslinked networks[32]. The study found that the polymer networks achieved maximum conductivity at a critical PEO molecular weight. Galvanostatic plating-stripping and impedance tests revealed stable cycling, attributed to good interfacial contact at elevated temperatures. However, cyclic voltammetry highlighted that the balance between Li^+ diffusion in SPE and the reaction kinetics at the interface is critical in designing crosslinked SPEs.

In conclusion, to fully realize the benefits of the crosslinking strategy, it is important to select suitable crosslinking methods and crosslinkers, manage crosslinking density and polymer molecular weight, and deepen the understanding of ion transport mechanisms within the crosslinked network and at the interface.

2.2.4 Charaterization Methods

Research methodologies in this field range from experimental synthesis and characterization of crosslinked SPEs to computational modelling of ionic transport. Experimental techniques such as Fourier Transform Infrared Spectroscopy (FTIR),

Raman spectroscopy, Nuclear Magnetic Resonance (NMR), and impedance spectroscopy are commonly used to study the relationships between structure and properties in these materials.

FTIR and NMR help investigate the chemical structure and transport properties of crosslinked SPEs. They provide insights into the degree of crosslinking and the interaction between polymer chains and ionic species. Studies by Nguyen et al. used FTIR and Raman techniques to examine the chemical structure, crosslinking mechanisms, and ion–ion and ion–polymer interactions in crosslinked SPE systems[92–94]. Similarly, Herbers et al. used FTIR analysis to verify the crosslinking process of the designed PEO-based ternary polymer electrolyte for LMBs[95]. FTIR analysis was further employed by the same group to study the impact of PEO degradation in the ternary SPE when used in high energy NMC||Li cells[96]. Wang et al. reported a composite SPE consisting of PEO, triethylmethylammonium bis(fluorosulfonyl)imide (N_{1222}FSI) and LiFSI. FTIR study was conducted to examine the potential ion-polymer interactions[97]. Very recently, Zhang et al. reported a novel design of crosslinked PEO-based SPE based on concentrated ionic liquid (CIL)[83]. Raman analysis was conducted to reveal the ion-polymer and ion-ion interactions. The research demonstrated a synergistic effect from combining crosslinking with CIL, which led to an increase in free Li^+ and a decrease in ion pairs. The crosslinked SPE showed high ionic conductivity of 4×10^{-4} S cm^{-1} at 30 °C. Additionally, Yang et al. reported a crosslinked polymer-in-salt SPE with multiple ion transport pathways for solid-state LMBs[98]. Both ^{13}C solid-state NMR and FTIR were used to study the structural characteristics of the designed SPEs. Han et al. reported a fluorine-containing crosslinked SPE which has a bi-continuous structure[99]. ^{7}Li solid-state NMR was used to investigate the interaction of Li^+ ion with polymers. The results indicate that ion pair dissociation and local ion hopping are more efficient in the phase-separated F-containing SPE compared to the homogeneous F-free SPE.

Computational modelling is another important tool for studying crosslinked SPEs. These models can simulate how ions behave within the polymer matrix, providing valuable insights into ion transport mechanisms and the effects of crosslinking. Research on crosslinked SPEs in lithium batteries using molecular dynamics (MD) simulations has shown various advancements. Ceder et al. reviewed the latest progress in computational modelling and simulation for rechargeable batteries, highlighting the benefits of using these techniques in researching and designing battery materials (Figure 2-14)[100]. Chua et al. conducted a MD study of crosslinked phthalonitrile (PN) systems to show the impact of crosslinking density on thermal, mechanical, and dielectric properties of the SPE[101]. The predicted linear thermal expansion coefficient aligns well with experimental results, indicating the good thermal stability of the SPE. Simulations also reveal that the SPE has excellent mechanical properties, with improved strength as crosslink density increases. Additionally, the calculated dielectric constant shows an inverse relationship between crosslink density and dielectric constant. Fischer et al. investigated structure and transport properties of PEO-based crosslinked polymers with LiTFSI and LiDFOB salts by MD simulation, demonstrating

improved ion dynamics due to favourable network structures[102]. Verners et al. applied MD to study Li ion diffusivity in crosslinked polymer electrolytes with added plasticizers or anions[103]. They found that ion diffusivity improved due to changes in solvation structures and plasticizing mechanisms. Additionally, Hosseinioun et al. used *ab initio* calculations to study the solvation and transport properties PMMA-based gel polymer electrolytes. They highlighted the positive effects of ester group interactions on lithium transport, showing higher cationic conductivity despite overall conductivity loss[104]. Wu et al. conducted molecular dynamics studies to explore the link between ion transport and segmental motion in crosslinked PEO SPEs[105]. The study showed that interactions between EO and Li^+ decrease PEO segmental mobility, confirming the connection between segmental mobility and ion transport. Zhu et al. investigated PEO-POSS based SPEs through MD simulations[106]. They revealed that POSS effectively prevents PEO crystallization, resulting in the formation of more amorphous phases. Furthermore, the simulations showed that POSS offers additional transport sites for Li^+ ions.

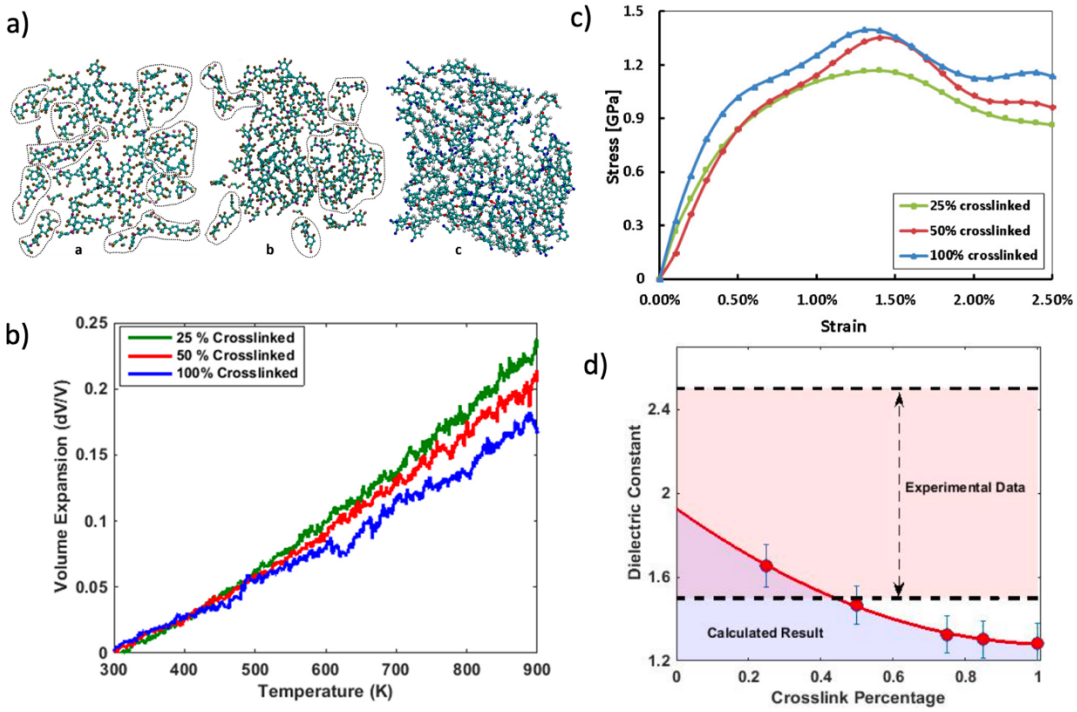

Figure 2 - 14. a) Simulations of crosslinked phthalonitrile system with different crosslinking densities (a. 25%, b. 50% and c. 100%). Clusters of uncrosslinked polymers are circled. b) Temperature-dependent volume expansion of different crosslinked structures. c) Stress vs. strain at different crosslink percentage under tensile test. d) Relationship of dielectric constant vs. crosslink percentage. Adapted from Ref. 100, with permission from MRS Bulletin. Copyright 2022.

Additionally, one common method for measuring crosslinking density is the swelling tests, which involve putting the crosslinked sample into a chosen solvent

at a specific temperature and measuring either the change in mass or volume[107]. The degree of swelling inversely correlates with the extent of crosslinking. Based on the degree of swelling, sample-solvent interaction, and the solvent density, the theoretical degree of crosslinking can be calculated using the Flory Interaction Parameter.

2.3 Applications in Advanced Lithium Batteries

Crosslinked SPEs have shown significant potential for use in advanced battery technologies, such as lithium-ion, lithium-metal, Li-S, and lithium-air batteries. Their enhanced performance and durability make them suitable for high-performance batteries.

Yerkinbekova et al. reported a UV-crosslinked separator based on lignin/ polyacrylonitrile (PAN) for safe LIBs. The obtained separator exhibited high porosity, allowing better electrolyte uptake and higher ionic conductivity[108]. Yin et al. developed a dual-bond crosslinked SPE aimed at overcoming the trade-offs between mechanical properties, ionic conductivity, and recyclability[109]. This SPE is elastically resilient, highly conductive, and chemically recyclable, making it suitable for high voltage room-temperature LMBs. Sheng et al. designed a PEO-PAN copolymer SPE[110]. The PAN fibers function as both a filler and crosslinker. This structure offers high mechanical strength and effectively blocks lithium dendrite formation. It also prevents the polysulfide shuttling effect, enhancing safety, cycling stability, and rate capability of Li-S batteries. A 96% capacity retention after 1000 cycles is achieved due to its high mechanical integrity. Zou et al. developed a water-resistant, nonvolatile, and flexible lithium-air battery using a hydrogen-bond crosslinking approach[111]. This innovation offers valuable insights into designing oxygen-permeable membranes with optimal properties for versatile metal-air battery applications. Similarly, Lei et al. reported a flexible lithium-air battery that operates efficiently in ambient air conditions[112]. The use of an in situ crosslinking significantly enhances the battery's functionality and practical applicability.

2.4 Future Research Directions

Looking ahead, the future of crosslinking technology is pointing towards sustainability and advanced functionalities. Future research should focus on exploring new crosslinking agents, advanced characterization techniques, industrial scalability, and sustainability. Additionally, computational modelling should be considered to gain deeper insights into the relationships between structure and properties in the crosslinked network. Computational modelling is a powerful tool in predicting the behavior of crosslinked SPEs and guiding the design of new materials. By combining experimental and computational methods, researchers can better understand the factors that influence the performance of crosslinked SPEs and find ways for improvements.

Hybrid Crosslinking Systems

One promising area in electrolyte research is the development of hybrid crosslinking systems that enhance multiple properties of SPEs simultaneously. MOFs[33], nanoparticles[113], nanowires[114], or other species[115] are often used in hybrid crosslinking systems. For example, adding inorganic nanoparticles to crosslinked polymer matrices has been explored to enhance the properties of SPEs. These polymer-inorganic hybrid electrolytes combine the benefits of mechanical reinforcement by crosslinking with ionic conductivity provided by the inorganic fillers. Tang et al. prepared hybrid polymer electrolyte based on crosslinked PPO–PEO–PPO triblock copolymers and surface-modified SiO_2 nanoparticles[116]. The obtained electrolyte exhibited high ionic conductivity of 1.32×10^{-3} S cm^{-1} at 20°C and excellent mechanical stability with 700% ultimate elongation. Ionic liquid is another promising multifunctional crosslinking agent for high performance SPEs in LMBs.

Advanced Characterization Techniques

Advanced characterization techniques, such as X-ray imaging, solid-state NMR, neutron scattering, operando characterizations and non-destructive techniques, have been promising to study the ion transport mechanisms within crosslinked SPEs[117,118]. Very recently, Mouravieff et al. reviewed the recent progress in non-destructive characterization methods (Figure 2-15)[119]. These techniques can help deepen our understanding of battery degradation, cut down on time and costs, and boost battery performance during manufacturing, usage, and end-of-life.

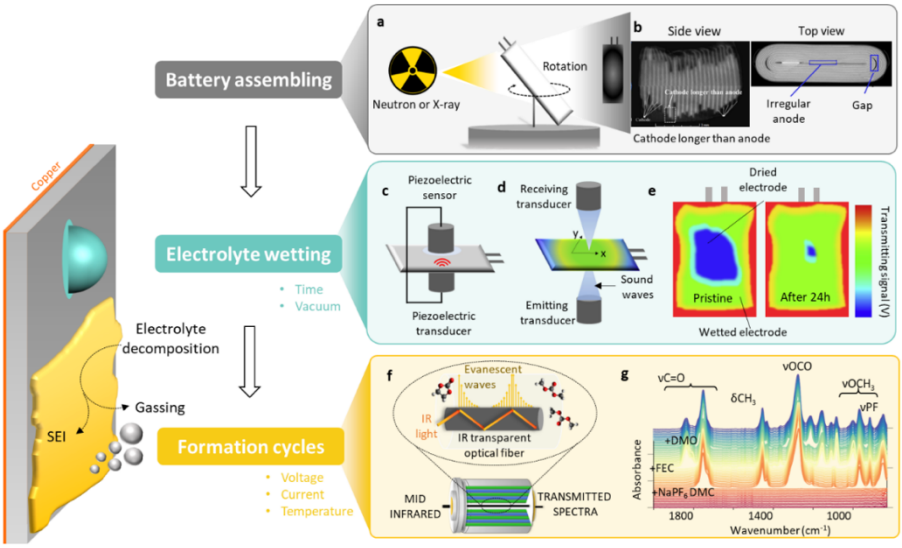

Figure 2 - 15. Non-destructive characterization techniques in different stages battery manufacturing. Adapted from Ref.119, with permission from Nature Reviews Electrical Engineering. Copyright 2024.

Scalability and Industrial Applications

The scalability of crosslinking techniques for SPEs production remains a significant concern. Although lab-scale research has shown promising results, more research and development are needed to translate these findings into industrial-scale applications. This includes exploring cost-effective and efficient methods for producing crosslinked SPEs on a large scale, as well as ensuring the consistency and reliability in real-world applications. Various strategies have been employed by different companies (Figure 2-16)[120]. For example, Blue Solution, the pioneering company that commercialized the lithium metal polymer technology using of a PEO-LiTFSI-based SPE, has conducted extensive research on SPEs derived from crosslinked copolymers[121,122]. Hydro-Québec works with Mercedes-Benz on solid-state batteries for EVs. They developed a SPE composed of an ethylene oxide copolymer and a substituted oxirane with a crosslinkable function. The obtained SPE has excellent mechanical properties, high cationic conductivity, and good chemical compatibility with Li/Na electrodes[123]. Recently, they also patented a hybrid electrolyte that includes LLZO inorganic particles and a crosslinked PEO-based aprotic polymer, which remains stable over 4 V[124]. LG Chemical Ltd. synthesized a variety of solid electrolytes, finding that the best balance between ionic conductivity and mechanical stability was achieved by crosslinking PEO with acrylate-based polymers to create semi-IPN[125]. Using a similar approach, they also crosslinked fluorinated polyether diacrylate with thiol-based polymer[126]. The fluorinated crosslinking agent was found to be more effective in reducing heat generation in lithium batteries compared to the non-fluorinated counterpart, demonstrating improved ionic conductivity, oxidation stability, and leakage prevention. Samsung SDI Co., Ltd., developed a catholyte that includes crosslinked polymer. This catholyte effectively delays dendrite formation and enhances the ionic conductivity of the LMB[127].

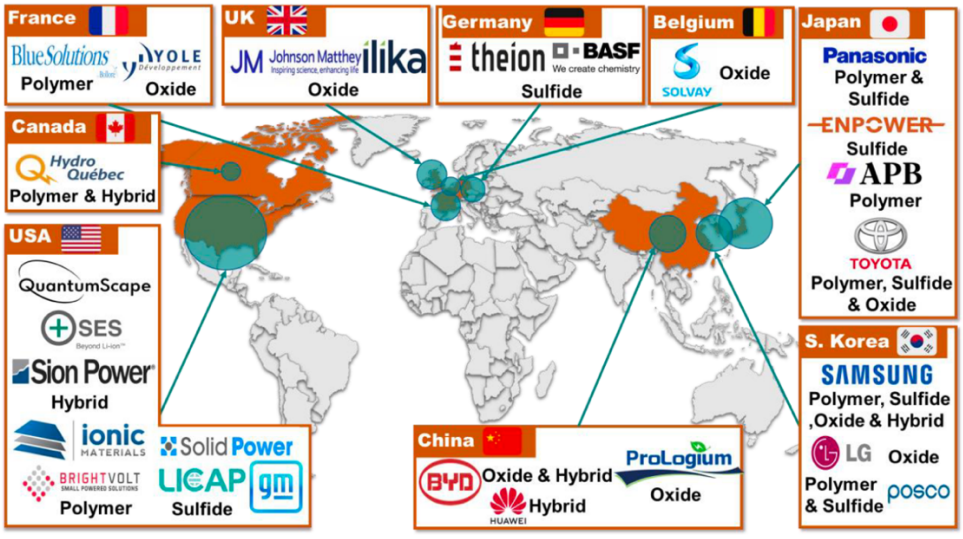

Figure 2 - 16. Location overview of companies developing solid-state technology. Adapted from Ref.120, with permission from Batteries. Copyright 2024.

Environmental Impact and Sustainability

As the demand for advanced batteries grows, it's important to develop materials and processes that are environmentally friendly and sustainable. This includes exploring biodegradable and recyclable crosslinking agents and creating production methods that reduce waste and energy use. For example, Chowdhury et al. developed a biodegradable SPE using a natural compound called sinapic acid as the crosslinker to improve the mechanical and electrochemical properties of the SPE[128]. Reddy et al. reported a low-cost and sustainable 3D crosslinked binder for Li-S batteries[129]. This binder improved mechanical properties and reduced the polysulfide effect during cycling.

Research on in situ crosslinking methods and solvent-free polymerization techniques, as discussed earlier, shows more efficient and environmentally friendly ways to develop sustainable crosslinking strategies.

2.5 Concluding Remarks

Crosslinking is a powerful tool that addresses many challenges associated with traditional electrolytes. Various crosslinking methods, including UV-induced, chemical, thermal, and in situ crosslinking, have shown great improvements in ionic conductivity, mechanical strength, thermal stability, and electrochemical properties of SPEs. These enhancements are crucial for developing safer and high-performance batteries. Despite the significant progress made in this field, several challenges and research gaps remain. Optimizing the crosslinking density, designing hybrid crosslinking systems, and developing scalable production methods are key areas that require further research. Additionally, ensuring environmental sustainability and integrating computational modeling with experimental studies are important considerations. Furthermore, the principles of crosslinking can be used in various fields, including biomedical devices, aerospace, and construction. This shows the broader impact of research on crosslinking and its potential to drive innovation across multiple industries. Continued in this field is essential for realizing the full potential of crosslinking with many opportunities for advancements and applications.

2.6 References

1. Armand, M. Polymer solid electrolytes - an overview. *Solid State Ion.* **9–10**, 745–754 (1983).
2. Song, Z. *et al.* A reflection on polymer electrolytes for solid-state lithium metal batteries. *Nat. Commun.* **14**, 4884 (2023).
3. Yue, L. *et al.* All solid-state polymer electrolytes for high-performance lithium ion batteries. *Energy Storage Mater.* **5**, 139–164 (2016).
4. Tarascon, J.-M. & Armand, M. Issues and challenges facing rechargeable lithium batteries. *Nature* **414**, 359–367 (2001).
5. Lopez, J., Mackanic, D. G., Cui, Y. & Bao, Z. Designing polymers foradvanced battery chemistries. *Nat. Rev. Mater.* **4**, 312–330 (2019).
6. Ye, T., Li, L. & Zhang, Y. Recent Progress in Solid Electrolytes for Energy Storage Devices. *Adv. Funct. Mater.* **30**, 2000077 (2020).
7. Wang, H. *et al.* Reviewing the current status and development of polymer electrolytes for solid-state lithium batteries. *Energy Storage Mater.* **33**, 188–215 (2020).
8. Fenton, D. E., Parker, J. M. & Wright, P. V. Complexes of alkali metal ions with poly(ethylene oxide). *Polymer* **14**, 589 (1973).
9. Watanabe, M., Nagano, S., Sanui, K. & Ogata, N. Ionic Conductivity of Network Polymers from Poly(ethylene oxide) Containing Lithium Perchlorate. *Polym. J.* **18**, 809–817 (1986).
10. Nair, J. R. *et al.* UV-cured methacrylic membranes as novel gel–polymer electrolyte for Li-ion batteries. *J. Power Sources* **178**, 751–757 (2008).
11. Kim, G. T. *et al.* UV cross-linked, lithium-conducting ternary polymer electrolytes containing ionic liquids. *J. Power Sources* **195**, 6130–6137 (2010).
12. Khurana, R., Schaefer, J. L. & Archer, L. A. Suppression of Lithium Dendrite Growth Using Cross-Linked Polyethylene/Poly(ethylene oxide) Electrolytes: A New Approach for Practical Lithium-Metal Polymer Batteries. *J Am Chem Soc* (2014).
13. Porcarelli, L., Gerbaldi, C., Bella, F. & Nair, J. R. Super Soft All-Ethylene Oxide Polymer Electrolyte for Safe All-Solid Lithium Batteries. *Sci. Rep.* **6**, 19892 (2016).
14. Li, S. *et al.* A Superionic Conductive, Electrochemically Stable Dual-Salt Polymer Electrolyte. *Joule* **2**, 1838–1856 (2018).
15. Choudhury, S. Solid-state polymer electrolytes for high-performance lithium metal batteries.
16. Falco, M. *et al.* Understanding the Effect of UV-Induced Cross-Linking on the Physicochemical Properties of Highly Performing PEO/LiTFSI-Based Polymer Electrolytes. *Langmuir*. 2019, 35, 25, 8210–8219 (2019)
17. Ahmed, F. *et al.* UV-Cured Cross-Linked Astounding Conductive Polymer Electrolyte for Safe and High-Performance Li-Ion Batteries. *ACS Appl. Mater. Interfaces* **13**, 34102–34113 (2021).

18. Xue, Z., He, D. & Xie, X. Poly(ethylene oxide)-based electrolytes for lithium-ion batteries. *J. Mater. Chem. A* **3**, 19218–19253 (2015).
19. Xin, C. *et al.* A Cross-Linked Poly(Ethylene Oxide)-Based Electrolyte for All-Solid-State Lithium Metal Batteries With Long Cycling Stability. *Front. Mater.* **9**, 864478 (2022).
20. Nair, J. R. *et al.* UV-Induced Radical Photo-Polymerization: A Smart Tool for Preparing Polymer Electrolyte Membranes for Energy Storage Devices. *Membranes* **2**, 687–704 (2012).
21. Homann, G., Stolz, L., Neuhaus, K., Winter, M. & Kasnatscheew, J. Effective Optimization of High Voltage Solid-State Lithium Batteries by Using Poly(ethylene oxide)-Based Polymer Electrolyte with Semi-Interpenetrating Network. *Adv. Funct. Mater.* **30**, 2006289 (2020).
22. Song, M.-K., Cho, J.-Y., Cho, B. W. & Rhee, H.-W. Characterization of UV-cured gel polymer electrolytes for rechargeable lithium batteries. *J. Power Sources* **110**, 209–215 (2002).
23. Lehmann, M. L. *et al.* Tailored crosslinking of Poly(ethylene oxide) enables mechanical robustness and improved sodium-ion conductivity. *Energy Storage Mater.* **21**, 85–96 (2019).
24. Chaudoy, V., Ghamouss, F., Luais, E. & Tran-Van, F. Cross-Linked Polymer Electrolytes for Li-Based Batteries: From Solid to Gel Electrolytes. *Ind. Eng. Chem. Res.* **55**, 9925–9933 (2016).
25. Decker, C. Photoinitiated crosslinking polymerisation. *Prog. Polym. Sci.* **21**, 593–650 (1996).
26. Luo, D., Li, Y. & Yang, M. Crosslinked poly(acrylonitrile–glycidyl methacrylate) as a novel gel polymer electrolyte. *Mater. Chem. Phys.* **125**, 231–235 (2011).
27. Doytcheva, M. *et al.* Ultraviolet-induced crosslinking of solid poly(ethylene oxide). *J. Appl. Polym. Sci.* **64**, 2299–2307 (1997).
28. Rupp, B., Schmuck, M., Balducci, A., Winter, M. & Kern, W. Polymer electrolyte for lithium batteries based on photochemically crosslinked poly(ethylene oxide) and ionic liquid. *Eur. Polym. J.* **44**, 2986–2990 (2008).
29. Armand, M., Endres, F., MacFarlane, D. R., Ohno, H. & Scrosati, B. Ionic-liquid materials for the electrochemical challenges of the future. *Nat. Mater.* **8**, 621–629 (2009).
30. Wetjen, M., Kim, G.-T., Joost, M., Winter, M. & Passerini, S. Temperature dependence of electrochemical properties of cross-linked poly(ethylene oxide)–lithium bis(trifluoromethanesulfonyl)imide–N-butyl-N-methylpyrrolidinium bis(trifluoromethanesulfonyl)imide solid polymer electrolytes for lithium batteries. *Electrochimica Acta* **87**, 779–787 (2013).
31. Ha, H.-J. *et al.* UV-curable semi-interpenetrating polymer network-integrated, highly bendable plastic crystal composite electrolytes for shape-conformable all-solid-state lithium ion batteries. *Energy Environ. Sci.* **5**, 6491 (2012).
32. Stalin, S. *et al.* Achieving Uniform Lithium Electrodeposition in Cross-Linked Poly(ethylene oxide) Networks: “Soft” Polymers Prevent Metal Dendrite Proliferation. *Macromolecules* **53**, 5445–5454 (2020).

33. Xu, R. *et al.* Double Crosslinked Polymer Electrolyte by C–S–C Group and Metal–Organic Framework for Solid-State Lithium Batteries. *Small Struct.* **4**, 2200206 (2023).
34. Mackanic, D. G. *et al.* Crosslinked Poly(tetrahydrofuran) as a Loosely Coordinating Polymer Electrolyte. *Adv Energy Mater* (2018).
35. He, Y., Liu, N. & Kohl, P. A. Difunctional block copolymer with ion solvating and crosslinking sites as solid polymer electrolyte for lithium batteries. *J. Power Sources* **481**, 228832 (2021).
36. Nishimoto, A., Agehara, K., Furuya, N., Watanabe, T. & Watanabe, M. High Ionic Conductivity of Polyether-Based Network Polymer Electrolytes with Hyperbranched Side Chains. *Macromolecules* **32**, 1541–1548 (1999).
37. Shim, J. *et al.* All-solid-state lithium metal battery with solid polymer electrolytes based on polysiloxane crosslinked by modified natural gallic acid. *Polymer* **122**, 222–231 (2017).
38. Shim, J. *et al.* Solid Polymer Electrolytes Based on Functionalized Tannic Acids from Natural Resources for All-Solid-State Lithium-Ion Batteries. *ChemSusChem* **8**, 4133–4138 (2015).
39. Liang, W., Shao, Y., Chen, Y.-M. & Zhu, Y. A 4 V Cathode Compatible, Superionic Conductive Solid Polymer Electrolyte for Solid Lithium Metal Batteries with Long Cycle Life. *ACS Appl. Energy Mater.* **1**, 6064–6071 (2018).
40. Stettner, T., Lingua, G., Falco, M., Balducci, A. & Gerbaldi, C. Protic Ionic Liquids-Based Crosslinked Polymer Electrolytes: A New Class of Solid Electrolytes for Energy Storage Devices. *Energy Technol.* **8**, 2000742 (2020).
41. Xue, X. *et al.* Crosslinked network solid polymer electrolyte with self-healing ability and high stability for lithium metal battery. *Polym. Int.* **71**, 1201–1209 (2022).
42. Lee, Y. M., Ko, D.-H., Lee, J. Y. & Park, J.-K. Highly ion-conductive solid polymer electrolytes based on polyethylene non-woven matrix. *Electrochimica Acta* **52**, 1582–1587 (2006).
43. Lee, J. Y., Ko, D.-H., Lee, Y. M., Seol, W.-H. & Park, J.-K. New crosslinking agent as a Lewis acid for solid polymer electrolytes. *J. Power Sources* **174**, 603–606 (2007).
44. Lin, Y.-C., Ito, K. & Yokoyama, H. Solid polymer electrolyte based on crosslinked polyrotaxane. *Polymer* **136**, 121–127 (2018).
45. Bao, W. *et al.* An H2O-Initiated Crosslinking Strategy for Ultrafine-Nanoclusters-Reinforced High-Toughness Polymer-In-Plasticizer Solid Electrolyte. *Adv. Mater.* **35**, 2304712 (2023).
46. Sakakibara, T. *et al.* Cross-linked polymer electrolyte and its application to lithium polymer battery. *Electrochimica Acta* **296**, 1018–1026 (2019).
47. Sylla, S., Sanchez, J.-Y. & Armand, M. Electrochemical study of linear and crosslinked POE-based polymer electrolytes. *Electrochimica Acta* **37**, 1699–1701 (1992).

48. Matoba, Y., Ikeda, Y. & Kohjiya, S. Ionic conductivity and mechanical properties of polymer networks prepared from high molecular weight branched poly(oxyethylene)s. *Solid State Ion.* **147**, 403–409 (2002).
49. Lee, K.-H., Kim, K.-H. & Lim, H. S. Studies on a New Series of Cross-Linked Polymer Electrolytes for a Lithium Secondary Battery. *J. Electrochem. Soc.* **148**, A1148 (2001).
50. Pan, Q., Smith, D. M., Qi, H., Wang, S. & Li, C. Y. Hybrid Electrolytes with Controlled Network Structures for Lithium Metal Batteries. *Adv. Mater.* **27**, 5995–6001 (2015).
51. Li, X. *et al.* Designing Comb-Chain Crosslinker-Based Solid Polymer Electrolytes for Additive-Free All-Solid-State Lithium Metal Batteries. *Nano Lett.* **20**, 6914–6921 (2020).
52. Zheng, Y., Li, X. & Li, C. Y. A novel de-coupling solid polymer electrolyte via semi-interpenetrating network for lithium metal battery. *Energy Storage Mater.* **29**, 42–51 (2020).
53. Lehmann, M. L. Well-designed Crosslinked Polymer Electrolyte Enables High Ionic Conductivity and Enhanced Salt Solvation. *J. Electrochem. Soc.* (2020).
54. Rymarczyk, J. *et al.* A novel ternary polymer electrolyte for LMP batteries based on thermal cross-linked poly(urethane acrylate) in presence of a lithium salt and an ionic liquid. *Eur. Polym. J.* **44**, 2153–2161 (2008).
55. Whiteley, J. M., Taynton, P., Zhang, W. & Lee, S. Ultra-thin Solid-State Li-Ion Electrolyte Membrane Facilitated by a Self-Healing Polymer Matrix. *Adv. Mater.* **27**, 6922–6927 (2015).
56. Lopez, J. *et al.* A Dual-Crosslinking Design for Resilient Lithium-Ion Conductors. *Adv. Mater.* **30**, 1804142 (2018).
57. Zhang, Y., Kim, J. & Miyatake, K. Effect of thermal crosslinking on the properties of sulfonated poly(phenylene sulfone)s as proton conductive membranes. *J. Appl. Polym. Sci.* **133**, app.44218 (2016).
58. Di Vona, M. L. *et al.* Stabilized Sulfonated Aromatic Polymers by in situ Solvothermal Cross-Linking. *Front. Energy Res.* **2**, (2014).
59. Niu, Y.-B. *et al.* In Situ Copolymerizated Gel Polymer Electrolyte with Cross-Linked Network for Sodium-Ion Batteries. *CCS Chem.* **2**, 589–597 (2020).
60. Lim, J. Y., Kang, D. A., Kim, N. U., Lee, J. M. & Kim, J. H. Bicontinuously crosslinked polymer electrolyte membranes with high ion conductivity and mechanical strength. *J. Membr. Sci.* **589**, 117250 (2019).
61. Liu, T. *et al.* Review—In Situ Polymerization for Integration and Interfacial Protection Towards Solid State Lithium Batteries. *J. Electrochem. Soc.* **167**, 070527 (2020).
62. Vijayakumar, V., Anothumakkool, B., Kurungot, S., Winter, M. & Nair, J. R. *In situ* polymerization process: an essential design tool for lithium polymer batteries. *Energy Environ. Sci.* **14**, 2708–2788 (2021).
63. Choi, W. *et al.* Stable Cycling of a 4 V Class Lithium Polymer Battery Enabled by In Situ Cross-Linked Ethylene Oxide/Propylene Oxide Copolymer

Electrolytes with Controlled Molecular Structures. *ACS Appl. Mater. Interfaces* **13**, 35664–35676 (2021).
64. Nair, J. R. Thermally cured semi-interpenetrating electrolyte networks (s-IPN) for safe and aging-resistant secondary lithium polymer batteries. *J. Power Sources* (2016).
65. Wang, Z., Shen, L., Deng, S., Cui, P. & Yao, X. 10 μm-Thick High-Strength Solid Polymer Electrolytes with Excellent Interface Compatibility for Flexible All-Solid-State Lithium-Metal Batteries. *Adv. Mater.* **33**, 2100353 (2021).
66. Wang, Z. *et al.* Porous poly(vinylidene fluoride) supported three-dimensional poly(ethylene glycol) thin solid polymer electrolyte for flexible high temperature all-solid-state lithium metal batteries. *Chem. Eng. J.* **435**, 135106 (2022).
67. Duan, H. *et al.* In situ plasticized polymer electrolyte with double-network for flexible solid-state lithium-metal batteries. *Energy Storage Mater.* **10**, 85–91 (2018).
68. Qiu, Z. *et al.* High Conductive Composite Polymer Electrolyte via in Situ UV-Curing for All-Solid-State Lithium Ion Batteries. *ACS Sustain. Chem. Eng.* **7**, 9875–9880 (2019).
69. Röchow, E. T. *et al.* In Situ Preparation of Crosslinked Polymer Electrolytes for Lithium Ion Batteries: A Comparison of Monomer Systems. *Polymers* **12**, 1707 (2020).
70. Zhang, Y. *et al.* Cross-linking network based on Poly(ethylene oxide): Solid polymer electrolyte for room temperature lithium battery. *J. Power Sources* **420**, 63–72 (2019).
71. Chen, X. *et al.* An Ultra-Thin Crosslinked Carbonate Ester Electrolyte for 24 V Bipolar Lithium-Metal Batteries. *J. Electrochem. Soc.* **169**, 090509 (2022).
72. Wen, S. *et al.* Integrated design of ultrathin crosslinked network polymer electrolytes for flexible and stable all-solid-state lithium batteries. *Energy Storage Mater.* **47**, 453–461 (2022).
73. Cui, Y. *et al.* High Performance Solid Polymer Electrolytes for Rechargeable Batteries: A Self-Catalyzed Strategy toward Facile Synthesis. *Adv Sci* (2017).
74. Nest, J. L., Gandini, A. & Cheradame, H. Crosslinked polyethers as media for ionic conduction. *Br. Polym. J.* **20**, 253–268 (1988).
75. Zhang, Z. *et al.* Ion conductive characteristics of cross-linked network polysiloxane-based solid polymer electrolytes. *Solid State Ion.* **170**, 233–238 (2004).
76. Thiam, A., Antonelli, C., Iojoiu, C., Alloin, F. & Sanchez, J.-Y. Optimizing ionic conduction of poly(oxyethylene) electrolytes through controlling the cross-link density. *Electrochimica Acta* **240**, 307–315 (2017).
77. Cui, Y. *et al.* A Fireproof, Lightweight, Polymer–Polymer Solid-State Electrolyte for Safe Lithium Batteries. *Nano Lett. 2020, 20, 3, 1686–1692*.
78. Chen, K., Sun, Y., Zhang, X., Liu, J. & Xie, H. A Self-Healing and Nonflammable Cross-Linked Network Polymer Electrolyte with the Combination of Hydrogen Bonds and Dynamic Disulfide Bonds for Lithium Metal Batteries. *ENERGY Environ. Mater.* **6**, e12568 (2023).

79. Oh, B. *et al.* New interpenetrating network type poly(siloxane-g-ethylene oxide) polymer electrolyte for lithium battery. *J. Power Sources* **119–121**, 442–447 (2003).
80. Sung, S.-J., Kim, D.-H., Kim, M. R. & Cho, K. Y. Effect of molecular weight of biscinnamated poly(ethylene glycol) oligomers on the photocycloaddition reaction. *Macromol. Res.* **18**, 614–617 (2010).
81. Zheng, Q., Ma, L., Khurana, R., Archer, L. A. & Coates, G. W. Structure–property study of cross-linked hydrocarbon/poly(ethylene oxide) electrolytes with superior conductivity and dendrite resistance. *Chem. Sci.* **7**, 6832–6838 (2016).
82. Kang, Y., Lee, W., Hack Suh, D. & Lee, C. Solid polymer electrolytes based on cross-linked polysiloxane-g-oligo(ethylene oxide): ionic conductivity and electrochemical properties. *J. Power Sources* **119–121**, 448–453 (2003).
83. Zhang, M. *et al.* Synergistic Combination of Crosslinked Polymer and Concentrated Ionic Liquid for Electrolytes with High Stability in Solid-State Lithium Metal Batteries. ACS Appl. Polym. Mater. 6, 14469–14476 (2024).
84. Tang, L. *et al.* Polyfluorinated crosslinker-based solid polymer electrolytes for long-cycling 4.5 V lithium metal batteries. *Nat. Commun.* **14**, 2301 (2023).
85. Mu, K. *et al.* Hybrid Crosslinked Solid Polymer Electrolyte via In situ Solidification Enables High-Performance Solid-State Lithium Metal Batteries. *Adv. Mater.* **35**, 2304686 (2023).
86. Khan, K. *et al.* PEO-Based Solid Composite Polymer Electrolyte for High Capacity Retention All-Solid-State Lithium Metal Battery. *Small* **20**, 2305772 (2024).
87. Xu, L., Xin, H. & Su, C. Effect of cross-linking on electrochemical performances of polyaniline as the cathode material of lithium-ion batteries. *Polym. Bull.* **79**, 5261–5278 (2022).
88. Cabañero Martínez, M. A. *et al.* Are Polymer-Based Electrolytes Ready for High-Voltage Lithium Battery Applications? An Overview of Degradation Mechanisms and Battery Performance. *Adv. Energy Mater.* **12**, 2201264 (2022).
89. Chelmecki, M., Meyer, W. H. & Wegner, G. Effect of crosslinking on polymer electrolytes based on cellulose. *J. Appl. Polym. Sci.* **105**, 25–29 (2007).
90. Zhang, W. *et al.* Cross-Linked Gel Polymer Electrolyte Based on Multiple Epoxy Groups Enabling Conductivity and High Performance of Li-Ion Batteries. *Gels* **9**, 384 (2023).
91. Baroncini, E. A., Rousseau, D. M., Strekis, C. A. & Stanzione, J. F. Optimizing conductivity and cationic transport in crosslinked solid polymer electrolytes. *Solid State Ion.* **345**, 115161 (2020).
92. Nguyen, H. T. T. *et al.* A scaffold membrane of solid polymer electrolytes for realizing high-stability and dendrite-free lithium-metal batteries. *J. Mater. Chem. A* **9**, 25408–25417 (2021).
93. Nguyen, H. T. T. *et al.* Facile Li^+ Transport in Interpenetrating O- and F-Containing Polymer Networks for Solid-State Lithium Batteries. *Adv. Funct. Mater.* **33**, 2213469 (2023).

94. Nguyen, M. L., Nguyen, V.-C., Lee, Y.-L., Jan, J.-S. & Teng, H. Synergistic combination of ether-linkage and polymer-in-salt for electrolytes with facile Li+ conducting and high stability in solid-state lithium batteries. *Energy Storage Mater.* **65**, 103178 (2024).
95. Herbers, L., Küpers, V., Winter, M. & Bieker, P. An ionic liquid- and PEO-based ternary polymer electrolyte for lithium metal batteries: an advanced processing solvent-free approach for solid electrolyte processing. *RSC Adv.* **13**, 17947–17958 (2023).
96. Herbers, L. *et al.* The Influence of Polyethylene Oxide Degradation in Polymer-Based Electrolytes for NMC and Lithium Metal Batteries. *Adv. Energy Sustain. Res.* **4**, 2300153 (2023).
97. Wang, W. *et al.* Solid polymer electrolytes based on the composite of PEO–LiFSI and organic ionic plastic crystal. *Chem. Phys. Lett.* **747**, 137335 (2020).
98. Yang, J. *et al.* Crosslinked polymer-in-salt solid electrolyte with multiple ion transport paths for solid-state lithium metal batteries. *Energy Storage Mater.* **64**, 103088 (2024).
99. Han, J. *et al.* Fluorine-Containing Phase-Separated Polymer Electrolytes Enabling High-Energy Solid-State Lithium Metal Batteries. *Adv. Funct. Mater.* **34**, 2310801 (2024).
100. Ceder, G., Doyle, M., Arora, P. & Fuentes, Y. Computational Modeling and Simulation for Rechargeable Batteries. *MRS Bull.* **27**, 619–623 (2002).
101. Chua, J. & Tu, Q. A Molecular Dynamics Study of Crosslinked Phthalonitrile Polymers: The Effect of Crosslink Density on Thermomechanical and Dielectric Properties. *Polymers* **10**, 64 (2018).
102. Fischer, M., Heuer, A. & Diddens, D. Structure and Transport Properties of Poly(ethylene oxide)-Based Cross-Linked Polymer Electrolytes─A Molecular Dynamics Simulations Study. *Macromolecules* **55**, 10229–10242 (2022).
103. Verners, O. Molecular dynamics modeling of structural battery components. (2015).
104. Hosseinioun, A., Nürnberg, P., Schönhoff, M., Diddens, D. & Paillard, E. Improved lithium ion dynamics in crosslinked PMMA gel polymer electrolyte. *RSC Adv.* **9**, 27574–27582 (2019).
105. Wu, T. & Zhang, P. Structure and dynamics of dynamic covalent cross-linked PEOs and PEO/LiPF6 electrolytes: a coarse-grained simulation study. *Phys. Chem. Chem. Phys.* **25**, 14530–14537 (2023).
106. Zhu, Y., Cao, S. & Huo, F. Molecular dynamics simulation study of the solid polymer electrolyte that PEO grafted POSS. *Chem. Phys. Lett.* **756**, 137834 (2020).
107. Flory, P. J. & Rehner, J. Statistical Mechanics of Cross-Linked Polymer Networks I. Rubberlike Elasticity. *J. Chem. Phys.* **11**, 512–520 (1943).
108. Yerkinbekova, Y. *et al.* Photo-crosslinked lignin/PAN electrospun separator for safe lithium-ion batteries. *Sci. Rep.* **12**, 18272 (2022).

109. Yin, L. *et al.* A Dual-Bond Crosslinking Strategy Enabling Resilient and Recyclable Electrolyte Elastomers for Solid-State Lithium Metal Batteries. *Angew. Chem.* **n/a**, e202404769.
110. Sheng, J. *et al.* Crosslinked Nanofiber-Reinforced Solid-State Electrolytes with Polysulfide Fixation Effect Towards High Safety Flexible Lithium–Sulfur Batteries. *Adv. Funct. Mater.* **32**, 2203272 (2022).
111. Zou, X. *et al.* Water-proof, electrolyte-nonvolatile, and flexible Li-Air batteries via O2-Permeable silica-aerogel-reinforced polydimethylsiloxane external membranes. *Energy Storage Mater.* **27**, 297–306 (2020).
112. Lei, X. *et al.* Flexible Lithium–Air Battery in Ambient Air with an In Situ Formed Gel Electrolyte. *Angew. Chem. Int. Ed.* **57**, 16131–16135 (2018).
113. Chai, J. *et al.* Dendrite-Free Lithium Deposition via Flexible-Rigid Coupling Composite Network for $LiNi_{0.5}Mn_{1.5}O_4$/Li Metal Batteries. *Small* **14**, 1802244 (2018).
114. Lei, D. *et al.* Cross-linked beta alumina nanowires with compact gel polymer electrolyte coating for ultra-stable sodium metal battery. *Nat. Commun.* **10**, 4244 (2019).
115. Cao, X. *et al.* High-performance fully-stretchable solid-state lithium-ion battery with a nanowire-network configuration and crosslinked hydrogel. *J. Mater. Chem. A* **10**, 11562–11573 (2022).
116. Tang, S. *et al.* A novel cross-linked nanocomposite solid-state electrolyte with super flexibility and performance for lithium metal battery. *Nano Energy* **71**, 104600 (2020).
117. Xiang, Y., Li, X., Cheng, Y., Sun, X. & Yang, Y. Advanced characterization techniques for solid state lithium battery research. *Mater. Today* **36**, 139–157 (2020).
118. Strauss, F. *et al.* Operando Characterization Techniques for All-Solid-State Lithium-Ion Batteries. *Adv. Energy Sustain. Res.* **2**, 2100004 (2021).
119. Gervillié-Mouravieff, C., Bao, W., Steingart, D. A. & Meng, Y. S. Non-destructive characterization techniques for battery performance and life-cycle assessment. *Nat. Rev. Electr. Eng.* **1**, 547–558 (2024).
120. Karkar, Z., Houache, M. S. E., Yim, C.-H. & Abu-Lebdeh, Y. An Industrial Perspective and Intellectual Property Landscape on Solid-State Battery Technology with a Focus on Solid-State Electrolyte Chemistries. *Batteries* **10**, 24 (2024).
121. Bouchet, R. & Deschamps, M. Batterie lithium metal polymere a haute densite d'energie. (2017).
122. Pavlenko, E. *et al.* Électrolyte polymère pour batterie lithium métal polymère à performances ameliorées. (2020).
123. Harvey, P.-E., Sanchez, J.-Y. & Alloin, F. Copolymer of ethylene oxide and at least one substituted oxirane carrying a cross-linkable function, process for preparation thereof and use thereof for producing materials with ionic conduction. (2005).
124. KIM, C. *et al.* Cellules électrochimiques à l'état solide, procédés pour leur préparation et leurs utilisations. (2021).

125. Kim, D., CHAE, J., Kim, S., LIM, S. C. & AHN, J. Solid electrolyte, method for preparing same, and all-solid-state battery including same. (2021).
126. Ahn, K.; Kim, D.; Lee, W.; Jeong, B.; Lim, D.; Lee, C.; Jeong, Y. Gel Polymer Electrolyte and Lithium Secondary Battery Comprising Same. WO2023008970A1. (2023).
127. Lee, E.G.; Cho, B.G.; Han, S.I. Catholyte for Lithium Metal Battery Composite Cathode for Lithium Metal Battery Including the Same Preparing Method Thereof and Lithium Metal Battery Comprising the Same. KR20210112925A. (2021).
128. Chowdhury, P. *et al.* Biodegradable Solid Polymer Electrolytes from the Discarded Cataractous Eye Protein Isolate. *ACS Appl. Bio Mater.* **7**, 2240–2253 (2024).
129. Reddy, B. R. S., Ahn, J.-H., Ahn, H.-J., Cho, G.-B. & Cho, K.-K. Low-Cost and Sustainable Cross-Linked Polyvinyl Alcohol–Tartaric Acid Composite Binder for High-Performance Lithium–Sulfur Batteries. *ACS Appl. Energy Mater.* **6**, 6327–6337 (2023).

Chapter 3

Characterization Techniques

This chapter provides an overview of the key characterization techniques used to analyze the structural, thermal, and electrochemical properties of solid polymer electrolytes (SPEs) developed in this PhD work. Each method is discussed in terms of its principles, relevance to SPE research, and the insights it offers into the material properties, followed by the general measurement setup used in this research work. For specific experimental details and conditions tailored to the studies in Chapters 4 and 5, please refer to those chapters individually.

3.1 Differential Scanning Calorimetry

Differential Scanning Calorimetry (DSC) is a widely used technique to analyze thermal transitions such as melting, crystallization, and glass transition temperatures, as well as thermodynamic properties like enthalpy and heat capacity. Additionally, DSC is effective for analysing purity, reaction kinetics, and thermal history of materials. The thermal profile obtained from DSC can also serve as a unique fingerprint for compound identification.

In a DSC measurement, the sample is heated or cooled in parallel with an inert reference material. This allows the instrument to detect and compensate for heat changes that occur in the sample during thermal transitions or reactions, ensuring the same temperature between the sample and reference (empty crucible).[1] The difference in heat flow is given by:

$$\Delta(dH/dt) = (dH/dt) - (dH/dt)_{ref}$$

In endothermic transitions or reactions, where heat is absorbed, $\Delta(dH/dt) > 0$. Conversely, during exothermic processes like crystallization, the sample releases heat, leading to $\Delta(dH/dt) < 0$. DSC allows for the quantification of heat absorbed or released during material changes by measuring the heat flow difference between the sample and the reference. The data is typically presented as a plot of heat flow versus temperature.

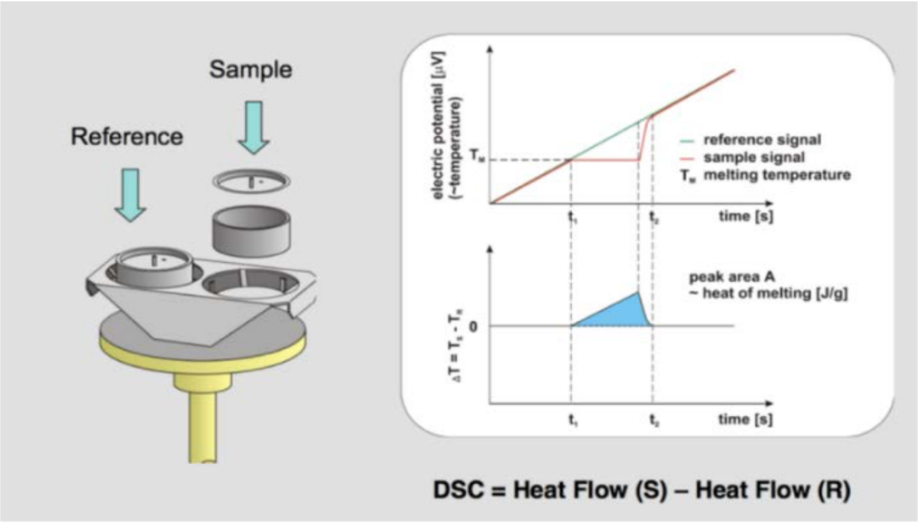

Figure 3 - 1. A DSC holder and heat flow measurement during operation.[1]

This technique is valuable for characterizing SPEs, as it helps determine the degree of crystallinity within the polymer matrix—a key factor in ionic conductivity. By heating or cooling a sample alongside an inert reference material, DSC measures heat flow differences that indicate endothermic or exothermic transitions in the sample.

DSC measurements:

In this work, a Netzsch DSC 214 Polyma instrument with Proteus 70 software was used to analyze the phase behavior of PEO and the designed SPEs. Cyclohexane was used for temperature calibration. T_g and melting transitions were determined by the midpoints. For specific experimental setups, please refer to Chapter 4 and 5.

3.2 Scanning Electron Microscopy

Scanning Electron Microscopy (SEM) provides detailed images of the surface morphology and topography by directing a focused electron beam at the sample. When electrons interact with the atoms in a sample, they produce signals that provide detailed information of the surface structure and the material composition.[2]

SEM helps to analyze the surface structure, including homogeneity, phase separation, and microstructure, which are critical for assessing the stability and integrity of SPEs. This technique was particularly useful for examining pristine SPEs and post-cycling morphology of lithium metal anodes.

SEM measurement:

In this work, to investigate the morphology of the designed SPEs and the Li metal surface after cycling, we used a JEOL JSM-IT300 microscope. For Li samples, a sealed argon-filled canister was used for sample transfer as shown in

Figure 3-2. The SEM with a load-lock chamber (LLC) used in this PhD thesis is shown in Figure 3-3. Images were acquired using an accelerating voltage of 10 KV.

Figure 3 - 2. A sealed canister used to transfer samples for SEM.

Figure 3 - 3. The JEOL JSM-IT300 SEM used in this PhD thesis.

3.3 Electrochemical Impedance Spectroscopy

Electrochemical Impedance Spectroscopy (EIS) is widely used for evaluating the ionic conductivity and electrochemical behavior of SPEs. By applying an alternating voltage across a sample and measuring the resulting current, EIS assesses impedance over a wide frequency range, providing insights into electron transfer rates and ion mobility. EIS data are typically represented in Nyquist plots to reveal resistive and capacitive characteristics.

EIS is determined by applying an alternating voltage to a system and measuring the resulting alternating current (AC). Due to the nonlinear nature of the current

response, a small AC voltage is used across a wide frequency spectrum (typically from 10 MHz to 1 mHz) to approximate a linear behavior. In the near-linear systems, the current maintains a sinusoidal shape with the same frequency as the applied voltage, but with a phase-shifted, as illustrated in Figure 3-4. This phase shift allows for a detailed analysis of the system's electrochemical properties across different frequencies.

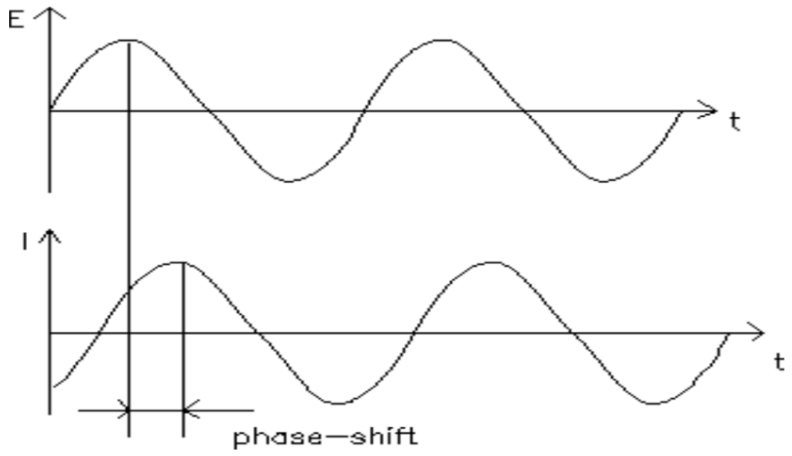

Figure 3 - 4. Current response vs. time.[3]

At each frequency, based on the excitation signal and current response, the impedance (Z) can be calculated by Ohm's Law:

$Z = E_t / I_t$

where potential (E_t) and current response (I_t) are given by:
$E_t = E_0 \exp(j\omega t)$
$I_t = I_0 \exp(j\omega t) - \varphi$

where ω is the angular frequency and φ is the phase shift.

The impedance is then divided into real and imaginary parts:

$$Z = \frac{E_0 \sin(\omega t)}{I_0 \sin(\omega t + \varphi)} = Z_0 \frac{\sin(\omega t)}{\sin(wt + \varphi)} = Z_0(cos\varphi + jsin\varphi)$$

EIS data is typically illustrated in a Nyquist plot, where the imaginary part (indicative of capacitance) is plotted against the real part (indicative of resistance).[4] As shown in Figure 3-7, the semicircle represents a paralleled resistor and capacitor, reflecting both resistive and capacitive characteristics of the material. The intercept of the plot at ω = 0 represents the bulk resistance of the sample, which is used to determine its conductivity. However, in some cases, where multiple conduction processes occur (indicated by multiple semicircles in the Nyquist plot), the measurement of conductivity becomes more complex. In such cases, the Nyquist

plot needs to be analysed using an appropriate equivalent circuit model. A commonly used model for this analysis is shown in the inset of Figure 3-5.

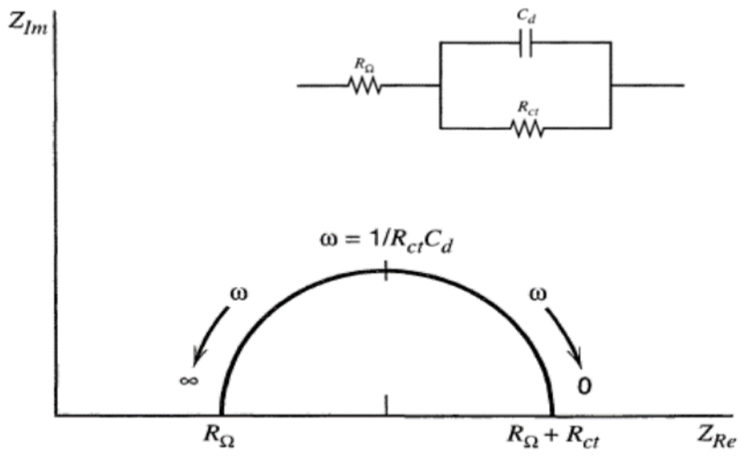

Figure 3 - 5. A Nyquist plot with equivalent circuit.[4]

Figure 3 - 6. Barrel cell used for conductivity measurements.

EIS measurement:

For measuring the conductivity of the designed SPEs in this thesis, a barrel cell configuration is used. (Figure 3-6). The sample was sandwiched in a SS||SS coin cell (CR2032 type) before putting into the barrel cell for conductivity measurement. A Biologic MTZ-35 Analyser with MT-Lab software was used for all EIS measurements. A frequency range of 10 MHz to 0.1 Hz was used under DC potential. A 10 mV voltage amplitude was applied. Temperature was automatically controlled by a Eurotherm 2204 temperature controller. Details are reported in Chapters 4 and 5.

3.4 Linear Sweep Voltammetry

Linear Sweep Voltammetry (LSV) assesses the electrochemical stability of SPEs by gradually increasing the applied voltage and monitoring the resulting current. This technique is critical for defining the electrochemical stability window, indicating the maximum voltage the SPE can sustain without decomposition.[5] In this study, LSV was performed to determine the oxidative stability of SPEs in Li||SS cells, detailed further in Chapters 4 and 5.

LSV measurements:

In this thesis, a Biologic VMP3/Z potentiostat with EC-lab software was used to perform the LSV to investigate the oxidation stability of the designed SPE. A Li||SS cell configuration was used. The voltage applied was increased linearly from open-circuit voltage to 6 V vs. Li^+/Li at a sweeping rate of 0.1 mV s^{-1}.

3.5 Fourier Transform Infrared Spectroscopy

Fourier Transform Infrared (FTIR) Spectroscopy characterizes molecular interactions by measuring the absorption of infrared light, which corresponds to specific vibrational modes of molecular bonds. The basic principle of FTIR involves passing IR light through a sample and detecting the wavelengths that are absorbed by the sample (Figure 3-7). Molecules absorb IR at specific frequencies, which correspond to the vibrational modes of the molecular bonds. These vibrational frequencies are highly specific to the types of bonds and chemical environments present in the sample, making FTIR a sensitive technique for identifying chemical species and their interactions.[6]

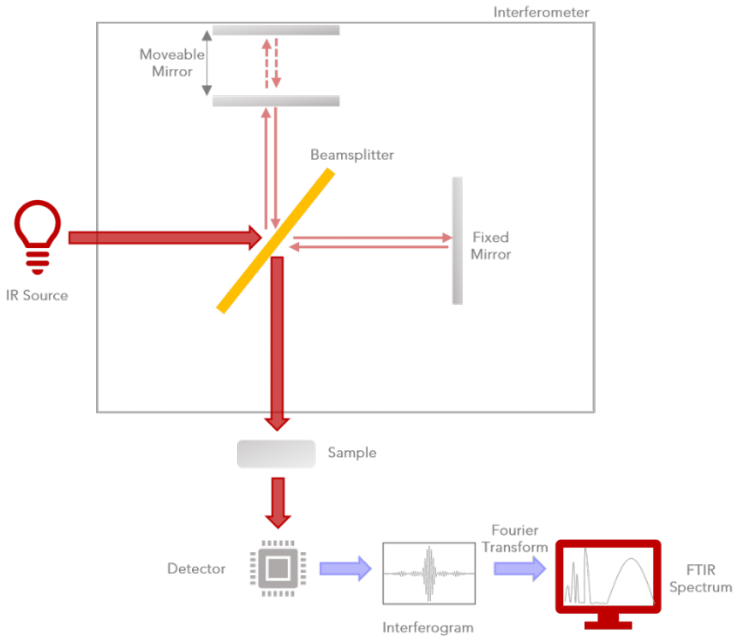

Figure 3 - 7. Basics of FTIR spectroscopy.[6]

In SPE research, FTIR is commonly used to

- Verify the crosslinking progress and the degree of crosslinking
- Analyse how lithium salts interact with the polymer backbone.
- Detect changes in polymer structure due to the addition of ionic liquids (ILs) or salts.
- Study the coordination of ions with polymer chains or other components.
- Monitor the formation of complexes, ion clusters, or dissociated ions, which impact ion transport and conductivity.

By examining vibrational modes, FTIR helps to clarify how the polymer and ions interact and what molecular rearrangements occur under various conditions.

FTIR measurements:

In this PhD thesis, FTIR was applied to assess ion-polymer and ion-ion interactions in the SPEs, revealing how lithium salts and ionic liquids influence polymer structures. This technique also helped verify crosslinking and detect changes in polymer structure due to ionic liquid integration. FTIR spectra were obtained using a Perkin Elmer Spectrum from 650 to 4000 cm^{-1} at room temperature. 32 scans were accumulated per sample.

3.6 Raman Spectroscopy

Raman Spectroscopy is a complementary technique to FTIR, useful for studying molecular interactions and ion transport mechanisms in SPEs. By analyzing the vibrational modes of the molecules, Raman spectroscopy provides insights into lithium-ion coordination and the structural dynamics of the polymer matrix. This technique was particularly effective for probing ion coordination and anion interactions in the studied SPE systems.

When light interacts with a molecule, some of the light may be absorbed by molecular vibration. This absorption changes the frequency of the scattered light (Figure 3-8). By detecting the difference in frequency between the original light and the scattered light (Raman shift), we can identify the specific vibrational modes of the molecules.[7]

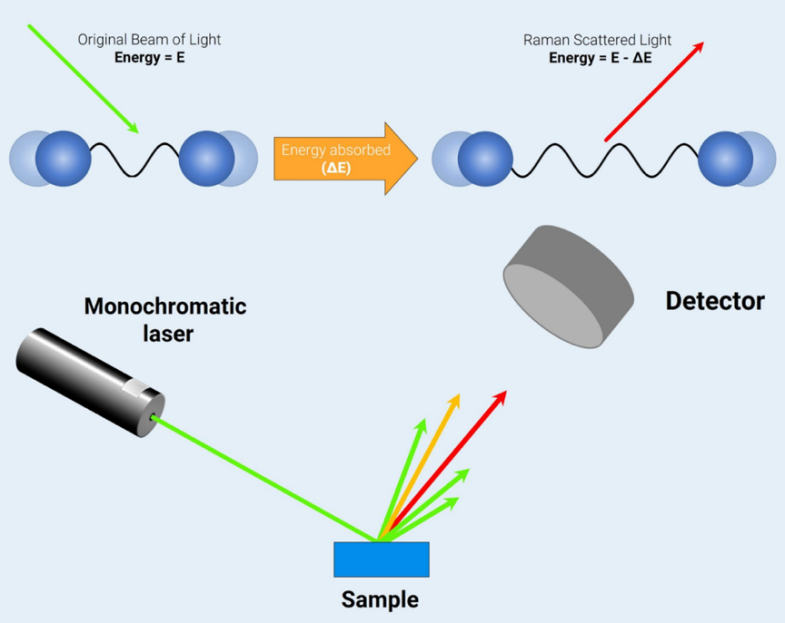

Figure 3 - 8. Basics of Raman spectroscopy.[7]

Raman measurements:

In this PhD thesis, Raman spectra were obtained by a Renishaw Invia microscope at room temperature. The laser power generates 633 nm light and delivers 13.0 mW at the sample. The measurement were done in the frequency range of 100 to 3200 cm^{-1}. After obtaining the Raman spectra, baseline correction and normalization were applied and Voigt function was used for peak deconvolution for further analysis.

3.7 Thermal Gravimetric Analysis

Thermogravimetric Analysis **(**TGA**)** is a powerful method to monitor the mass loss of a sample under a controlled temperature program (Figure 3-9).[8] It is widely used in the thermal analysis of SPEs. It provides key insights into the thermal stability, decomposition mechanisms, and compositional analysis of SPEs, making it a powerful tool to evaluate the thermal resilience of the SPEs under varying conditions, which is essential for assessing the long-term stability of materials intended for high-temperature battery applications.

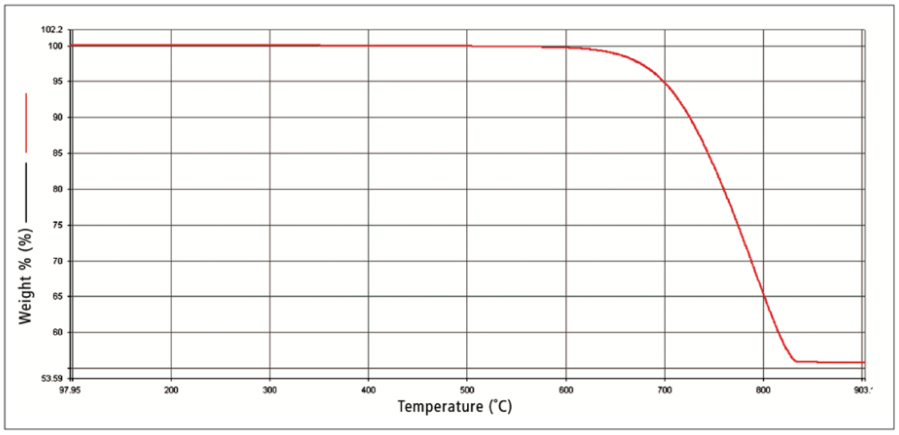

Figure 3 - 9. A typical TGA thermogram.[8]

TGA measurements:

In this thesis, a Mettler Toledo TGA STAR instrument was used to conduct the TGA experiment. Over the temperature 30-600 °C, the mass loss was monitored at a heating rate of 10 °C min^{-1} under constant N_2 flow.

3.8 The Bruce & Vincent Method for Li^+ Transference Number

Ionic conductivity is a key property to reveal ion transport in batteries. However, it is also important to understand which ions are primarily responsible for carrying the current. In the present work, it is important to assess how much current is contributed by Li^+ rather than other ionic species in the SPE. Since the overall ionic conductivity considers the movement of all present ions, it is possible that only a small fraction of the current is from Li^+. Therefore, a high ionic conductivity does not necessarily imply efficient Li-ion transport. If the Li^+ transference (t_{Li+}) is low, there will be insufficient Li^+ supply at the cathode or an excessive accumulation of Li^+ at the anode during discharge, resulting in quick polarization and battery deterioration.

Several methods have been developed to measure t_{Li+}. Among these, the Bruce-Vincent method, which is based on potentiostatic polarization and EIS measurements, is widely used due to its simplicity[9–11]. When a small voltage is applied to a Li symmetric cell, Li oxidation occurs at the positive electrode, and Li deposition happens at the negative electrode. This process drives ion movement through the electrolyte. However, since anions do not undergo oxidation or reduction at the electrodes, some Li ions must migrate along with the anions to keep the charge balanced and avoid anion buildup at the positive electrode. This creates a concentration gradient, and over time, the system reaches a steady state.

In the Bruce-Vincent method, with a small applied voltage, at **t = 0**, all ions in the electrolyte participate in the ionic movement, and the initial current reflects the contribution of all ions. As concentration gradient forms, the number of active Li

ions carrying charge decreases, leading to a decay in the current over time as illustrated in Figure 3-10. t_{Li+} can be calculated:

$$tLi^{+} = I_{ss} / I_0$$

where I_{ss} and I_0 are the initial and steady state current respectively.

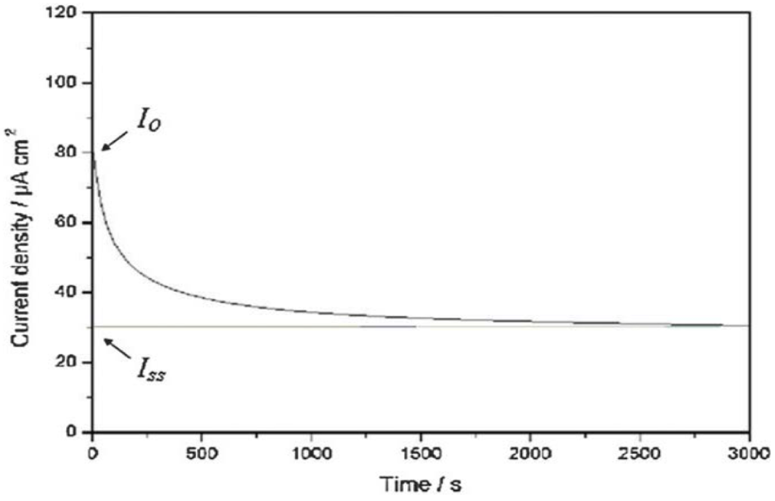

Figure 3 - 10. Current change over time. I_0 is the initial current and Iss is the steady state current.[11]

In practical systems, the presence of multiple charge-carrying ionic species and the formation of the passivation layer on the electrode surfaces complicate the situation, making the basic equation insufficient for accurate analysis. To account for these factors, correction terms were added to the Bruce and Vincent equation:

$$tLi^{+} = I_{ss} (V - I_0 R_0) / I_0 (V - I_{ss} R_{ss})$$

where R_0 and R_{ss} are the initial and steady state resistance of passivation layer respectively, and V is the applied constant potential. The impedance is characterized by EIS analysis before and after voltage polarization as shown in Figure 3-11.

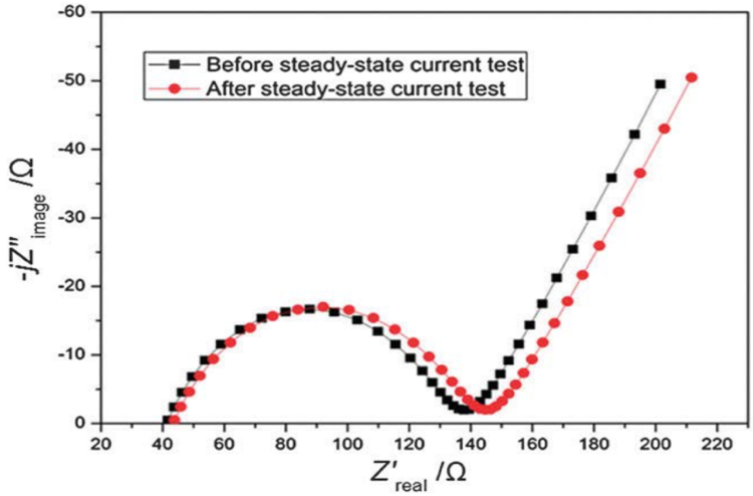

Figure 3 - 11. EIS impedance before and after polarization.[11]

t_{Li+} measurements:

In this PhD thesis, we assembled a Li||Li symmetric cell for the t_{Li+} measurement. A small 10 mV voltage polarization was applied, and the initial and steady state currents were then recorded. The electrode impedance before and after polarization was obtained by EIS measurements. The measurement was repeated several times to ensure reliable results. All measurements were conducted by Bio-Logic VMP3 Multi Potentiostat with EC-Lab for EIS spectra fitting.

3.9 Solid-State Nuclear Magnetic Resonance

Nuclear Magnetic Resonance (NMR) spectroscopy is a non-destructive technique that studies the electronic environment of specific nuclei, providing detailed structural information at the molecular level. Unlike diffraction techniques, NMR does not require the material to be crystalline and can therefore be applied to disordered or amorphous systems, offering complementary insights into molecular structures that diffraction methods cannot access. Additionally, NMR can be used to study the dynamic behavior of nuclei within materials, such as motion and diffusion.

Every nucleus has an intrinsic "spin" associated with a non-zero quantum number, which generates its magnetic moment (μ). This magnetic moment interacts with an external magnetic field, causing the nucleus to rotate around the direction of the external field. The rate of this rotation known as the Larmor frequency is unique to each type of nucleus, the gyromagnetic ratio (γ) and the magnetic field (B).[12]

$$\omega_L = -\gamma B$$

When a magnetic field is applied, longitudinal relaxation occurs as the individual magnetic moments reorient to align with the field, leading to the establishment of a bulk magnetization. This process continues until thermal equilibrium is reached where the time need is known as longitudinal relaxation time (T1). This relaxation time represents how quickly the magnetization recovers to its equilibrium state, and is typically measured as 5 × T1, as illustrated in Figure 3-12.

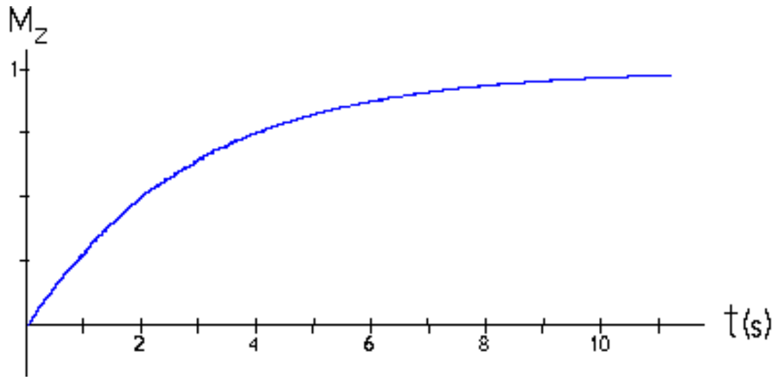

Figure 3 - 12. Longitudinal relaxation.[13]

To produce a strong NMR signal, a radiofrequency (RF) pulse close to the Larmor frequency is applied. This RF pulse causes the bulk magnetization (M) to rotate 90° away from the external magnetic field. As the magnetization processes around the external magnetic field, it generates an alternating electric field, which induces an AC current in a coil surrounding the sample. This produces the detectable NMR signal. Over time, the AC current decreases in magnitude, finally reaching zero, causing the NMR signal to decay. This decaying signal is referred to as Free Induction Decay (FID), as illustrated in Figure 3-13. The NMR signal is initially recorded in the time domain, but to obtain an NMR spectrum, the FID is converted to frequency by Fourier transformation. This conversion allows the signal to be represented in a form that reflects the frequencies of the molecular environments in the sample.[12]

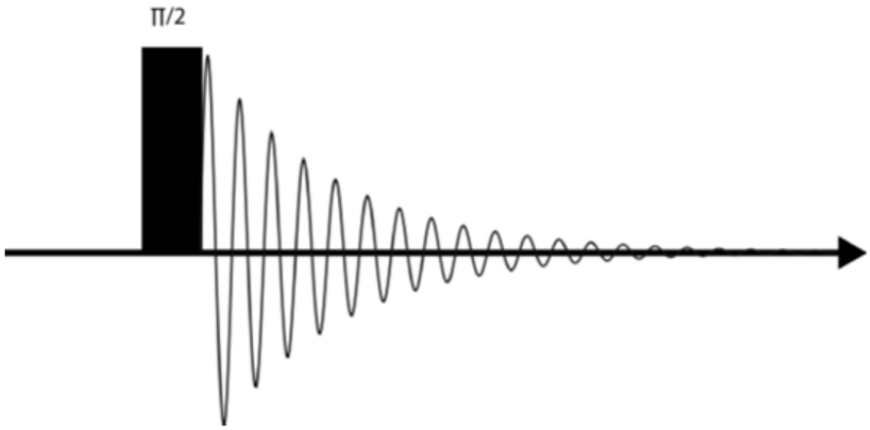

Figure 3 - 13. A simple one-pulse sequence.[14]

The electron clouds surrounding each nucleus create internal magnetic fields that influence the overall magnetic field experienced by each nucleus. The size and orientation of these internal fields depend on the chemical structure and local molecular mobility, which alters the precession frequency of each nucleus.

This variation in the local magnetic environment is referred to as chemical shielding. Due to chemical shielding, the NMR signals of nuclei in different environments will appear at different frequencies. To standardize NMR spectra, chemical shifts δ is given by:

$$\delta = \frac{\nu - \nu_{ref}}{\nu_{ref}} \times 10^6$$

where ν and ν_{ref} is the resonance frequency.

When two nuclear spins are close to each other, their magnetic fields can interact. One spin may feel the magnetic field of the other, leading to dipolar (dipole-dipole) interactions, as shown in Figure 3-14. These interactions are commonly seen in solid samples and are a major cause of NMR spectral broadening, which can obscure fine details. To minimize this broadening, a technique called

Magic Angle Spinning (MAS) is used. In MAS, the sample is rotated at a specific angle of 54.7° relative to the external magnetic field. This rotation helps to average out some of the dipolar interactions, significantly enhancing the spectral resolution and reducing broadening, thereby making the NMR spectra of solid-state samples clearer and more detailed.[13]

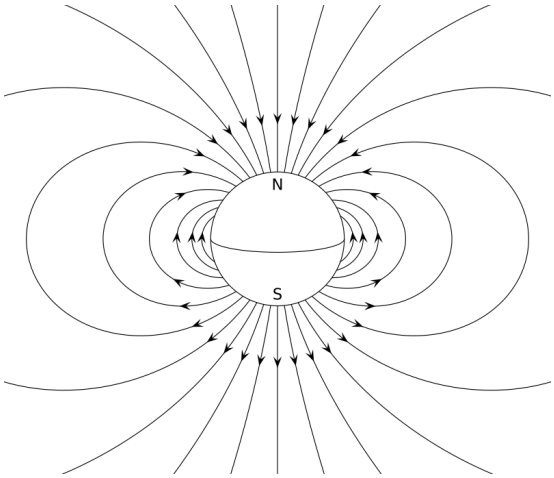

Figure 3 - 14. Dipole-dipole magnetic field around a nuleus.[15]

Nuclei with a quantum number greater than 1/2 have a non-spherical charge distribution and are referred to as quadrupolar nuclei. The interaction between these nuclei and the local electric field is another key factor that causes line broadening in solid-state NMR spectra. Quadrupolar interactions, similar to dipolar interactions, contribute to the complexity of NMR spectra in solid materials, making it more challenging to resolve distinct signals.

NMR measurements:

In this thesis, Solid-State MAS NMR was used to study the Li ion environment. Zirconia rotors with a diameter of 2.5 mm were used sample packing. the experiment was conducted using a Bruker 2.5 mm HXY probe, which spins at 25 kHz under 11.7 T magnetic field (500 MHz ^{1}H frequency). One-dimensional ^{7}Li and ^{19}F spectra and two-dimensional ^{19}F–^{7}Li heteronuclear correlation (HETCOR) spectrum were acquired.

3.10 References

1. Principle of a heat-flux DSC. *NETZSCH - Analyzing and Testing. Leading in Thermal Analysis, Rheology and Fire Testing* https://analyzing-testing.netzsch.com/en/landingpages/principle-of-a-heat-flux-dsc. Date of the last visit 25/10/2024.
2. Scanning Electron Microscope A To Z.
3. Basics of EIS: Electrochemical Research-Impedance Gamry Instruments. https://www.gamry.com/application-notes/EIS/basics-of-electrochemical-impedance-spectroscopy/. Date of the last visit 25/10/2024.
4. Bard, A. J. & Faulkner, L. R. *Electrochemical Methods: Fundamentals and Applications*. (Wiley, 2012).
5. Bontempelli, G., Dossi, N. & Toniolo, R. Linear Sweep and Cyclic☆. in *Reference Module in Chemistry, Molecular Sciences and Chemical Engineering* (Elsevier, 2016).
6. Griffiths, P. R. & Haseth, J. A. D. *Fourier Transform Infrared Spectrometry*. (John Wiley & Sons, 2007).
7. Guide to Raman Spectroscopy. https://www.bruker.com/en/products-and-solutions/infrared-and-raman/raman-spectrometers/what-is-raman-spectroscopy.html. Date of the last visit 25/10/2024.
8. faq_beginners-guide-to-thermogravimetric-analysis_009380c_01.pdf.
9. Bruce, P. G. & Vincent, C. A. Steady state current flow in solid binary electrolyte cells. *J. Electroanal. Chem. Interfacial Electrochem.* **225**, 1–17 (1987).
10. Evans, J., Vincent, C. A. & Bruce, P. G. Electrochemical measurement of transference numbers in polymer electrolytes. *Polymer* **28**, 2324–2328 (1987).
11. Zhang, J. *et al.* Preparation and electrochemical behaviors of composite solid polymer electrolytes based on polyethylene oxide with active inorganic–organic hybrid polyphosphazene nanotubes as fillers. *New J. Chem.* **35**, 614–621 (2011).
12. Understanding NMR Spectroscopy, 2nd Edition | Wiley. *Wiley.com*
13. Spin Dynamics: Basics of Nuclear Magnetic Resonance, 2nd Edition | Wiley. *Wiley.com*
14. Pulse Sequences. *Chemistry Libre Texts* https://chem.libretexts.org/Bookshelves/Physical_and_Theoretical_Chemistry_Textbook_Maps/Supplemental_Modules_(Physical_and_Theoretical_Chemistry)/Spectroscopy/Magnetic_Resonance_Spectroscopies/Nuclear_Magnetic_Resonance/NMR%3A_Experimental/Pulse_Sequences (2014). Date of the last visit 25/10/2024.
15. Landé, A. (1988). Nuclear Magnetic Moments and Their Origin. In: Barut, A.O., van der Merwe, A. (eds) Selected Scientific Papers of Alfred Landé. Fundamental Theories of Physics, vol 22. Springer, Dordrecht.

Chapter 4

Synergistic Combination of Crosslinked Polymer and Concentrated Ionic Liquid for Electrolytes with High Stability in Solid-State Lithium Metal Batteries

4.1 Introduction

The advancement of energy storage technologies has become increasingly vital, with LMBs at the forefront due to their high energy density and potential for supporting applications like long-range EVs. However, the practical deployment of LMBs is significantly limited by safety concerns, particularly those associated with conventional LEs, which are prone to flammability and instability issues. In light of these challenges, there has been growing interest in solid electrolytes as a safer alternative, leading to intensified research in SPEs over the past decades.

The initial exploration of SPEs was pioneered in the 1970s by Wright and Armand, who investigated the potential of PEO as a solid polymer electrolyte.[1,2] Since then, PEO has emerged as a promising material for SPEs, primarily due to its

safety profile, ease of processing, low cost, and effective compatibility with lithium metal.[3,4] However, while high molecular weight PEO offers the added advantage of dendrite suppression due to its superior mechanical properties and improved cycling stability.[5] PEO-based SPEs face significant limitations, such as low ionic conductivity at ambient temperature (up to 10^{-6} S cm^{-1}). This low conductivity is attributed to the semi-crystalline nature of PEO, which restricts the mobility of polymer chains necessary for ion transport, thereby necessitating higher operating temperatures. Furthermore, the electrochemical stability of PEO-based SPEs remains a critical barrier, with a limited electrochemical stability window (ESW) of less than 4 V vs. Li^+/Li due to the oxidative vulnerability of the ether oxygen in PEO.[1,4,5] These limitations significantly hinder the potential of PEO-based SPEs for high-voltage, solid-state LMBs, highlighting the need for modifications that could improve their ionic conductivity and oxidative stability. Recent studies have focused on several strategies to address these limitations, including the incorporation of inorganic fillers,[6–8] plasticizing ionic liquids,[10] copolymerization,[11] and crosslinking of PEO matrices.[9,10]

Among these approaches, ionic liquid (IL)-based electrolytes have gained particular interest due to their inherent properties, such as low vapor pressure, nonflammability, and exceptional thermal and chemical stability.[11] For example, the integration of ionic liquids has been shown to substantially enhance the ionic conductivity of PEO-based SPEs, as demonstrated by Shin et al., who studied the effects of C3mpyrTFSI ionic liquid on PEO-based ternary polymer electrolytes.[12] Their findings indicated that the addition of conductive, room-temperature ionic liquids enabled significant enhancements in conductivity, surpassing the levels achievable by IL-free electrolytes.

Crosslinking represents another promising modification strategy, enabling improved mechanical properties and reduced crystallization in PEO-based SPEs. This method has been shown to enhance the phase behavior and ionic conductivity of SPEs by creating a stable polymer network.[10,13] Early work by Watanabe et al. on crosslinked PEO-$LiClO_4$ systems demonstrated that reducing crystallinity through crosslinking could effectively increase ionic conductivity and reduce the glass transition temperature (Tg) in comparison to linear PEO systems.[14] Similarly, Joost et al. observed that incorporating C4mpyrTFSI ionic liquid within crosslinked PEO matrices could further enhance ionic mobility, particularly by decreasing interactions between Li^+ ions and EO groups due to the presence of additional $TFSI^-$ anions.[15] The crosslinking process, typically induced by UV irradiation, forms a stable polymer network that reinforces the mechanical integrity of the SPE while retaining the beneficial characteristics of ionic liquids. The effectiveness of UV-induced crosslinking in polymer-plasticizer-salt ternary systems has been further confirmed by other studies, validating its role in advancing SPE design.[16,17]

In recent years, the concept of highly concentrated electrolytes, originally applied to traditional liquid electrolytes, has also gained traction in ionic liquid-based systems.[18–20] Concentrated ionic liquid (CIL) electrolytes offer several advantages, such as expanded electrochemical stability window,[21] higher transference number,[22] enhanced rate capability,[23] and improved cycling stability.[24]

For example, recent works by Pal et al. have demonstrated that the use of ether-aided, concentrated LiFSI-C3mpyrFSI ionic liquid electrolyte could effectively enhance ion transport, interfacial stability, and fast-charging capability.[25–27] These desirable features make CILs strong candidates for integration with crosslinking strategies to develop high-performance PEO-based SPEs. By combining crosslinking with CILs, there is considerable potential to further reduce PEO crystallinity, improve ionic conductivity, expand electrochemical stability, and maintain safety and mechanical integrity.

Building upon these concepts, the current study introduces a novel crosslinked polymer-in-concentrated ionic liquid (PCIL) system composed of PEO, lithium bis(fluorosulfonyl)imide (LiFSI), and N-propyl-N-methylpyrrolidinium bis(fluorosulfonyl)imide (C3mpyrFSI) ionic liquid, with a Li^+:IL molar ratio of 1:1. This system integrates the advantages of UV-induced crosslinking and concentrated ionic liquid environments to create a highly amorphous, robust SPE with enhanced ionic conductivity and electrochemical stability. Through this approach, the study aims to bridge a critical knowledge gap in PEO-based SPEs, particularly by addressing the demands for high-performance solid-state LMBs that can operate at ambient temperatures with extended cycling stability.

4.2 Methodology

This section outlines the preparation and characterization of the polymer-in-concentrated ionic liquid solid polymer electrolytes (PCIL-SPEs) developed in this study. These materials were synthesized using a solvent casting technique, followed by UV crosslinking to achieve a stable, amorphous structure with enhanced ionic conductivity and mechanical integrity.

4.2.1 Materials

PEO with a molecular weight of 5,000,000 (Sigma-Aldrich) was used as the polymer matrix. Prior to synthesis, PEO was vacuum-dried at 50 °C for 24 hours to remove any residual moisture, ensuring a dry environment suitable for SPE preparation. The ionic liquid, N-propyl-N-methylpyrrolidinium bis(fluorosulfonyl)imide (C3mpyrFSI), with a purity of 99.5%, was obtained from Solvionic and similarly subjected to vacuum drying at 50 °C for 48 hours. LiFSI salt (99.9% purity, Nippon Shokubai) underwent the same drying protocol. Benzophenone (BP), sourced from Sigma-Aldrich, was used as the photoinitiator in the crosslinking process without further purification. LFP with an areal capacity of 1 mAh cm^{-2} and a mass loading of approximately 6 mg cm^{-2} was obtained from Custom Cells, while lithium manganese oxide (LMO) powder was provided by Calix Ltd. All materials were stored in an argon-filled glovebox to maintain a controlled, moisture-free environment.

4.2.2 Membrane Preparation

The PCIL-SPEs were prepared in an argon-filled glovebox to prevent moisture interference, which is critical for maintaining the electrochemical performance of the final SPEs. The synthesis involved a solvent casting method, which allowed for precise control over the composition and structural characteristics of the SPEs. The preparation steps are illustrated in Figure 4-1.

- **Solution Preparation**: Predetermined amounts of LiFSI salt and C3mpyrFSI ionic liquid were combined in a Li^+:IL molar ratio of 1:1. This mixture was dissolved at room temperature overnight to ensure homogeneity.
- **Polymer Mixture**: The LiFSI/C3mpyrFSI solution was then mixed with varying amounts of PEO in acetonitrile, adjusting the EO molar ratio to 10:1:1. This controlled ratio ensured an optimized balance between ion transport and structural stability. The resulting solutions were poured into silicon molds and left to stand for 48 hours, allowing for slow evaporation of the solvent and formation of free-standing solid membranes.
- **Hot Pressing**: The membranes were sandwiched between two Mylar foils and hot-pressed at 70 °C under a pressure of 2 MPa for 10 minutes. This step improved the homogeneity and mechanical consistency of the membranes, resulting in a uniform thickness of approximately 150 ± 10 µm.
- **Crosslinking**: To induce crosslinking, 5 wt% benzophenone (relative to the weight of PEO) was added as a photoinitiator. Crosslinking was carried out in a TBK 905 UV curing chamber at a power setting of 200 W for 3 minutes, immediately following the hot-pressing step. UV crosslinking created a stable polymer network, reducing PEO crystallinity and enhancing mechanical integrity.
- **Secondary Drying**: The crosslinked membranes were then transferred to a Büchi® oven for a secondary vacuum drying process at 50 °C for 24 hours to remove any residual solvents. All prepared SPEs were stored in an argon-filled glovebox until further characterization.

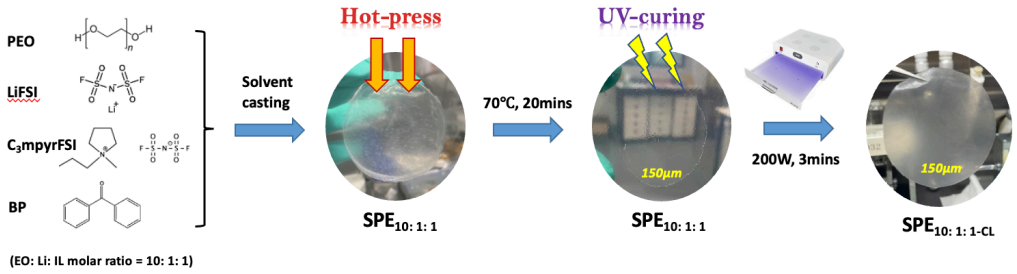

Figure 4 - 1. PCIL-SPEs (linear and crosslinked) prepared by solvent casting followed by hot-press and UV-crosslinking. Adapted from Zhang et al. ACS Appl. Polym. Mater. 2024, 6, 23, 14469–14476. Copyright 2024.

4.2.3 Characterization Techniques

A range of analytical techniques was employed to comprehensively assess the physical, thermal, and electrochemical properties of the PCIL-SPEs.

- **Differential Scanning Calorimetry (DSC)**: A Mettler Toledo DSC instrument was used to examine the thermal phase behavior of the SPEs. Approximately 10 mg of each sample was loaded, and measurements were conducted over a temperature range of -120 to 80 °C at a heating/cooling rate of 10 °C min^{-1}. This analysis helped evaluate the degree of crystallinity in the crosslinked and non-crosslinked samples.
- **Electrochemical impedance spectroscopy (EIS)**: Ionic Conductivity was measured by the EIS method using an MTZ-35 impedance analyzer (Biologic). Stainless steel (SS) was used in the SS|PCIL-SPEs|SS coin cell configuration, and impedance was measured over a frequency range of 1 MHz to 0.1 Hz at temperatures between 30 and 50 °C. The ionic conductivity (σ) was calculated from the bulk resistance (R_b), determined from the high-frequency region of the impedance spectrum, using the equation: $\sigma = l/R_b*A$ where l is the membrane thickness and A is the area of the electrode.
- **Raman Spectroscopy**: To investigate cation-anion interactions and identify the state of the FSI- anions, Raman spectroscopy was conducted with a Renishaw Invia microscope equipped with a 633 nm laser (13.0 mW at sample, 10% laser power, 60 s exposure). All measurements were carried out at room temperature within a custom-built sample holder with a quartz window, and spectra were acquired over a range of 100 to 3200 cm^{-1}. Baseline correction and normalization were applied, and the Voigt function was used to deconvolute the Raman bands into constituent peaks.
- **Thermogravimetric Analysis (TGA)**: Thermal stability was assessed using a Mettler Toledo TGA STAR instrument. Approximately 10 mg of each sample was loaded, and mass loss was recorded over a temperature range of 30 to 600 °C at a heating rate of 10 °C min^{-1} under a constant N_2 flow. This analysis provided insights into the thermal degradation properties of the crosslinked and non-crosslinked SPEs.
- **Scanning Electron Microscopy (SEM)**: Surface morphology and structural characteristics of the SPEs were analyzed using a JEOL JSM-IT300 SEM with an acceleration voltage of 10 kV. Cycled cells were disassembled in an argon-filled glovebox using a coin cell disassembly unit (Hohsen) to examine changes in the membrane morphology post-cycling.

4.2.4 Electrode Preparation, Cell Assembly and Electrochemical Measurements

The performance of the synthesized PCIL-SPEs was evaluated in LFP||Li and LMO||Li cell configurations.

- **Electrode Preparation**: LMO cathodes were prepared by mixing LMO powder, Super C65, and PVDF binder (80:10:10 wt.%) in NMP solvent. The resulting slurry was cast and dried according to established protocols[28], resulting in electrodes with a loading of approximately 7 mg cm^{-2} and an areal capacity of 1 mAh cm^{-2}. For LFP cathodes, pre-fabricated electrodes with a similar areal capacity and 6 mg cm^{-2} active mass loading were used. The electrodes were then cut into 8 mm diameter discs before coin cell assembly.
- **Cell Assembly**: All cells were assembled in an argon-filled glovebox. Each cell consisted of a Li metal anode, a free-standing PCIL-SPE membrane, and either an LFP or LMO cathode. The cells were assembled in CR2032 coin cell configurations (Hohsen Corp.), as shown in Figure 4-2.

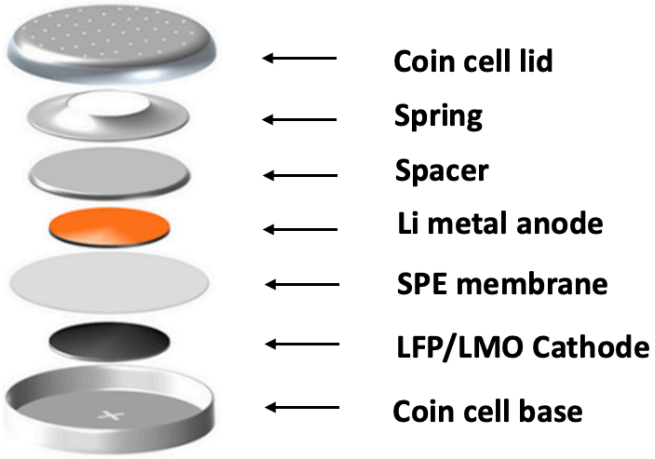

Figure 4 - 2. Coin cell assembly in this work.

- **Electrochemical Testing**: Electrochemical measurements were conducted using a VMP3 potentiostat (BioLogic). Linear sweep voltammetry (LSV) was performed with Li||SS cells at 50 °C, scanning from the open-circuit voltage up to 6 V vs. Li^+/Li at a rate of 0.1 mV s^{-1}. Galvanostatic cycling was carried out for Li||Li, LFP||Li, and LMO||Li cells at 50 °C, with voltage limits set to 2.5–4 V for LFP||Li cells and 3–4.3 V for LMO||Li cells. Two formation cycles were applied prior to long-term cycling to stabilize the cells.

4.3 Results and Discussion

This section presents the key findings from the synthesis and characterization of the PCIL-SPEs, comparing linear and crosslinked versions to demonstrate the impact of crosslinking on the structural, thermal, and electrochemical properties of the materials.

4.3.1 Thermal Properties and Phase Behavior

Both linear and crosslinked PCIL-SPEs were synthesized from homogeneous mixtures of PEO, LiFSI and C_3mpyrFSI (EO:Li:IL molar ratio=10:1:1) by solvent casting and UV-crosslinking processes, namely $SPE_{10:1:1}$ and $SPE_{10:1:1\text{-}CL}$ respectively (Figure 4-1). TGA of both $SPE_{10:1:1}$ and $SPE_{10:1:1\text{-}CL}$ confirms the thermal stability up to 220 °C which is sufficiently high for the safe operation of solid-state LMB (Figure 4-3).

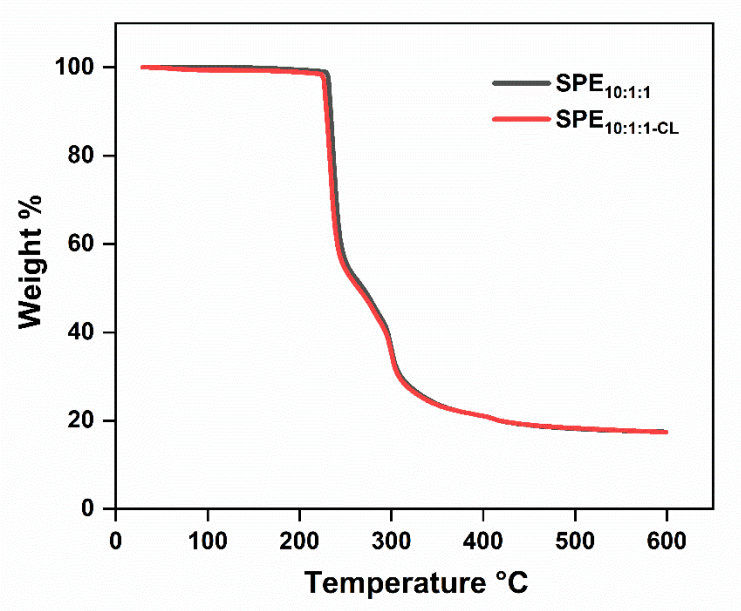

Figure 4 - 3. TGA analysis of the linear $SPE_{10:1:1}$ and crosslinked $SPE_{10:1:1\text{-}CL}$. Adapted from Zhang et al. ACS Appl. Polym. Mater. 2024, 6, 23, 14469–14476. Copyright 2024.

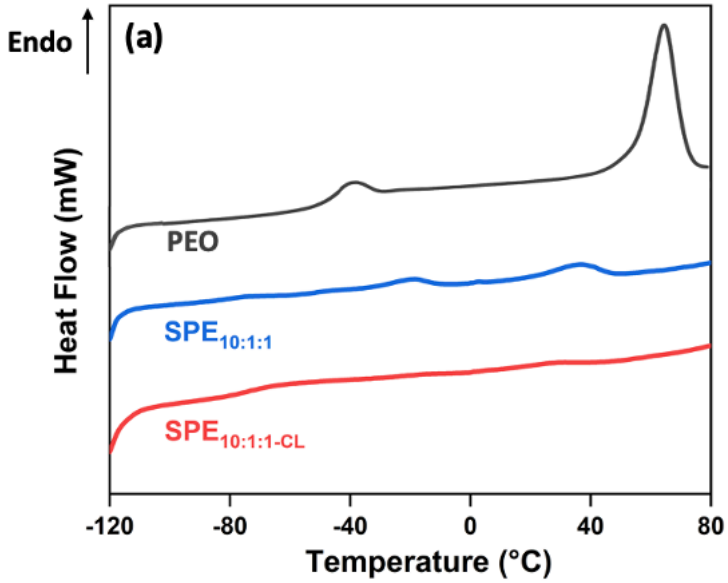

Figure 4 - 4. Phase behaviour of crosslinked $SPE_{10:1:1\text{-}CL}$ compared with linear $SPE_{10:1:1}$ and pure PEO. Adapted from Zhang et al. ACS Appl. Polym. Mater. 2024, 6, 23, 14469–14476. Copyright 2024.

The phase behavior of the prepared PCIL-SPEs was characterized by DSC to evaluate the effect of crosslinking on crystallinity and glass transition. As shown in Figure 4-4, the incorporation of C3mpyrFSI ionic liquid at a Li:IL molar ratio of 1:1 significantly altered the phase behavior of PEO, lowering the melting point from 65 °C in pure PEO to 38 °C in the linear SPE ($SPE_{10:1:1}$). Additionally, the glass transition temperature (Tg) broadened, indicating the development of a more heterogeneous system. This shift in phase behavior aligns with previous studies, which demonstrate that adding ionic liquids can suppress PEO crystallinity and enhance amorphicity, a factor crucial for improving ionic conductivity.[29,30] Notably, a small peak at approximately -20°C appears in linear $SPE_{10:1:1}$, attributed to a phase transition in the C_3mpyrFSI/LiFSI mixture, suggesting IL solubility limits in PEO and potential phase separation.[31,32]

In the crosslinked PCIL-SPE ($SPE_{10:1:1\text{-}CL}$), both the melting and phase transition peaks disappeared, and a pronounced Tg was observed at -74 °C. This suggests that crosslinking leads to a highly amorphous structure and enhances the uptake of IL in PEO matrix.[10] Additionally, the emergence of a single Tg in the crosslinked $SPE_{10:1:1\text{-}CL}$ points to a good miscibility between the ionic liquid and the PEO matrices.[33] Crosslinking has been shown in literature to hinder PEO crystallization by forming an interconnected network that restricts chain mobility, effectively enhancing the uptake of ionic liquid into the PEO matrix. The enhanced amorphicity in $SPE_{10:1:1\text{-}CL}$ supports higher ionic conductivity, as reduced crystallinity facilitates the movement of Li ions through the polymer matrix.

4.3.2 Ionic Conductivity

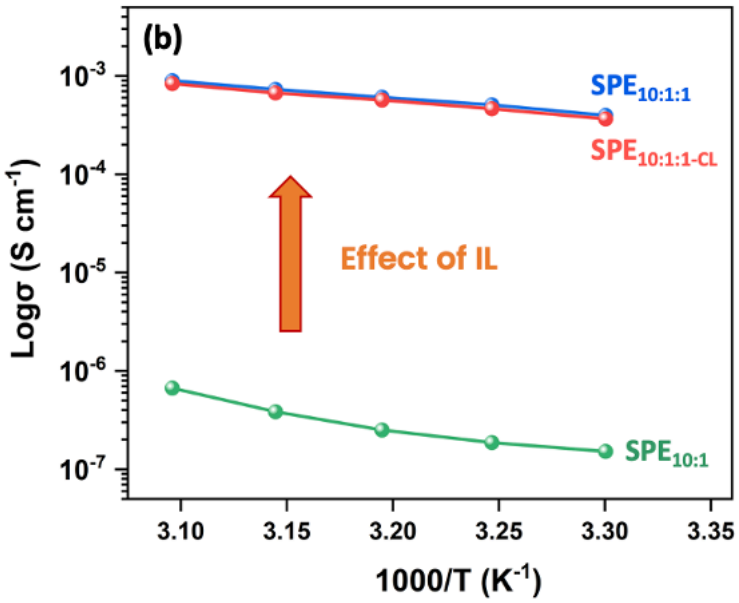

Figure 4 - 5. Ionic conductivity of crosslinked $SPE_{10:1:1\text{-}CL}$ (red) compared with linear $SPE_{10:1:1}$ (blue) and linear IL-free $SPE_{10:1}$ (orange). Adapted from Zhang et al. ACS Appl. Polym. Mater. 2024, 6, 23, 14469–14476. Copyright 2024.

The ionic conductivity of both linear and crosslinked PCIL-SPEs was measured by electrochemical impedance spectroscopy (EIS) over a temperature range of 30–50 °C. Figure 4-5 illustrates a significant increase in conductivity when C3mpyrFSI ionic liquid is added to the PEO matrix, with $SPE_{10:1:1}$ exhibiting an ionic conductivity of 4 $x10^{-4}$ S cm^{-1} at 30 °C, over three orders of magnitude higher than that of IL-free PEO systems as reported in our previous study.[30] Our previous work showed that the ionic conductivity of the CIL electrolyte is 6 $x10^{-4}$ S cm^{-1} at 30°C,[25] indicating that the ion transport property of CIL is very well maintained after mixing with PEO. This enhancement in ionic conductivity underscores the substantial role of ionic liquids in promoting ion transport within SPEs.

Upon crosslinking, the conductivity of $SPE_{10:1:1\text{-}CL}$ decreased slightly compared to the linear $SPE_{10:1:1}$. This is consistent with literature reports that crosslinking can restrict polymer chain mobility, which, while increasing mechanical stability, can also impede ion transport, especially in high salt content systems.[34] Whereas in high polymer content systems, crosslinking generally increases the amount of amorphous region which therefore contribute to higher ionic conductivities.[35] Despite this minor decrease, the crosslinked SPE retained high conductivity levels, suggesting that the benefits of reduced crystallinity and enhanced ionic liquid uptake offset the limitations imposed by restricted chain mobility. Thus, while crosslinking introduces minor trade-offs in terms of ion transport, the overall impact remains favorable due to the significant increase in amorphous content.

4.3.3 Morphological Analysis

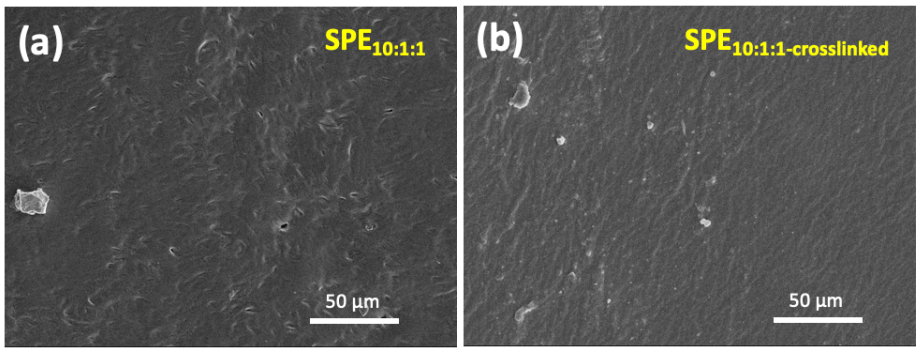

Figure 4 - 6. SEM surface morphology of linear $SPE_{10:1:1}$ and crosslinked $SPE_{10:1:1\text{-}CL}$. Adapted from Zhang et al. ACS Appl. Polym. Mater. 2024, 6, 23, 14469–14476. Copyright 2024.

Scanning electron microscopy (SEM) was employed to examine the surface morphology of the PCIL-SPEs. As shown in Figure 4-6, the crosslinked $SPE_{10:1:1\text{-}CL}$ displayed a denser and smoother surface compared to the liner $SPE_{10:1:1}$, which exhibited a more heterogeneous and less uniform texture. The wrinkled texture observed in $SPE_{10:1:1\text{-}CL}$ can be attributed to the increased incorporation of lithium salt and ionic liquid, which results in a more cohesive and mechanically robust structure. The increased uniformity and amorphous nature of the crosslinked

material align with findings from prior studies that highlight the role of crosslinking in promoting homogeneity in SPE networks.[13,36]

4.3.4 Raman Spectroscopy Analysis

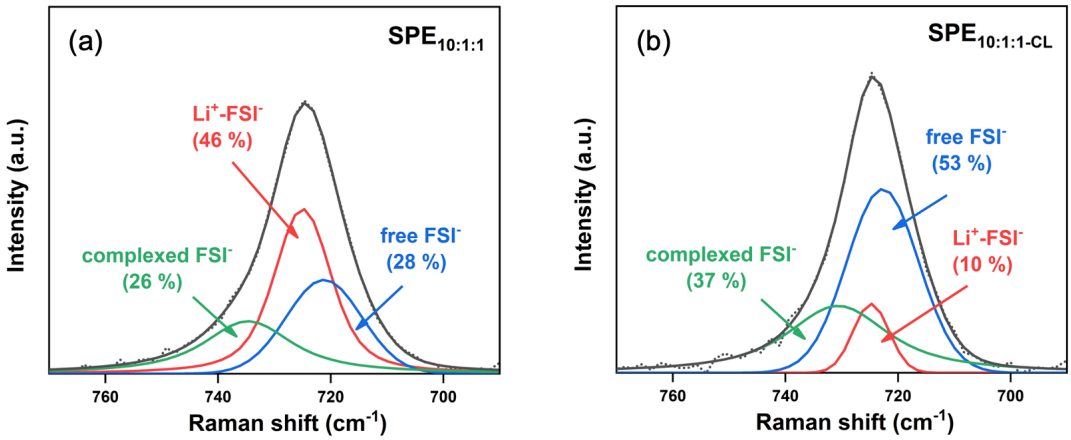

Figure 4 - 7. Raman spectra of -SNS stretching vibration mode of FSI^- anions in (a) linear $SPE_{10:1:1}$ and (b) crosslinked $SPE_{10:1:1\text{-}CL}$. The spectra were deconvoluted to three FSI^- states, including free FSI^-, Li^+-FSI^- ion pairs, and complexed FSI^-. Adapted from Zhang et al. ACS Appl. Polym. Mater. 2024, 6, 23, 14469–14476. Copyright 2024.

Raman spectroscopy provided insights into the ion-ion interactions within the PCIL-SPEs by deconvoluting the -SNS stretching mode of the FSI^- anions. The analysis revealed distinct differences between linear and crosslinked systems (Figure 4-7). The -SNS stretching mode of FSI^- in the PCIL-SPEs was deconvoluted into three constituent peaks: free FSI^- at 721-723 cm^{-1}, Li^+-FSI^- ion pairs at 725 cm^{-1}, and complexed FSI^- anions at 730-735 cm^{-1} (aggregated ion clusters).[37] In the linear $SPE_{10:1:1}$, the proportion of free FSI^- was relatively low (28%), with a higher fraction of Li^+-FSI^- ion pairs (46%). However, in the crosslinked $SPE_{10:1:1\text{-}CL}$, the free FSI^- anions increased to 53%, while Li^+-FSI^- ion pairs were reduced to 10%. In this system, the plasticizing effect of the concentrated IL is likely the primary driver of Li^+ solvation by weakening the strong Li-EO interactions. Crosslinking, meanwhile, reduces the crystallinity of PEO and making the polymer more homogeneously amorphous, which in turn facilitates Li^+-FSI^- ion pair dissociation.[37,38] This dissociation increases the availability of Li^+ for Li^+-EO coordination. Furthermore, the spatial segregation of PEO chains due to crosslinking likely promotes a more uniform distribution of FSI^- anions and ion clusters.[38]

The observed increase in complexed FSI^- anions in the crosslinked SPE indicates the presence of aggregated ion clusters. The crosslinked network may help to segregate the large, aggregated domains and facilitates the formation of dispersed ion clusters. These more uniformly distributed domains could contribute to improved ionic conductivity by promoting efficient Li^+ transport across the SPE, a phenomenon supported by previous studies showing that crosslinking can enhance

ion mobility through improved distribution of ionic clusters.[38] Therefore, we believe that crosslinking results in enhanced Li^+-FSI^- ion pairs dissociation and more uniformly distributed ion clusters which would account for the high ionic conductivity and the potential high electrochemical stability of the crosslinked $SPE_{10:1:1\text{-}CL}$.

4.3.5 Electrochemical Stability

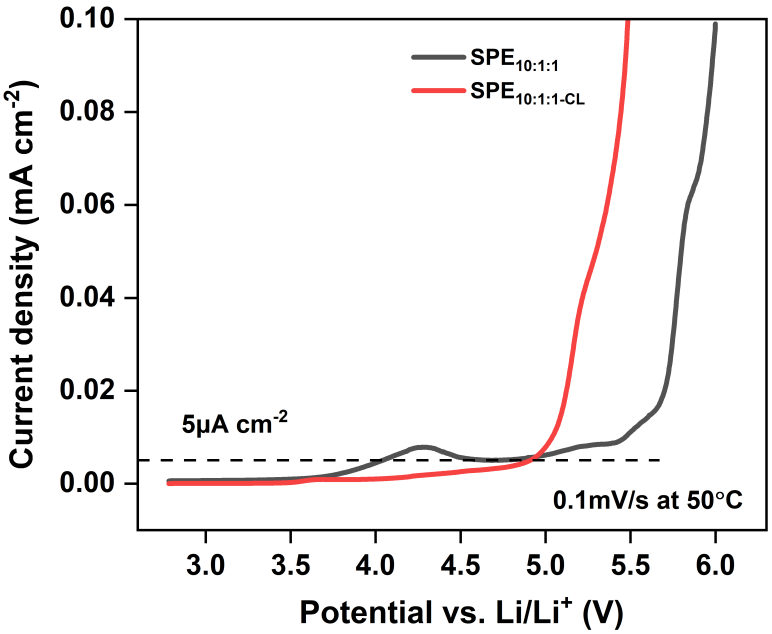

Figure 4 - 8. Linear sweep voltammetry of $SPE_{10:1:1}$ and $SPE_{10:1:1\text{-}CL}$ in a Li||SS cell with a scan rate of 0.1 mV s^{-1} at 50 °C. Adapted from Zhang et al. ACS Appl. Polym. Mater. 2024, 6, 23, 14469–14476. Copyright 2024.

The electrochemical stability window (ESW) of the linear $SPE_{10:1:1}$ and crosslinked $SPE_{10:1:1\text{-}CL}$ was evaluated in a Li||SS cell by LSV measurements. As shown in Figure 4-8, the linear $SPE_{10:1:1}$ begins to oxidize slowly above 4V vs. Li^+/Li, a common behaviour in PEO-based SPEs. In contrast, the crosslinked $SPE_{10:1:1\text{-}CL}$ showed high electrochemical stability up to 4.9V vs. Li^+/Li (5μA cm^{-2} current density was used as the cut-off of a current rise[39,40]). This indicates its excellent oxidation stability and suitability for use with high-energy 4V-classs electrodes. The enhanced electrochemical stability of $SPE_{10:1:1\text{-}CL}$ can be attributed to its crosslinked network, which limits the mobility of linear EO chains and therefore reduces their likelihood of oxidation at the cathode surface. Furthermore, the crosslinking changes the coordination environment enhancing more Li^+-EO coordination and promoting the formation of FSI^--rich ion clusters, as evidenced by Raman analysis. These coordinated ions and surrounding ion clusters likely form a protective layer that prevents further oxidation of EO, synergistically contributing to the enhanced oxidation stability.

4.3.6 Lithium Metal Stability

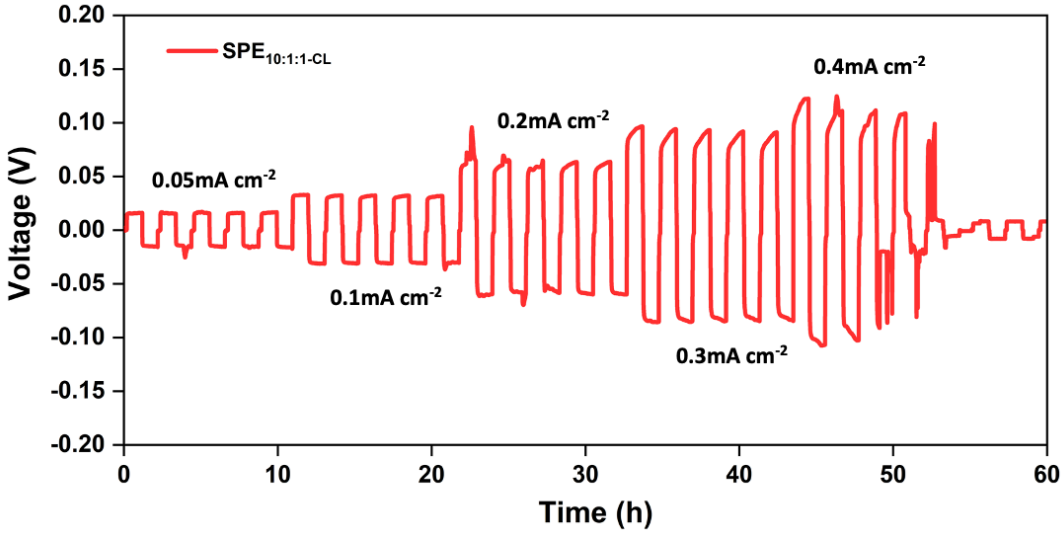

Figure 4 - 9. Voltage profiles upon Li plating/stripping of the Li|$SPE_{10:1:1\text{-}CL}$|Li cell at different current densities (0.05–0.4 mA cm^{-2}). Adapted from Zhang et al. ACS Appl. Polym. Mater. 2024, 6, 23, 14469–14476. Copyright 2024.

The ability of the crosslinked $SPE_{10:1:1\text{-}CL}$ to support lithium plating-stripping at various current densities was assessed using Li||Li symmetrical cells at 50 °C, with current densities ranging from 0.05 up to 0.4 mA cm^{-2}. The cells showed overpotentials of 20 mV and 125 mV at 0.05 and 0.4 mA cm^{-2} respectively. As illustrated in Figure 4-9, the SPE can sustain plating-stripping polarization steps throughout the entire polarization period up to 0.4 mA cm^{-2}, demonstrating stable interfacial properties, thus compatibility with the lithium metal electrodes, and good cycling performance for a solid-state polymer electrolyte.

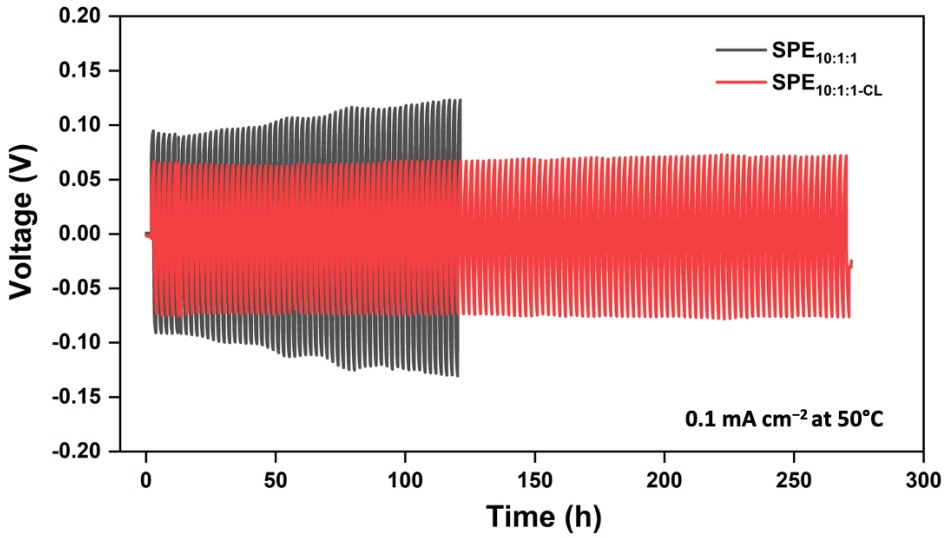

Figure 4 - 10. Voltage profiles of Li|$SPE_{10:1:1}$|Li and Li|$SPE_{10:1:1\text{-}CL}$|Li cells at 0.1 mA cm^{-2}. Adapted from Zhang et al. ACS Appl. Polym. Mater. 2024, 6, 23, 14469–14476. Copyright 2024.

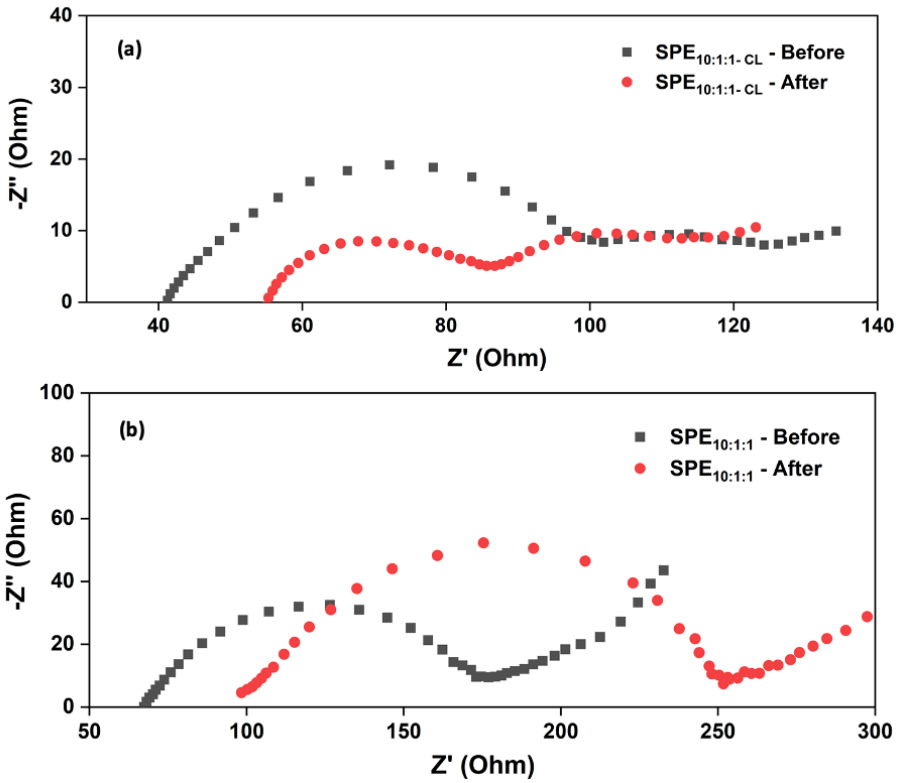

Figure 4 - 11. Impedance spectra of (a) Li|$SPE_{10:1:1-CL}$|Li and (b) Li|$SPE_{10:1:1}$|Li cells before and after polarization. The bulk resistance increase may be ascribed to the cumulative effect of SEI layer formation over cycling. Adapted from Zhang et al. ACS Appl. Polym. Mater. 2024, 6, 23, 14469–14476. Copyright 2024.

As shown in Figure 4-10, the long-term cycling of the Li|$SPE_{10:1:1-CL}$|Li cell cycled at 0.1 mA cm^{-2} for 1 hour polarisation demonstrated very stable performance, maintaining an overpotential of 60 mV over 130 cycles at 50°C, with no evidence of short circuit. This indicates that crosslinked $SPE_{10:1:1-CL}$ is highly compatible with the Li metal electrode. The interfacial resistance decreases after 130 cycles (shown in Figure 4-11-a), suggesting the formation of an ion-conductive and stable SEI layer at the electrode/electrolyte interface. In contrast, the Li|$SPE_{10:1:1}$|Li cell exhibits a steady increase in overpotential and a short circuit after just 60 cycles. The impedance spectra also showed an increase in interfacial resistance upon successive cycling as seen in Figure 4-11-b.

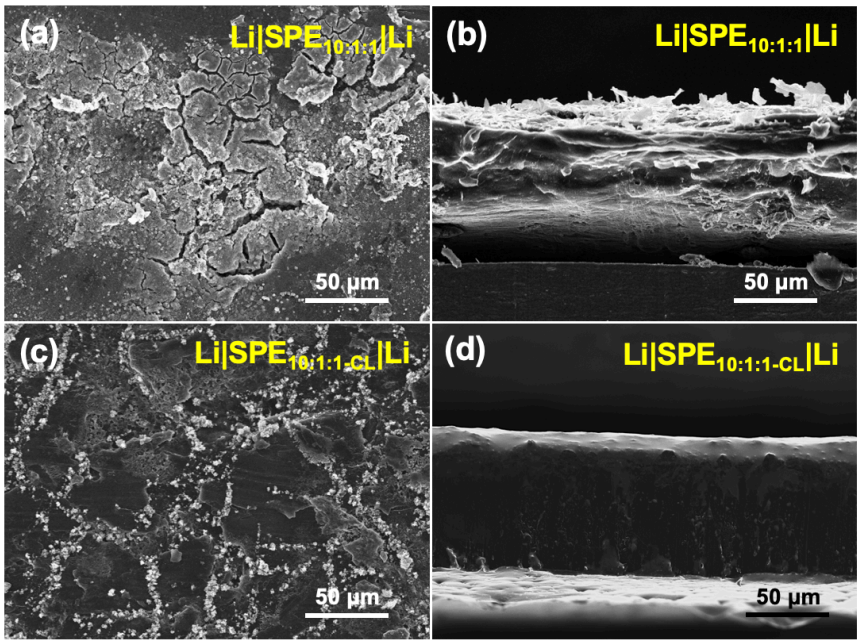

Figure 4 - 12. Surface (a, c) and Cross-section (b, d) SEM images of Li electrodes after cycling. Adapted from Zhang et al. ACS Appl. Polym. Mater. 2024, 6, 23, 14469–14476. Copyright 2024.

The top- and cross-section SEM images of the Li electrodes from both cells after cycling (Li|$SPE_{10:1:1}$|Li cell for 60 cycles, Li|$SPE_{10:1:1\text{-}CL}$|Li cell for 130 cycles) are shown in Figure 4-12. In the Li|$SPE_{10:1:1}$|Li cell, the electrode surface displays large cracks and mossy Li formations (Fig. 4-12-a), whereas the Li|$SPE_{10:1:1\text{-}CL}$|Li cell shows a smooth and dense Li metal surface (Fig. 4-12-c), indicating a uniform Li plating-stripping process. The cross-section images revealed a thick layer of dendritic/dead Li at the interface of the Li|$SPE_{10:1:1}$|Li cell (Fig. 4-12-b), in contrast to a dense and uniform interface observed in the Li|$SPE_{10:1:1\text{-}CL}$|Li cell (Fig. 4-12-d). This confirmed the formation of a smooth and compact interphase and SEI layer in the cell with crosslinked $SPE_{10:1:1\text{-}CL}$, contributing to its good cycling performance. UV-crosslinking appears to play a crucial role in suppressing Li-dendrite formation and facilitating facile and reversible Li plating-stripping.[41]

4.3.7 Performance of solid-state LMBs

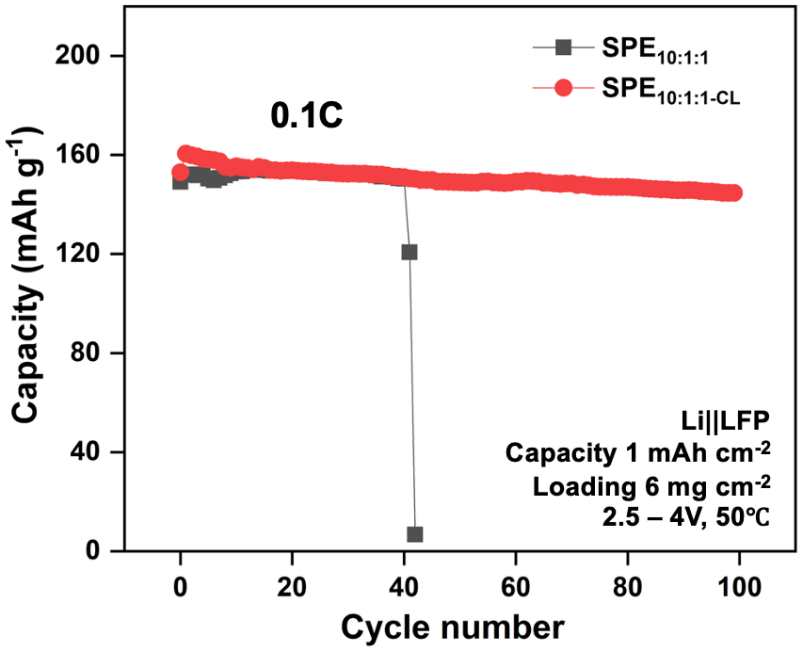

Figure 4 - 13. Cycling performance of LFP||Li (active mass loading 6 mg cm^{-2}) cell cycled at 0.1 C rate between 2.5−4.0 V for 100 cycles at 50°C. Adapted from Zhang et al. ACS Appl. Polym. Mater. 2024, 6, 23, 14469–14476. Copyright 2024.

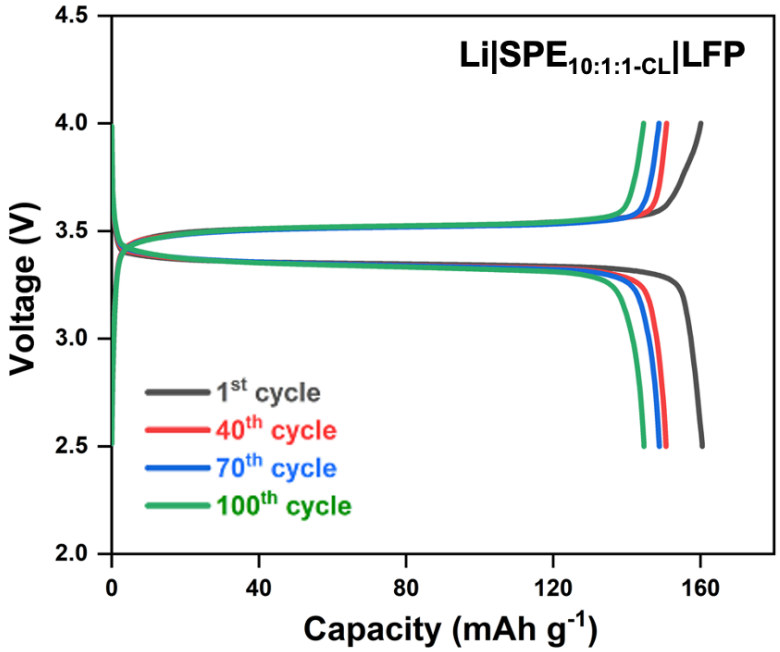

Figure 4 - 14. Charge-discharge profiles of different cycle numbers at 0.1 C rate. Adapted from Zhang et al. ACS Appl. Polym. Mater. 2024, 6, 23, 14469–14476. Copyright 2024.

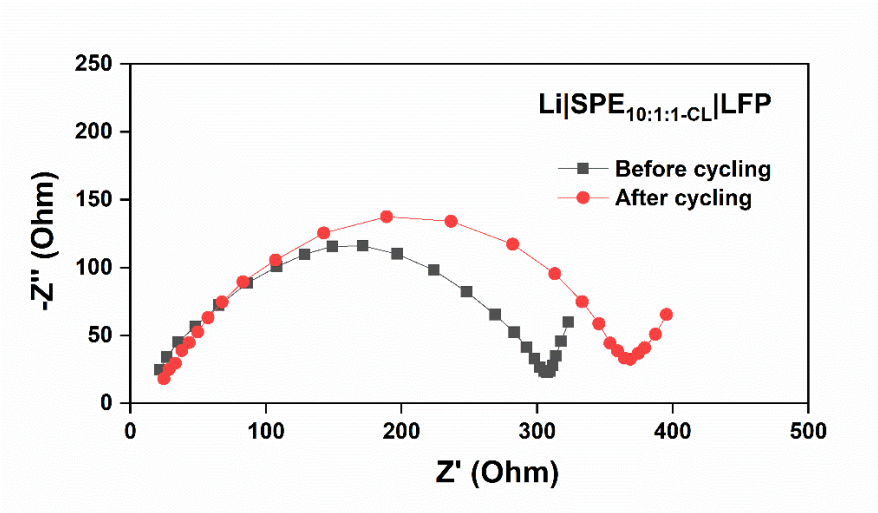

Figure 4 - 15. AC Impedance spectra of Li|$SPE_{10:1:1-CL}$|LFP cell before and after cycling. Adapted from Zhang et al. ACS Appl. Polym. Mater. 2024, 6, 23, 14469–14476. Copyright 2024.

The prepared $SPE_{10:1:1}$ and $SPE_{10:1:1-CL}$ membranes were first incorporated into high loading (6 mg cm^{-2}) LFP||Li cells to investigate their performance in solid-state LMBs. Figure 4-13 presents the prolonged cycling results for both LFP|$SPE_{10:1:1}$|Li and LFP|$SPE_{10:1:1-CL}$|Li cells at 0.1 C (0.05 mA cm^{-2} current density). The LFP|$SPE_{10:1:1-CL}$|Li cell incorporating a crosslinked membrane exhibits an initial discharge capacity of 160 mAh g^{-1}, maintaining 90% of its capacity after 100 cycles, achieving excellent coulombic efficiency of nearly 99.8% throughout cycling. In contrast, the LFP|$SPE_{10:1:1}$|Li cell with non-crosslinked membrane exhibits an initial capacity of 158 mAh g^{-1} but experienced a short circuit after 42 cycles. Figure 4-14 shows the charge–discharge profiles of the LFP|$SPE_{10:1:1-CL}$|Li cell at different cycle numbers, noting that while the discharge capacity decreased, the charge and discharge curves remained very stable over 100 cycles. Impedance profiles before and after cycling showed a slight increase due to interface stability (Figure 4-15).

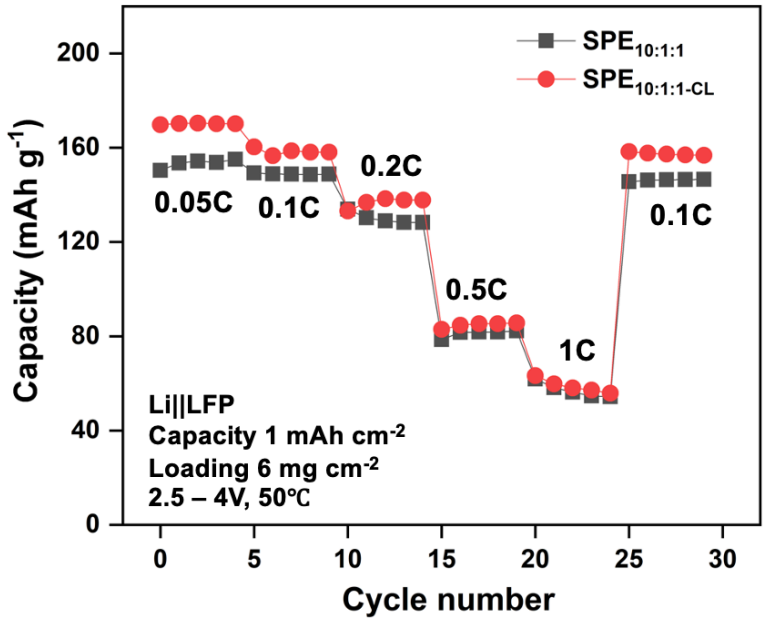

Figure 4 - 16. Rate performances of LFP||Li cell at different C rates. Adapted from Zhang et al. ACS Appl. Polym. Mater. 2024, 6, 23, 14469–14476. Copyright 2024.

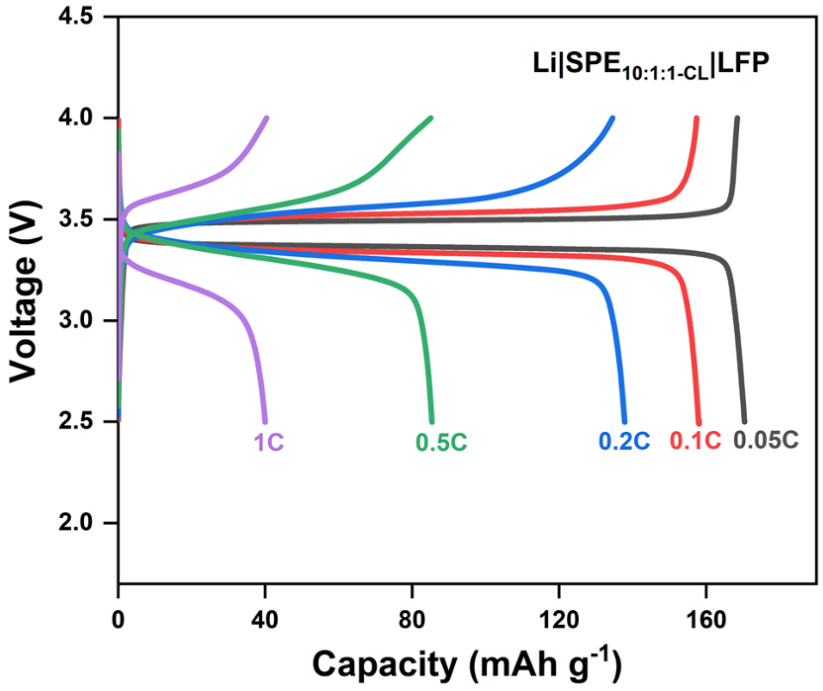

Figure 4 - 17. Voltage profile of Li|SPE$_{10:1:1-CL}$|LFP cell cycling at different C rates. Adapted from Zhang et al. ACS Appl. Polym. Mater. 2024, 6, 23, 14469–14476. Copyright 2024.

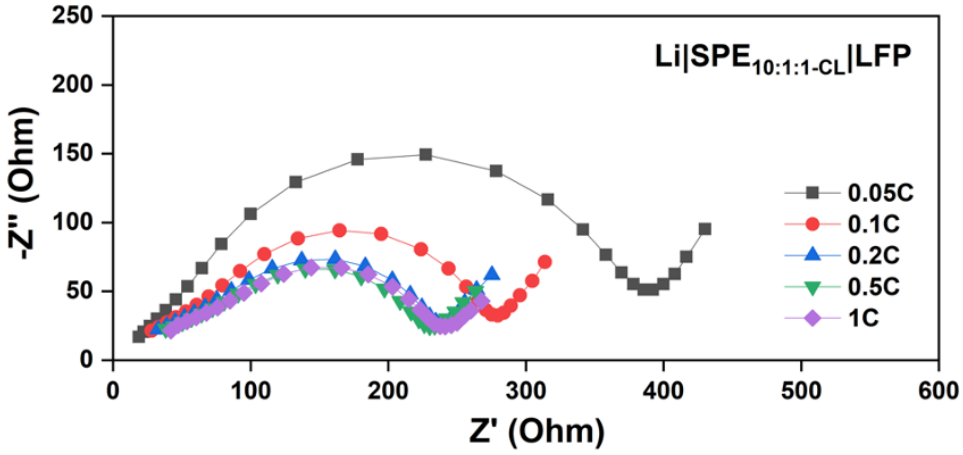

Figure 4 - 18. AC Impedance spectra of Li|$SPE_{10:1:1-CL}$|LFP cell cycling at different C rates. Adapted from Zhang et al. ACS Appl. Polym. Mater. 2024, 6, 23, 14469–14476. Copyright 2024.

A rate capability test, detailed in Figure 4-16, was conducted at current densities of 0.05 to 1 mA cm^{-2} (1C equals 1 mA cm^{-2}). Compared to the LFP|$SPE_{10:1:1}$|Li cells, the LFP|$SPE_{10:1:1-CL}$|Li cells exhibited improved rate capability, maintaining nearly full capacity at 0.05C. Overall, the battery delivered high discharge capacity ranging from 170–59 mAh g^{-1} at 0.05 to 1C. Figure 4-17 presents charge–discharge profiles of the LFP|$SPE_{10:1:1-CL}$|Li cell at various C-rates within a voltage range of 2.5–4.0 V vs. Li^+/Li, showing stable potential plateaus and increasing overpotential with higher C rates. AC impedance profiles (Figure 4-18) showed a steady decrease in interfacial resistance from 0.05C to 0.2C as the crosslinked membrane adapted itself with the electrode, followed by a slight increase at 0.5C and 1C rate due to interface stability. The improved rate performance and cycling stability of the LFP|$SPE_{10:1:1-CL}$|Li cell demonstrate the advantages of the crosslinked $SPE_{10:1:1-CL}$, providing superior electrochemical stability at 50°C.

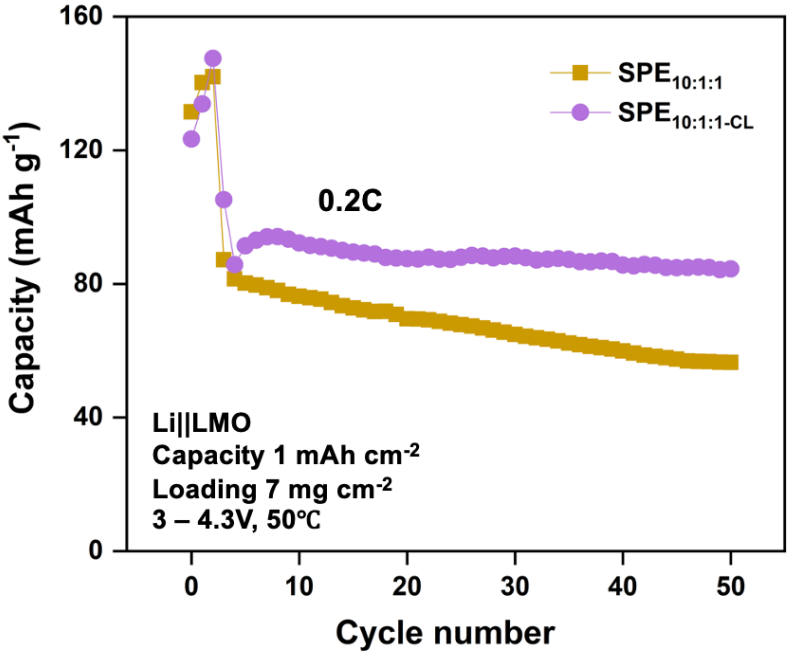

Figure 4 - 19. Cycling performance of LMO||Li (active mass loading 7 mg cm^{-2}) cell cycled at 0.2 C rate between 3−4.3 V for 50 cycles at 50°C. Adapted from Zhang et al. ACS Appl. Polym. Mater. 2024, 6, 23, 14469–14476. Copyright 2024.

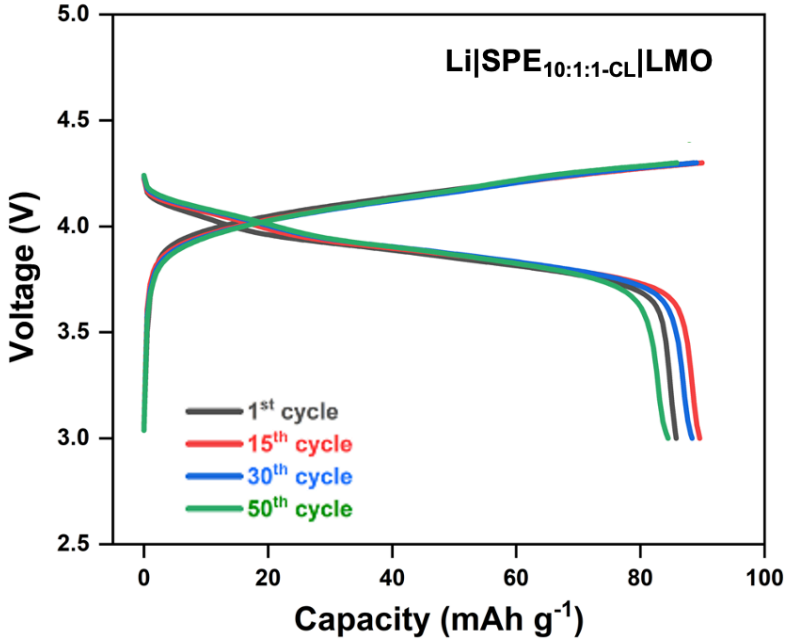

Figure 4 - 20. Charge-discharge profiles of different cycle numbers at 0.2 C rate. (f) Rate performances of LMO||Li cell at different C rates. Adapted from Zhang et al. ACS Appl. Polym. Mater. 2024, 6, 23, 14469–14476. Copyright 2024.

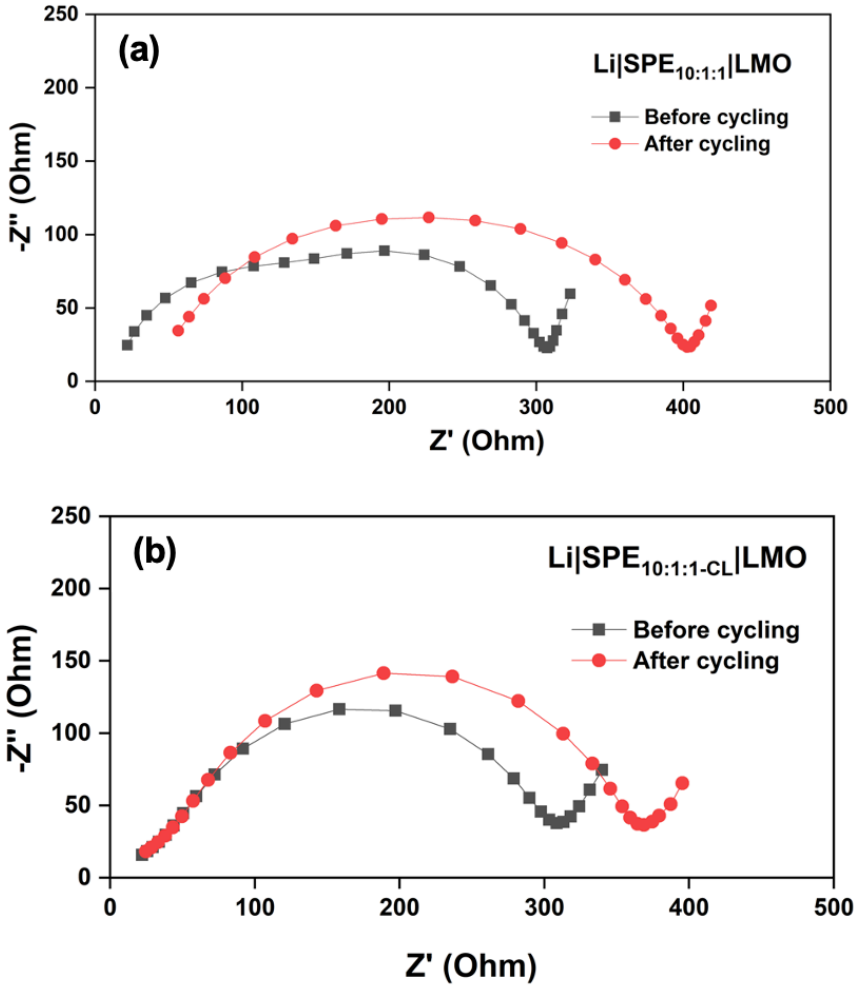

Figure 4 - 21. AC Impedance spectra of (a) Li|$SPE_{10:1:1}$|LMO cell and (b) Li|$SPE_{10:1:1\text{-}CL}$|LMO cell before and after cycling. Adapted from Zhang et al. ACS Appl. Polym. Mater. 2024, 6, 23, 14469–14476. Copyright 2024.

Given the high stability at anodic voltage observed from LSV tests, LMO||Li cells were explored using the crosslinked and non-crosslinked PCIL-SPEs. Figure 4-19 illustrates the cycling performance of both the LMO|$SPE_{10:1:1}$|Li and LMO|$SPE_{10:1:1\text{-}CL}$|Li cells at 0.2C (0.1 mA cm^{-2} current density) in the voltage range of 3–4.3V vs. Li^+/Li. The LMO|$SPE_{10:1:1\text{-}CL}$|Li cell with crosslinked membrane showed an initial discharge capacity of 91.4 mAh g^{-1}, maintaining 93% of its capacity after 50 cycles, whereas the LMO|$SPE_{10:1:1}$|Li cell experienced 25% discharge capacity loss after the same number of cycles. Figure 4-20 presents the corresponding charge–discharge profiles of the LMO|$SPE_{10:1:1\text{-}CL}$|Li cell at different cycle numbers, showing stable and relatively small over potential throughout cycling. Figure 4-21 shows the AC impedance profiles for both cells before and after cycling. Both cells exhibited an increase in interfacial resistance, but the LMO cell with the crosslinked membrane demonstrated a smaller increase after cycling, which correlates with its superior cycling performance, as shown in Figure 4-19.

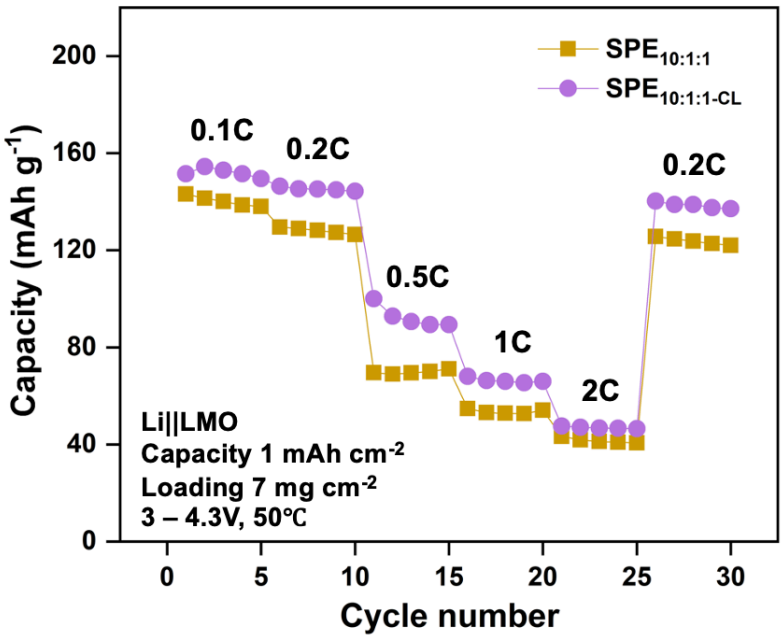

Figure 4 - 22. Rate performances of LMO||Li cell at different C rates. Adapted from Zhang et al. ACS Appl. Polym. Mater. 2024, 6, 23, 14469–14476. Copyright 2024.

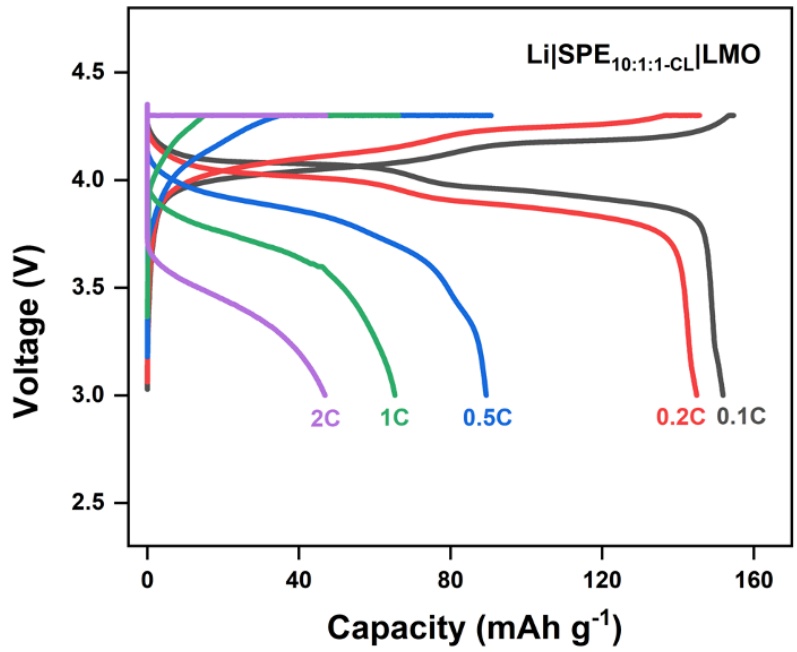

Figure 4 - 23. Voltage profile of Li|$SPE_{10:1:1-CL}$|LMO cell cycling at different C rates. Adapted from Zhang et al. ACS Appl. Polym. Mater. 2024, 6, 23, 14469–14476. Copyright 2024.

To evaluate the effect of crosslinking on fast charge/discharge capability, rate-capability tests were performed and compared across current densities from 0.05 to 1 mA cm^{-2} (shown in Figure 4-22). The LMO|$SPE_{10:1:1-CL}$|Li cell exhibited full capacity of 152 mAh g^{-1} at 0.1 mA cm^{-2} and a high capacity of 145 mAh g^{-1} at 0.1

mA cm^{-2}. The cell maintained 45% and 32% of its capacity at 1 mA cm^{-2} and 2 mA cm^{-2} (2C), respectively. Upon reducing the current density back to 0.1 mA cm^{-2}, the capacity was restored to 139 mAh g^{-1}. The voltage profiles of the LMO|$SPE_{10:1:1-CL}$|Li cell at different C rate are given in Figure 4-23.

Ref.	SPE System	EO/Li/IL Ratio	Additive	Cathode (loading)	Initial Capacity	T	Capacity Retention
2023 Herbers et al.[42]	(Liq)PEODA-LiTFSI-Pyr_{14}TFSI	4.4:1:1	BP 1%	LFP (7mg cm^{-2})	169 mAh g^{-1} (C/10)	60°C	88% (2.5-4V, 100 cycles)
2020 Homann et al.[43]	PEO/PEGDMA-LiTFSI	10:1	/	NMC622 (4mg cm^{-2})	140 mAh g^{-1} (C/10)	40°C	93% (3-4.3V, 50 cycles)
2020 Wang et al.[44]	PEO-LiFSI-N_{1222}FSI	20:1	/	LFP (2mg cm^{-2})	158.8 mAh g^{-1} (C/5)	50°C	95.4% (2.5-4V, 120 cycles)
2020 Ji et al.[45]	PEO/TEGDME/PEGMEMA-LiTFSI	24:1	BP 7.5wt%	LFP (2mg cm^{-2})	160 mAh g^{-1} (C/10)	RT	93.7% (2.5-3.8V, 100 cycles)
2019 Falco et al.[13]	PEO/G4-LiTFSI	17:1	BP 7.5wt%	LFP (1.3mg cm^{-2})	148 mAh g^{-1} (C/5)	RT	/
2019 Zhang et al.[46]	PEO/TEGDMA/TEGDME-LiTFSI	24:1	BP	LFP (1.3mg cm^{-2})	140 mAh g^{-1} (C/10)	RT	98.8% (2.5-4V, 100 cycles)
2013 Wetjen et al.[47]	PEO-LiTFSI-Pyr_{14} TFSI	10:1:2	BP 5% PEO	Composite LFP (2mg cm^{-2})	165 mAh g^{-1} (C/5)	60°C	/
This work	**PEO-LiFSI-C_3mpryFSI**	**10:1:1**	**BP 5% PEO**	**LFP (6mg cm^{-2}) LMO (7mg cm^{-2})**	**160 mAh g^{-1} (C/10) 91 mAh g^{-1} (C/5)**	**50°C**	**90% (2.5-4V, 100 cycles) 93.4% (3-4.3V, 50 cycles)**

Table 1. Comparison of the developed PEO-based PiCIL-SPE to PEO-based SPEs from literature. Adapted from Zhang et al. ACS Appl. Polym. Mater. 2024, 6, 23, 14469–14476. Copyright 2024.

Finally, compared with other types of PEO-based SPEs reported in the literature, the promising performances of the developed crosslinked $SPE_{10:1:1-CL}$ are highlighted (Table 1). It not only shows excellent cycling performance with high loading LFP cathodes, but also surprisingly good compatibility with very high loading, high voltage 4V-class LMO cathodes, which is a remarkable result within the PEO-based SPE family due to the low oxidative stability of PEO. Our findings collectively highlight the synergistic benefits of concentrated ionic liquid and the crosslinking approach in the designed PCIL-SPEs. The superior rate performance and prolonged cycling stability observed in the crosslinked PCIL-SPEs suggest they are a promising avenue for their deployment in high energy density solid-state LMBs.

4.4 Conclusion

A novel crosslinked polymer-in-concentrated ionic liquid (PCIL) solid polymer electrolyte (SPE) system was developed, incorporating PEO, LiFSI, and

C3mpyrFSI ionic liquid. By combining the advantages of UV-induced crosslinking and a concentrated ionic liquid environment, this research presents a robust SPE with promising electrochemical and structural properties that address critical limitations of traditional PEO-based electrolytes.

The crosslinked PCIL-SPE ($SPE_{10:1:1\text{-}CL}$) exhibited a highly amorphous structure with enhanced ionic conductivity and electrochemical stability compared to its linear counterpart. Key findings include the achievement of a high ionic conductivity (4×10^{-4} S cm^{-1} at ambient temperature) and an expanded electrochemical stability window up to 4.9 V vs. Li^+/Li. Crosslinking effectively reduced the crystallinity of the PEO matrix, facilitating ionic liquid uptake, while Raman spectroscopy results revealed improved ion dissociation within the crosslinked network.

Furthermore, the crosslinked SPE demonstrated excellent interfacial stability and compatibility with lithium metal anodes, as shown by stable lithium plating/stripping performance and minimized dendrite formation. In high-loading solid-state LFP||Li cells, the crosslinked SPE maintained over 90% capacity retention after 100 cycles at 50°C, while high-voltage LMO||Li cells exhibited 93% capacity retention at 0.2C over 50 cycles. These results highlight the crosslinked PCIL-SPE's ability to operate effectively in demanding solid-state lithium metal battery (LMB) configurations, even with high-energy-density cathodes.

Thus, the synergistic combination of crosslinking and concentrated ionic liquids provides a pathway for developing high-performance PEO-based SPEs that meet the rigorous demands of advanced energy storage systems. This study not only contributes to the advancement of PEO-based solid-state electrolytes but also underscores the potential of crosslinked ionic liquid systems for achieving high energy densities, enhanced safety, and extended cycling stability, paving the way for their practical application in next-generation battery technologies.

4.5 References

1. Armand, M. Polymer solid electrolytes - an overview. *Solid State Ion.* **9–10**, 745–754 (1983).
2. Fenton, D. E., Parker, J. M. & Wright, P. V. Complexes of alkali metal ions with poly(ethylene oxide). *Polymer* **14**, 589 (1973).
3. Xue, Z., He, D. & Xie, X. Poly(ethylene oxide)-based electrolytes for lithium-ion batteries. *J. Mater. Chem. A* **3**, 19218–19253 (2015).
4. Xiao, S., Ren, L., Liu, W., Zhang, L. & Wang, Q. High-voltage polymer electrolytes: Challenges and progress. *Energy Storage Mater.* **63**, 102970 (2023).
5. Gadjourova, Z., Andreev, Y. G., Tunstall, D. P. & Bruce, P. G. Ionic conductivity in crystalline polymer electrolytes. *Nature* **412**, 520–523 (2001).
6. Chen, L. *et al.* PEO/garnet composite electrolytes for solid-state lithium batteries: From "ceramic-in-polymer" to "polymer-in-ceramic". *Nano Energy* **46**, 176–184 (2018).
7. Song, X. *et al.* Unraveling the Synergistic Coupling Mechanism of Li^+ Transport in an "Ionogel-in-Ceramic" Hybrid Solid Electrolyte for Rechargeable Lithium Metal Battery. *Adv. Funct. Mater.* **32**, 2108706 (2022).
8. Zhang, X. *et al.* Vertically Aligned and Continuous Nanoscale Ceramic–Polymer Interfaces in Composite Solid Polymer Electrolytes for Enhanced Ionic Conductivity. *Nano Lett.* **18**, 3829–3838 (2018).
9. Porcarelli, L., Gerbaldi, C., Bella, F. & Nair, J. R. Super Soft All-Ethylene Oxide Polymer Electrolyte for Safe All-Solid Lithium Batteries. *Sci. Rep.* **6**, 19892 (2016).
10. Kim, G. T. *et al.* UV cross-linked, lithium-conducting ternary polymer electrolytes containing ionic liquids. *J. Power Sources* **195**, 6130–6137 (2010).
11. Armand, M., Endres, F., MacFarlane, D. R., Ohno, H. & Scrosati, B. Ionic-liquid materials for the electrochemical challenges of the future. *Nat. Mater.* **8**, 621–629 (2009).
12. Shin, J. Ionic liquids to the rescue? Overcoming the ionic conductivity limitations of polymer electrolytes. *Electrochem. Commun.* **5**, 1016–1020 (2003).
13. Falco, M. *et al.* Understanding the Effect of UV-Induced Cross-Linking on the Physicochemical Properties of Highly Performing PEO/LiTFSI-Based Polymer Electrolytes. *Langmuir*. 2019, 35, 25, 8210–8219 (2019)
14. Watanabe, M., Nagano, S., Sanui, K. & Ogata, N. Ionic Conductivity of Network Polymers from Poly(ethylene oxide) Containing Lithium Perchlorate. *Polym. J.* **18**, 809–817 (1986).
15. Joost, M. *et al.* Ionic mobility in ternary polymer electrolytes for lithium-ion batteries. *Electrochimica Acta* **86**, 330–338 (2012).
16. Gerbaldi, C. *et al.* UV-cured polymer electrolytes encompassing hydrophobic room temperature ionic liquid for lithium batteries. *J. Power Sources* **195**, 1706–1713 (2010).

17. Nair, J. R. *et al.* UV-cured methacrylic membranes as novel gel–polymer electrolyte for Li-ion batteries. *J. Power Sources* **178**, 751–757 (2008).
18. Yoshida, K. *et al.* Oxidative-Stability Enhancement and Charge Transport Mechanism in Glyme–Lithium Salt Equimolar Complexes. *J. Am. Chem. Soc.* **133**, 13121–13129 (2011).
19. Wang, J. *et al.* Superconcentrated electrolytes for a high-voltage lithium-ion battery. *Nat. Commun.* **7**, 12032 (2016).
20. Suo, L. *et al.* "Water-in-salt" electrolyte enables high-voltage aqueous lithium-ion chemistries. *Science* **350**, 938–943 (2015).
21. Gao, X., Wu, F., Mariani, A. & Passerini, S. Concentrated Ionic-Liquid-Based Electrolytes for High-Voltage Lithium Batteries with Improved Performance at Room Temperature. *ChemSusChem* **12**, 4185–4193 (2019).
22. Chen, F., Howlett, P. & Forsyth, M. Na-Ion Solvation and High Transference Number in Superconcentrated Ionic Liquid Electrolytes: A Theoretical Approach. *J. Phys. Chem. C* **122**, 105–114 (2018).
23. Chen, C.-Y. *et al.* Ionic liquid electrolytes with high sodium ion fraction for high-rate and long-life sodium secondary batteries. *J. Power Sources* **332**, 51–59 (2016).
24. Giffin, G. A., Moretti, A., Jeong, S. & Passerini, S. Decoupling effective Li+ ion conductivity from electrolyte viscosity for improved room-temperature cell performance. *J. Power Sources* **342**, 335–341 (2017).
25. Pal, U. *et al.* Enhanced ion transport in an ether aided super concentrated ionic liquid electrolyte for long-life practical lithium metal battery applications. *J. Mater. Chem. A* **8**, 18826–18839 (2020).
26. Pal, U. *et al.* Improved Li-Ion Transport by DME Chelation in a Novel Ionic Liquid-Based Hybrid Electrolyte for Li–S Battery Application. *J. Phys. Chem. C* **122**, 14373–14382 (2018).
27. Pal, U. *et al.* Interphase control for high performance lithium metal batteries using ether aided ionic liquid electrolyte. *Energy Environ. Sci.* **15**, 1907–1919 (2022).
28. Pal, U. *et al.* Developing a High-Performing Spinel LiMn2O4 Cathode Material with Unique Morphology, Fast Cycling and Scaled Manufacture. *Batter. Supercaps* **7**, e202400072 (2024).
29. He, R. & Kyu, T. Effect of Plasticization on Ionic Conductivity Enhancement in Relation to Glass Transition Temperature of Crosslinked Polymer Electrolyte Membranes. *Macromolecules* **49**, 5637–5648 (2016).
30. Zhang, M. et al. Advanced High-Voltage Electrolyte Design Using Poly(ethylene Oxide) and High-Concentration Ionic Liquids for All-Solid-State Lithium-Metal Batteries. ACS Appl. Mater. Interfaces 2024, 16, 56095−56105 (2024).
31. Al-Masri, D., Yunis, R., Hollenkamp, A. F. & Pringle, J. M. Designing Solid-State Electrolytes through the Structural Modification of a High-Performing Ionic Liquid. *ChemElectroChem* **7**, 4118–4123 (2020).

32. Jin, L. *et al.* Structure and Transport Properties of a Plastic Crystal Ion Conductor: Diethyl(methyl)(isobutyl)phosphonium Hexafluorophosphate. *J. Am. Chem. Soc.* **134**, 9688–9697 (2012).
33. Susan, Md. A. B. H., Kaneko, T., Noda, A. & Watanabe, M. Ion Gels Prepared by in Situ Radical Polymerization of Vinyl Monomers in an Ionic Liquid and Their Characterization as Polymer Electrolytes. *J. Am. Chem. Soc.* **127**, 4976–4983 (2005).
34. Joost, M., Kim, G. T., Winter, M. & Passerini, S. Phase stability of Li-ion conductive, ternary solid polymer electrolytes. *Electrochimica Acta* **113**, 181–185 (2013).
35. Berthier, Claude et al. "Microscopic investigation of ionic conductivity in alkali metal salts-poly(ethylene oxide) adducts." *Solid State Ionics* 11 (1983): 91-95.
36. Stettner, T., Lingua, G., Falco, M., Balducci, A. & Gerbaldi, C. Protic Ionic Liquids-Based Crosslinked Polymer Electrolytes: A New Class of Solid Electrolytes for Energy Storage Devices. *Energy Technol.* **8**, 2000742 (2020).
37. Kimura, K., Motomatsu, J. & Tominaga, Y. Correlation between Solvation Structure and Ion-Conductive Behavior of Concentrated Poly(ethylene carbonate)-Based Electrolytes. *J. Phys. Chem. C* **120**, 12385–12391 (2016).
38. Nguyen, H. T. T. *et al.* Facile Li^+ Transport in Interpenetrating O- and F-Containing Polymer Networks for Solid-State Lithium Batteries. *Adv. Funct. Mater.* **33**, 2213469 (2023).
39. Xu, K., Ding, S. P. & Jow, T. R. Toward Reliable Values of Electrochemical Stability Limits for Electrolytes. *J. Electrochem. Soc.* **146**, 4172–4178 (1999).
40. Herbers, L. *et al.* The Influence of Polyethylene Oxide Degradation in Polymer-Based Electrolytes for NMC and Lithium Metal Batteries. *Adv. Energy Sustain. Res.* **4**, 2300153 (2023).
41. Porcarelli, L., Gerbaldi, C., Bella, F. & Nair, J. R. Super Soft All-Ethylene Oxide Polymer Electrolyte for Safe All-Solid Lithium Batteries. *Sci. Rep.* **6**, 19892 (2016).
42. Herbers, L., Küpers, V., Winter, M. & Bieker, P. An ionic liquid- and PEO-based ternary polymer electrolyte for lithium metal batteries: an advanced processing solvent-free approach for solid electrolyte processing. *RSC Adv.* **13**, 17947–17958 (2023).
43. Homann, G. *et al.* Poly(Ethylene Oxide)-based Electrolyte for Solid-State-Lithium-Batteries with High Voltage Positive Electrodes: Evaluating the Role of Electrolyte Oxidation in Rapid Cell Failure. *Sci. Rep.* **10**, 4390 (2020).
44. Wang, W. *et al.* Solid polymer electrolytes based on the composite of PEO–LiFSI and organic ionic plastic crystal. *Chem. Phys. Lett.* **747**, 137335 (2020).
45. Ji, Y., Zhang, Y.-H., Shi, F.-N. & Zhang, L.-N. UV-derived double crosslinked PEO-based solid polymer electrolyte for room temperature. *J. Colloid Interface Sci.* **629**, 492–500 (2023).
46. Zhang, Y. *et al.* Cross-linking network based on Poly(ethylene oxide): Solid polymer electrolyte for room temperature lithium battery. *J. Power Sources* **420**, 63–72 (2019).

47. Wetjen, M., Kim, G.-T., Joost, M., Winter, M. & Passerini, S. Temperature dependence of electrochemical properties of cross-linked poly(ethylene oxide) lithium bis(trifluoromethanesulfonyl)imide–N-butyl-N-methylpyrrolidinium bis(trifluoromethanesulfonyl)imide solid polymer electrolytes for lithium batteries. *Electrochimica Acta* **87**, 779–787 (2013).

Chapter 5

Advanced High-Voltage Electrolyte Design Using Poly(ethylene oxide) and High-Concentration Ionic Liquids for All-Solid-State Lithium Metal Batteries

5.1 Introduction

The transition towards sustainable energy systems has heightened the demand for advanced energy storage technologies, particularly for applications in electric vehicles, aviation, and large-scale energy storage. Solid-state LMBs are increasingly viewed as the next-generation solution due to their superior energy density and enhanced safety compared to conventional LIBs.[1] However, substantial obstacles remain in developing suitable solid electrolytes that can deliver both high ionic conductivity and electrochemical stability, which are crucial for the performance and longevity of these batteries. Among the various solid electrolyte options, SPEs hold particular promise due to their inherent safety, processability, and compatibility with lithium metal anodes.[2,3] Despite these advantages, the majority of SPEs require liquid plasticizers to achieve adequate ionic conductivity and good electrode wettability, introducing risks such as flammability and leakage like liquid electrolytes that compromise the safety of solid state LMBs.[4–6] Consequently, designing all-solid-state SPE systems that maintain both high performance and safety is still a significant challenge.

PEO has been the most extensively studied polymer for SPEs, owing to its capacity to coordinate lithium ions and form a stable interface with lithium

metal.[7,8,9] High molecular weight PEO has demonstrated additional benefits, such as dendrite suppression and improved cycling stability due to its mechanical strength, making it suitable for flexible membrane formation.[10] However, PEO-based SPEs face two critical challenges: low room-temperature ionic conductivity (typically up to 10^{-6} S cm^{-1}) and a limited electrochemical stability window (ESW) of under 4 V vs. Li^+/Li. These limitations arise primarily from the semi-crystalline nature of PEO, which restricts ion mobility, and the oxidative instability of ether oxygen groups, which limits the operational voltage range of PEO-based electrolytes in high-voltage LMBs.[9]

To address these limitations, extensive research has focused on various strategies, including the incorporation of inorganic fillers,[11–13] ionic liquids,[14] and complex polymer architectures,[15–18], as well as the introduction of crosslinked networks.[19,20] Ionic liquid (IL)-based electrolytes have attracted particular interest due to their exceptional thermal and electrochemical stability, non-flammability, and low vapor pressure.[21] Studies have shown that incorporating ILs in SPEs can enhance ionic conductivity and broaden the electrochemical stability window. Early work by Howlett et al. and others demonstrated that ILs offer promising physical and electrochemical properties for LMBs,[22–24] while subsequent studies by Susan et al. revealed that combining ILs with compatible polymers can create "ion gels" with increased thermal stability and high ionic conductivity at ambient temperatures .[25]

The recent emergence of high-concentration ionic liquid (HCIL) electrolytes has provided a new pathway for improving ion transport and electrochemical stability in lithium metal batteries.[26–28] HCIL electrolytes leverage high salt concentrations to alter ion dynamics, creating more efficient transport pathways within the electrolyte matrix. This approach has been shown to improve lithium-ion transference numbers, enhance electrochemical stability, and support rapid charge-discharge rates.[29,30] Research by Pal et al. demonstrated that an ether-aided super-concentrated ionic liquid electrolyte could significantly enhance ion transport and interfacial stability with lithium metal electrodes.[31–33]

Building upon these insights, this study introduces a "polymer-in-high-concentrated ionic liquid" (PiHCIL) SPE, designed to optimize the ionic conductivity and electrochemical stability of PEO-based systems for all-solid-state LMBs. The PiHCIL-SPE is composed of high-molecular-weight PEO, lithium bis(fluorosulfonyl)imide (LiFSI) salt, and N-propyl-N-methylpyrrolidinium bis(fluorosulfonyl)imide (C3mpyrFSI) ionic liquid. By varying the ratio of PEO to LiFSI and IL, this study explores the impact of HCIL concentration on the physical and electrochemical properties of the PiHCIL-SPE. The structural and electrochemical behavior of these materials was analyzed using Fourier-transform infrared (FTIR) spectroscopy and solid-state magic angle spinning (MAS) nuclear magnetic resonance (NMR) spectroscopy, offering insights into the coordination and solvation environment of Li^+ ions within the polymer matrix.

Through this novel "PEO-in-HCIL" strategy, the study aims to address the existing limitations of PEO-based SPEs by enhancing ionic conductivity, expanding the electrochemical stability window, and maintaining mechanical

integrity. The research sheds light on the potential of HCILs to facilitate the development of high-performance SPEs for advanced all-solid-state LMBs, paving the way for safer, more efficient energy storage solutions.

5.2 Methodology

The preparation and characterization of the designed PiHCIL-SPEs were conducted following a similar solvent casting technique and experimental setup described in the previous chapter (see Chapter 4). To adapt the methodology for the various high-concentration ionic liquid systems, specific variations in processing and characterization parameters are highlighted below.

5.2.1 Preparation of PiHCIL-SPE Membranes

The PiHCIL-SPEs were synthesized using solvent casting in an argon-filled glovebox, as depicted in Chapter 4. The process involved dissolving LiFSI and C3mpyrFSI in a 1:1 molar ratio to form the high-concentration ionic liquid (HCIL) mixture, followed by mixing with various amounts of PEO in acetonitrile. Four compositions were prepared with EO:Li:IL molar ratios of 8:1:1, 10:1:1, 15:1:1, and 20:1:1. These solutions were cast into silicon molds, left for slow solvent evaporation over 48 hours, and then hot-pressed under conditions identical to those in chapter 4 to form homogenous, free-standing membranes with a thickness of 120 ± 10 µm (Figure 5-1). The membranes produced in this chapter are named PiHCIL-$SPE_{x:1:1}$, where *x* represents the PEO content.

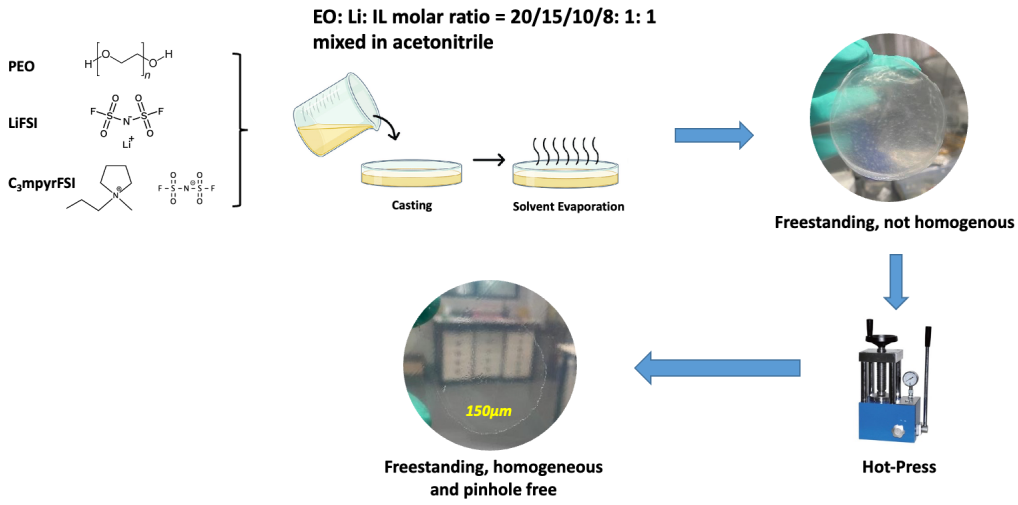

Figure 5 - 1. Free-standing PiHCIL-SPE membrane preparation by solvent casting. Adapted from Zhang et al. ACS Appl. Mater. Interfaces 2024, 16, 41, 56095–56105.

5.2.2 Characterization Techniques

The following characterization techniques were applied to assess the physical and electrochemical properties of the PiHCIL-SPEs. For detailed experimental setup and instrumentation specifications, refer to Chapter 3 and 4.

- **Differential Scanning Calorimetry (DSC)**: Used to assess phase behavior of the prepared PiHCIL-SPEs. DSC measurements were performed from -120 to 80 °C. A 10 °C min^{-1} heating and 20 °C min^{-1} cooling rate was used and the sample loading was about 15 mg. The DSC curves provide insights into the crystallinity and glass transition temperatures of the various PiHCIL-SPE compositions.
- **Scanning electron microscope (SEM)**: SEM analysis was carried out for the pristine PiHCIL-SPEs as well as cycled cells. A coin cell disassembly unit (Hohsen) was used inside glove-box to disassemble the cycled cells.
- **Electrochemical Impedance Spectroscopy (EIS)**: To measure ionic conductivity. EIS measurements were performed across a temperature range of 20–70 °C in a stainless steel (SS) coin cell configuration. The setup and calculation methods, including the calculation of bulk resistance, were consistent with the procedures detailed in Chapter 4.
- **Fourier-Transform Infrared (FTIR) Spectroscopy**: FTIR spectra were obtained to examine cation-polymer and cation-anion interactions in the PiHCIL-SPEs. This analysis specifically targeted the -SNS stretching modes of the FSI^- anions, facilitating comparison of coordination environments between different compositions.
- **Thermogravimetric Analysis (TGA)**: Thermal stability was assessed using TGA, following the same protocol as described in Chapter 4.
- **Solid-State Magic Angle Spinning (MAS) NMR**: To probe cation-polymer and cation-anion interactions at a molecular level, solid-state MAS NMR spectroscopy was employed. Both 1-D ^{7}Li and ^{19}F spectra and 2-D ^{19}F-^{7}Li heteronuclear correlation (HETCOR) spectra were acquired to analyze Li^+ coordination environments within the PiHCIL-SPE matrix.

5.2.3 Composite Cathode Preparation

The composite LFP (c-LFP) and LMO (c-LMO) electrodes were prepared by mixing LFP or LMO powder, Super C65 and our prepared $SPE_{20:1:1}$ as the binder in 80:10:10 wt% in acetonitrile. The slurry was mixed until smooth and cast using a doctor-blade on carbon-coated aluminium foil. The obtained c-LFP and c-LMO electrodes have an average cathode mass loading of 2.5 and 3 mg cm^{-2} and an areal capacity of 0.46 and 0.45 mAh cm^{-2}, respectively. The composite cathodes were then cut into 8 mm diameter discs and vacuum-dried at 50 °C for 24 h prior to cell assembly.

5.2.4 Cell Assembly and Electrochemical Measurements

Cell assembly of the all-solid-state LMB cells followed the protocols described in Chapter 4. All electrochemical measurements including Li transference number, electrochemical stability, and the galvanostatic cycling for Li||Li, Li||c-LFP, and Li||c-LMO cells were carried out following the same protocols described in Chapter 4. The reproducibility of the results has been checked by multiple tests.

5.3 Results and Discussion

This section presents the key findings from the characterization of prepared PiHCIL-SPEs, focusing on how different EO:Li:IL ratios influence the phase behavior, ionic conductivity, and electrochemical performance of the designed SPEs.

5.3.1 PiHCIL-SPE Membranes

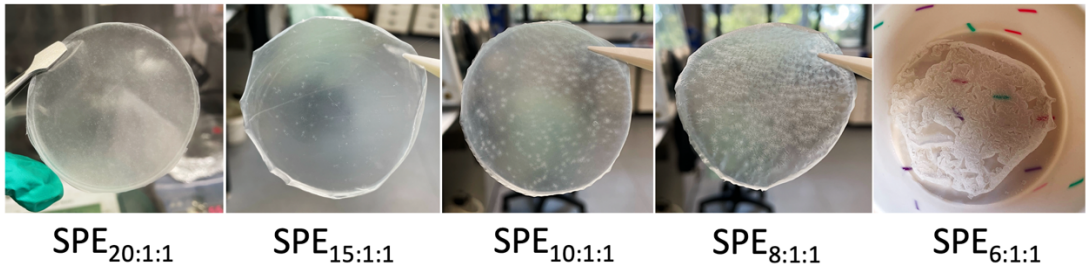

Figure 5 - 2. Different PiHCIL-SPE systems prepared by solvent casting. Adapted from Zhang et al. ACS Appl. Mater. Interfaces 2024, 16, 41, 56095–56105.

Various PiHCIL-SPE systems were prepared using a solvent casting method. As shown in Figure 5-2, phase separation was observed in higher HCIL concentration systems, such as $SPE_{10:1:1}$ and $SPE_{8:1:1}$. In the case of $SPE_{6:1:1}$, the PEO matrix is unable to accommodate the excess amount of HCIL, failing the formation of a homogenous, free-standing membrane. Therefore, we consider that $SPE_{6:1:1}$ surpasses the solubility limit of IL within the PEO matrix.

5.3.2 Phase Behavior

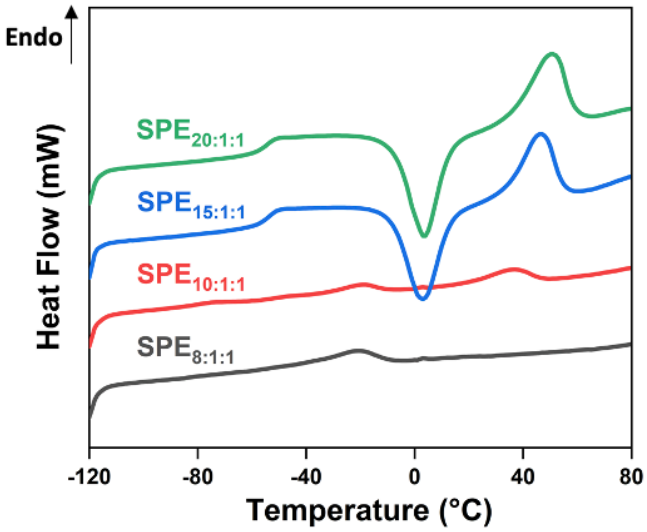

Figure 5 - 3. Phase behavior of different PiHCIL-SPE systems obtained from DSC measurements. Adapted from Zhang et al. ACS Appl. Mater. Interfaces 2024, 16, 41, 56095–56105.

Differential scanning calorimetry (DSC) was used to investigate the phase transitions and glass transition temperatures (T_g) of the PiHCIL-SPEs with varying EO:Li:IL ratios (Figure 5-3). PEO is a semi-crystalline polymer with a melting transition around 65 °C.[7] The results indicate that increasing the concentration of high-concentration ionic liquid (HCIL) in the PEO matrix progressively reduces the crystallinity of PEO. For instance, in the PiHCIL-SPE with a 20:1:1 ratio, a melting point transition is observed at 50 °C, with a T_g at -55 °C, suggesting a semi-crystalline structure with both amorphous and crystalline phases. By increasing the HCIL content to 10:1:1 ratio, the melting transition is further decreased in both temperature and enthalpy, accompanied by a significant reduction in T_g (-76 °C). This notable decrease in T_g in $SPE_{10:1:1}$, compared to $SPE_{20:1:1}$ or $SPE_{15:1:1}$, likely results from altered interactions between the polymer chains and the Li^+ ions in the presence of FSI^- anions which will be further discussed. As the ratio decreases to 8:1:1, the melting transition disappears entirely, and T_g shifts to -79 °C, indicating a fully amorphous structure that supports enhanced ionic mobility. Notably, in samples with higher HCIL content ($SPE_{8:1:1}$ and $SPE_{10:1:1}$), a small peak at approximately -20°C appears, attributed to a phase transition in C_3mpyrFSI/LiFSI ionic liquid, indicating the IL solubility limit in the PEO matrix and potential phase separation.[30,34]

This transition from semi-crystalline to amorphous structure as HCIL concentration increases supports the hypothesis that high HCIL concentrations create favorable ion transport pathways within the polymer matrix. The presence of both free and coordinated FSI^- anions in higher HCIL ratios likely contributes to a

more interconnected ion network, as confirmed by additional FTIR and NMR analyses discussed below.

5.3.3 Ionic Conductivity

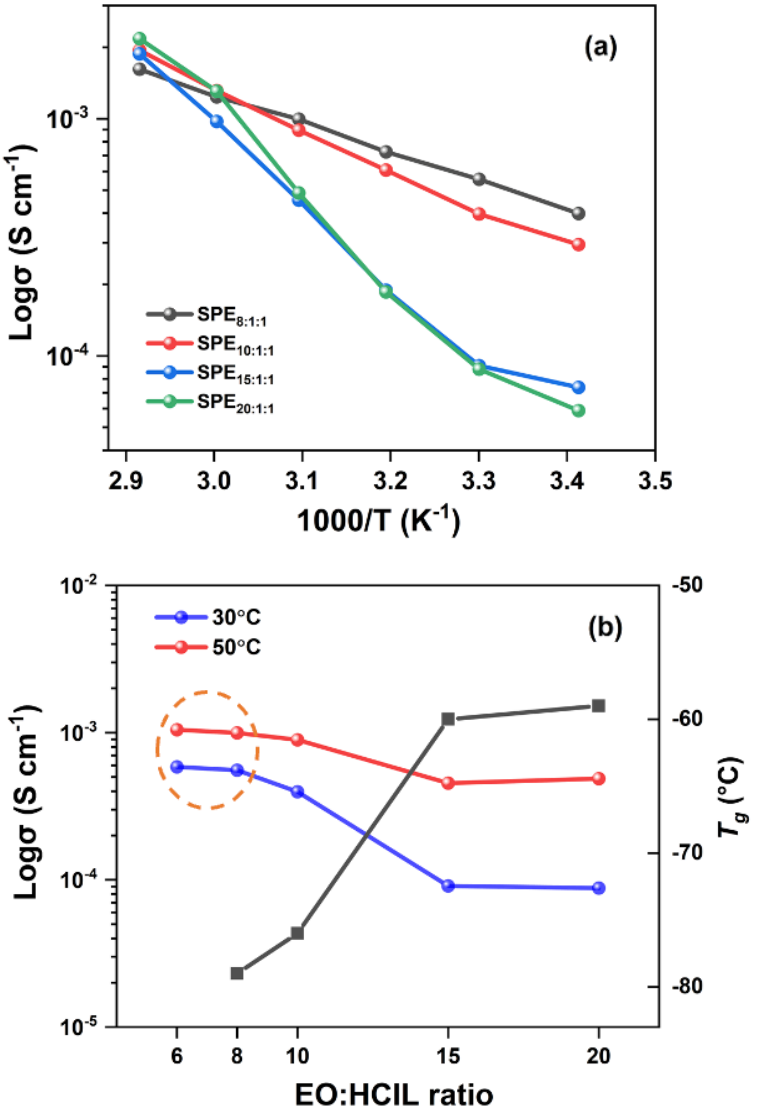

Figure 5 - 4. (a) Ionic conductivities of different PiHCIL-SPE systems in the temperature range 20−70°C. (b) Ionic conductivities of the PiHCIL-SPEs at 30 and 50 °C and their T_g as a function of EO:HCIL ratio. Adapted from Zhang et al. ACS Appl. Mater. Interfaces 2024, 16, 41, 56095–56105.

The impact of HCIL on the ionic conductivity of the prepared SPEs is detailed in Figure 5-4. The data reveal a clear trend of increasing ionic conductivity with higher HCIL content (Fig. a). The conductivity values for $SPE_{20:1:1}$ and $SPE_{15:1:1}$ are very similar, consisting with their comparable melting transitions and T_g values (Figure 5-2). They exhibit a sharp increase in ionic conductivity from the order of 10^{-5} S cm^{-1} at 30 °C to 10^{-3} S cm^{-1} at 70 °C, consistent with the DSC data showing a melting transition at 35 °C (onset) to 65 °C (end). Furthermore, there is a significant rise in ionic conductivity from $SPE_{15:1:1}$ (9.1 x10^{-5} S cm^{-1} at 30 °C) to

$SPE_{10:1:1}$ (4 $x10^{-4}$ S cm^{-1} at 30 °C) and $SPE_{8:1:1}$ (5.56 $x10^{-4}$ S cm^{-1} at 30 °C), suggesting that HCIL enhances overall ionic mobility. This is confirmed by DSC data, where the crystallization peak diminishes for $SPE_{10:1:1}$ and disappears for $SPE_{8:1:1}$. No gain in ionic conductivity is observed above 8:1:1 ratio (Fig. b) and excess IL starts to exude from the polymer matrix in $SPE_{6:1:1}$, indicating a potential HCIL solubility limit in the PEO chain.[35] Therefore, we speculate that $SPE_{8:1:1}$ represents an optimal EO:Li:IL ratio, favoring high ambient temperature ionic conductivity which is closely approximating that of HCIL liquid electrolytes.[31]

5.3.4 Microstructure

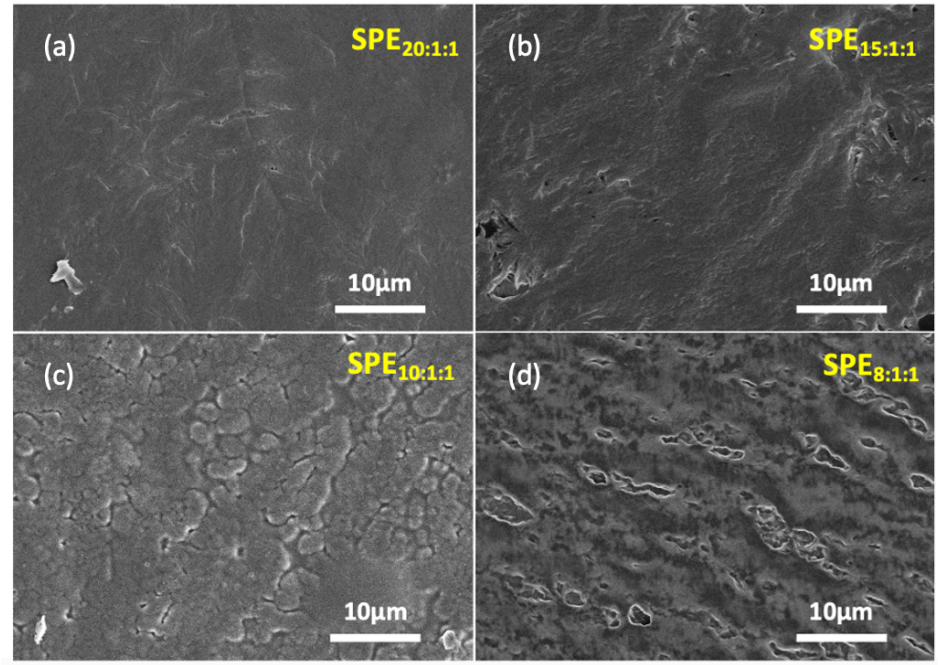

Figure 5 - 5. SEM revealing the surface morphology of different PiHCIL-SPEs. Adapted from Zhang et al. ACS Appl. Mater. Interfaces 2024, 16, 41, 56095–56105.

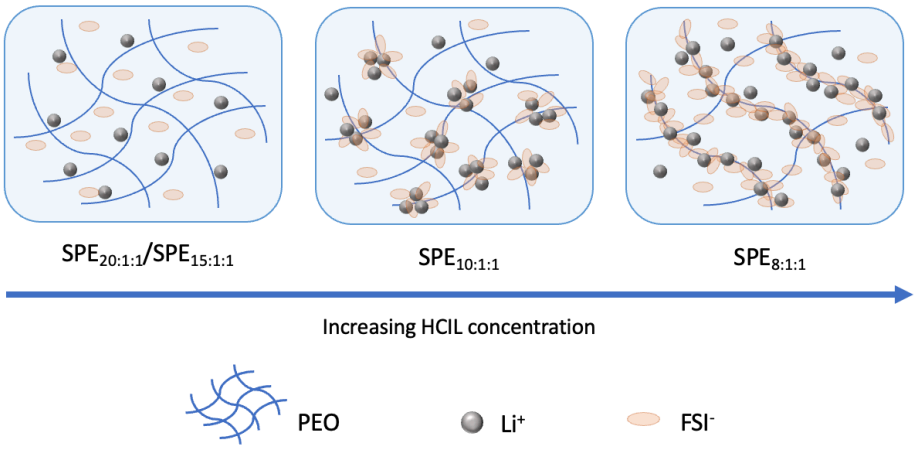

Figure 5 - 6. A schematic morphology model of different PiHCIL-SPEs systems. Adapted from Zhang et al. ACS Appl. Mater. Interfaces 2024, 16, 41, 56095–56105.

The surface morphology of the prepared PiHCIL-SPEs was characterized by SEM and shown in Figure 5-5. With high PEO content and low HCIL presence (i.e., $SPE_{20:1:1}$ and $SPE_{15:1:1}$), the SPEs show a relatively dense and smooth surface (Fig. a and b), highlighting the good miscibility of PEO and HCIL. With decreasing PEO content, a heterogeneous microstructure is observed (Fig. c), indicating the formation of separated phases, most likely approaching the miscibility limit of HCIL into the polymer. When the ratio reaches 8:1:1, a porous, interconnected and locally aligned ion conducting network is formed (Fig. d). It can be proposed that at high polymer content, most LiFSI can be dissociated by the PEO backbone, and most FSI^- anions exist as free ions. Li^+ ions mainly transfer via chain segmental motion.[36] Therefore, ionic conductivity increases slowly with increasing HCIL content due to increased charge carrier amounts; whereas at low polymer content, and high HCIL content, a considerable amount of LiFSI cannot be dissociated, and together with the anions from the IL they can form aggregated ion clusters, resulting in phase separation and pores in the system. The ion conduction behavior in this case can be explained by a "polymer-in-salt" percolation model where high salt content favors the formation of an ion conductive network composed of interconnected ion clusters that provide percolation pathways for fast ion transport.[37,38] Consistent with the polymer-in-salt system,[36] in $SPE_{8:1:1}$, the excessive FSI^- anions from both LiFSI and C_3mpyrFSI form interconnected cluster networks and pores as shown in Fig. d4. Interestingly, these connected ion clusters and pores also happen to be locally aligned, which can provide direct pathways for Li^+ transport, reducing tortuosity. This can lead to more efficient ion transport and higher conductivity. The pores may help accommodate volume change during cell cycling, potentially enhancing mechanical stability and longevity of the SPE. Figure 5-6 shows a proposed morphology model to help understand the structural change and ion dynamics in the prepared PiHCIL-SPEs.

5.3.5 Coordination Environment through FTIR and MAS solid-state NMR

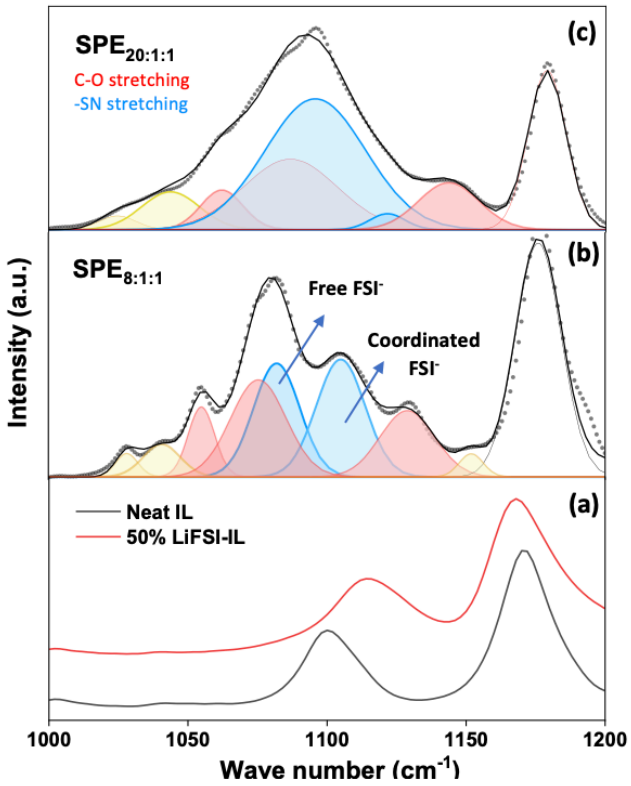

Figure 5 - 7. FTIR spectra of $SPE_{8:1:1}$ and $SPE_{20:1:1}$. Neat IL and 50 mol% LiFSI-IL were measured for reference. Adapted from Zhang et al. ACS Appl. Mater. Interfaces 2024, 16, 41, 56095–56105.

FTIR was used to investigate the changes of cation-polymer and cation-anion interactions in the prepared PiHCIL-SPEs as shown in Figure 5-7. In the region between 1000 and 1200 cm^{-1}, a vibrational peak at 1100 cm^{-1} from the neat IL (Fig. a) is assigned to the -SNS symmetric stretching from the FSI^- anions.[39] Our previous work showed that adding 50 mol% LiFSI salt to the neat IL shifted this peak to 1115 cm^{-1} which was attributed to the increased coordination between Li^+ and FSI^- anions.[31] After adding PEO (Fig. b), the -SNS stretching peak shifts to lower wavenumbers and splits into free FSI^- and coordinated FSI^- (blue), indicating a coordination environment change of the FSI^- anions that may be due to the introduced Li^+-EO coordination in $SPE_{8:1:1}$. As PEO content increases, the coordinated FSI^- peak dramatically decreased leaving mainly free FSI^- in the $SPE_{20:1:1}$ (Fig. c). Additionally, three -CO stretching peaks (red) from PEO shifted to higher wavenumbers, suggesting a coordination environment change of the -CO groups which may be due to increased Li^+-EO coordination and this is consistent with PEO-salt systems.[40,41] Therefore, summarily it can be stated that increasing HCIL concentration in the PEO matrix results in more coordinated FSI^- anions, leading to the formation of a connected anion-rich ion conducting phase that can be further supported by the microstructure analysis in Figure 5-5. These separated

phases might also decrease the crystalline regions of PEO, leading to higher chain mobility, improving the ionic conductivity and thus faster Li^+ transport.

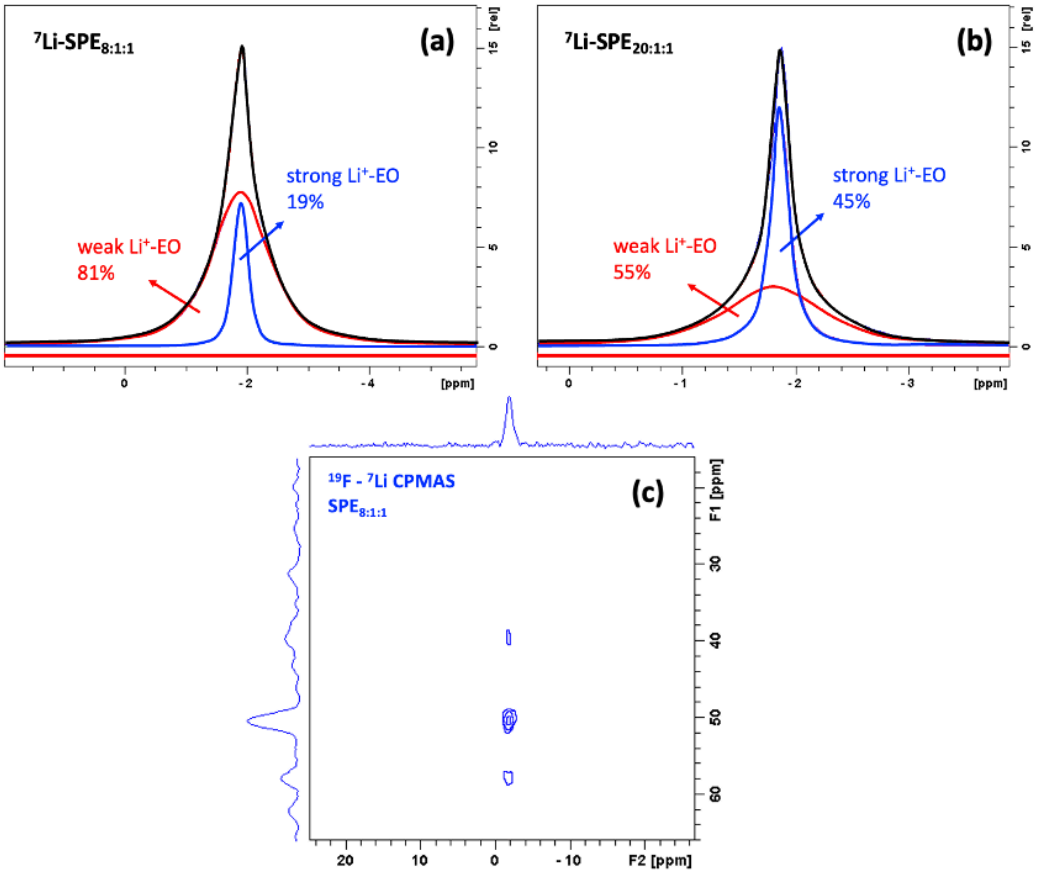

Figure 5 - 8. (a,b) Deconvoluted ^{7}Li solid-state MAS NMR spectra of $SPE_{8:1:1}$ and $SPE_{20:1:1}$. (c) $^{19}F-^7Li$ HETCOR spectrum of $SPE_{8:1:1}$. Adapted from Zhang et al. ACS Appl. Mater. Interfaces 2024, 16, 41, 56095–56105.

To further illustrate the Li^+ coordination environment in the PiHCIL-SPEs, solid-state MAS NMR experiments were performed (Figure 5-8). Analysis of the asymmetric ^{7}Li signals shows two Li^+ environments (Fig. a and b) Consistent with Greenbaum's work,[42] the right peak (45% of total integral) in $SPE_{20:1:1}$ is assigned to the Li^+ ions closely bound to the EO units which can be considered as solvated Li^+. The left peak (55% of total integral) represents Li^+ ions that have weakened Li^+-EO interactions which are less restricted and behave more as in ionic states. As HCIL concentration increases, $SPE_{8:1:1}$ shows 81% weakly coordinated Li^+ and only 19% strongly bonded Li^+, indicating more Li^+ ions escape from strong Li^+-EO interactions to the disordered environment where they possess a higher degree of freedom. Thus, the addition of HCIL can mitigate the affinity between EO and Li^+ interaction which is consistent with the FTIR results. Previous research has shown that Li^+ ions are more mobile in disordered environments, promoting faster ion transport.[43] This is consistent with our EIS analysis where $SPE_{8:1:1}$ shows the

highest ionic conductivity. The close interactions between Li^+ and FSI^- anions are established in the $^{19}F-^{7}Li$ HETCOR spectrum shown in Fig. c, where ^{19}F shows strong cross peaks with the ^{7}Li signal. Taken together, solid-state NMR results confirm the important role of Li^+ environment to the overall ionic conductivity. The favourable Li^+ ion environment of $SPE_{8:1:1}$ promotes its superior room temperature ionic conductivity among the prepared PiHCIL-SPEs.

5.3.6 Dimensional and Thermal Stability

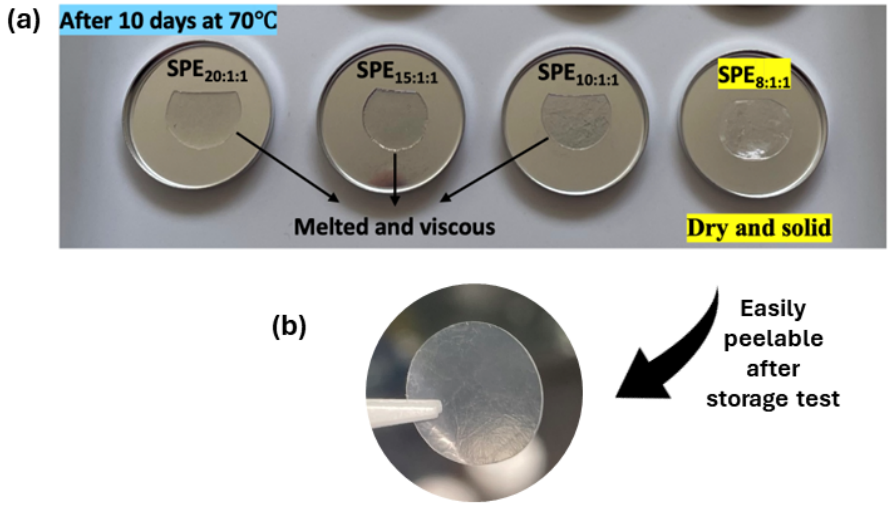

Figure 5 - 9. Thermal storage experiment. Adapted from Zhang et al. ACS Appl. Mater. Interfaces 2024, 16, 41, 56095–56105.

As Li^+ conduction in SPEs mainly relies on chain segmental motion within the polymer's amorphous regions, high salt concentration that leads to increased amorphous domains therefore facilitates faster ion transport, owing to its plasticizing effect.[44] However, this increase in ion conductivity often comes at the expense of mechanical robustness due to reduced crystallinity and increased segmental motion. This dynamic shifts with our PiHCIL-SPEs, where membrane robustness is not solely reliant on the crystalline domains. Conducting a simple storage experiment at 70 °C provides valuable insights into mechanical stability, as depicted in Figure 5-9. After 10 days storage at 70 °C, all SPEs above 8:1:1 ratio lost their dimensional integrity to some extent because of the existence of crystalline domains, as shown in the DSC results in Figure 5-3, whereas $SPE_{8:1:1}$ remained in its original shape and integrity. Hence, despite the absence of crystalline regions, $SPE_{8:1:1}$ shows high structural stability under elevated temperatures, pointing to sufficient mechanical robustness to prevent thermal deformation and potential Li dendrites penetration.

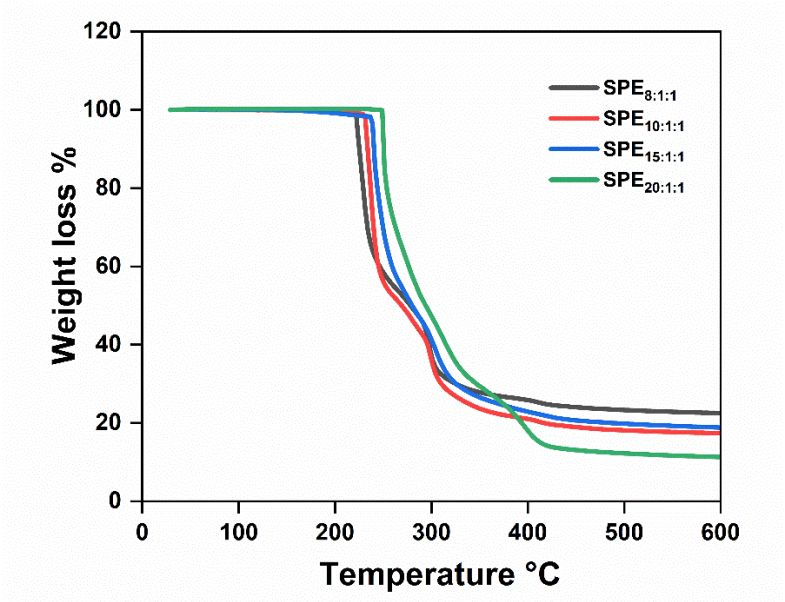

Figure 5 - 10. Thermal stability of the prepared PiHCIL-SPEs. Adapted from Zhang et al. ACS Appl. Mater. Interfaces 2024, 16, 41, 56095–56105.

Furthermore, thermal stability of SPEs is important for safe battery operation. Figure 5-10 presents the TGA results of the PiHCIL-SPEs. The negligible weight loss below 150 °C is ascribed to trapped moisture. The weight loss between 150 and 220 °C is because of the initial breakdown of LiFSI.[45] Extensive decomposition of the SPE started at above 220 °C. Adding LiFSI salt sped up the thermal breakdown of PiHCIL-SPEs.[46] Nevertheless, the PiHCIL-SPEs are still stable enough for safe use in solid-state LMBs.

5.3.7 Electrochemical Stability

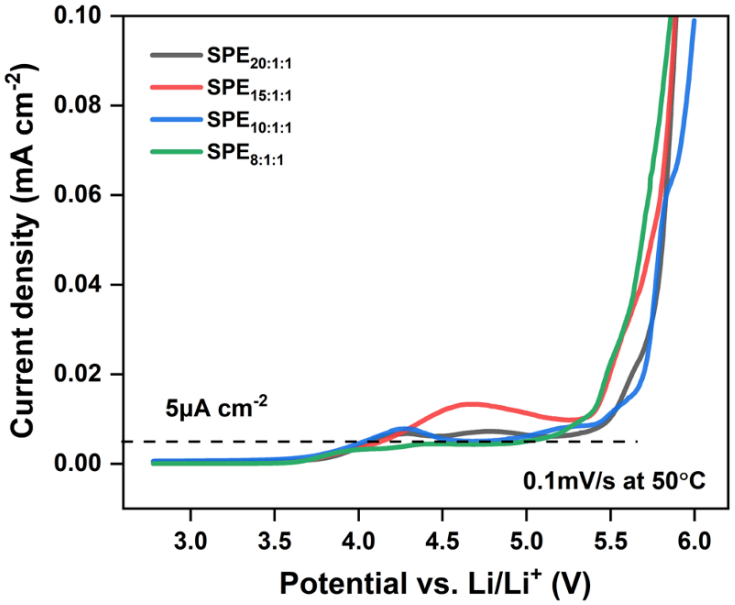

Figure 5 - 11. Electrochemical stability of the prepared PiHCIL-SPEs. Adapted from Zhang et al. ACS Appl. Mater. Interfaces 2024, 16, 41, 56095–56105.

The electrochemical stability window (ESW) of the PiHCIL-SPEs was measurred by LSV in a Li||SS cell configuration, scanning from open-circuit voltage to 6 V against Li^+/Li at a rate of 0.1 mV s^{-1}, as shown in Figure 5-11. Apart from $SPE_{8:1:1}$, all the other SPEs experienced oxidative degradation below 4 V which is commonly seen in PEO-based SPEs,[9] whereas $SPE_{8:1:1}$ showed high electrochemical stability of 5.1 V (5 µA cm^{-2} current density was used as the cut-off current [47]), far exceeding the typical stability range of PEO-based SPEs, indicating its excellent oxidation stability and potential to work with high-voltage materials. The excellent electrochemical stability of $SPE_{8:1:1}$ is likely due to the high concentration of HCIL, which promotes the polymer chains to strongly interact with Li^+ ions and FSI^- anion clusters.[48] The coordinated ions and surrounded ion clusters act like a shield, protecting EO from oxidation and reducing the highest occupied molecular orbital level of the PiHCIL-SPE,[26,49] all of which contribute to its improved oxidation stability. Thereby the $SPE_{8:1:1}$ has been chosen as the best candidate among others and will be investigated for the advanced electrochemical testing that will be discussed below.

The increased ESW highlights the potential of PiHCIL-SPEs to support high-voltage cathode materials, expanding their applicability for advanced solid-state LMBs. The presence of a shield-like layer formed by coordinated FSI^- clusters surrounding the EO units may act as a protective barrier, preventing direct oxidation of the polymer matrix and increasing the ESW.

5.3.8 Li^+ Transference Number

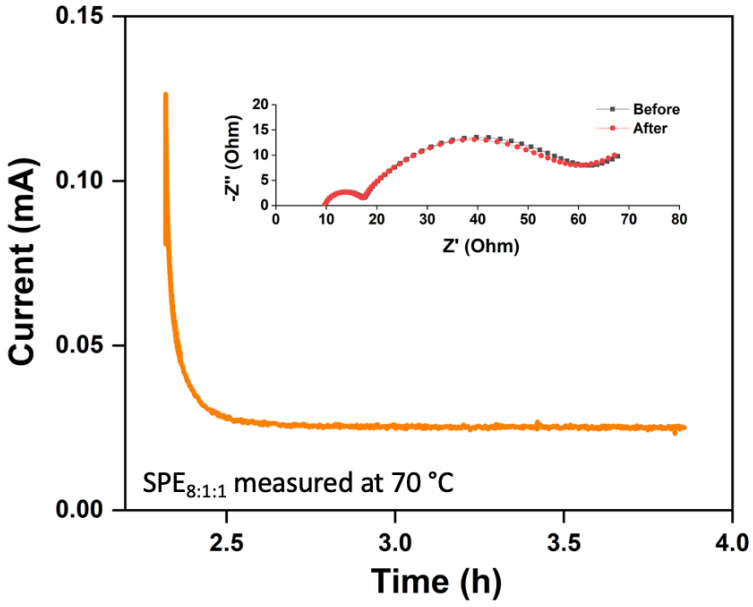

Figure 5 - 12. Change of current and impedance with time in symmetric Li|SPE8:1:1|Li cell under polarization at 10 mV and 70 °C. Adapted from Zhang et al. ACS Appl. Mater. Interfaces 2024, 16, 41, 56095–56105.

Li transference number (t_{Li+}) of the $SPE_{8:1:1}$ was measured using a Li|Li symmetric cell at 70 °C. Figure 5-12 displays the current profile following a 10 mV polarization and the insert shows the impedances of the initial state and steady state. The t_{Li+} of $SPE_{8:1:1}$ was calculated to be 0.2 which is consistent with the typical PEO system and the HCIL electrolyte.[23] Ionic conduction in PEO-based SPEs is attributed to the chain segmental motion,[50,51] where Li^+ ions coordinates with the ether oxygen on PEO backbone, leading to Li dissociation.[52] However, Li^+ movements are restricted by the strong Li^+-EO coordination, which results in relatively low ionic conductivity and low t_{Li+} (around 0.2 - 0.3).[53,54] Thereby, the transference number achieved by the $SPE_{8:1:1}$ falls within the well-accepted region supporting the previous literature reports.

5.3.9 Li Metal Stability

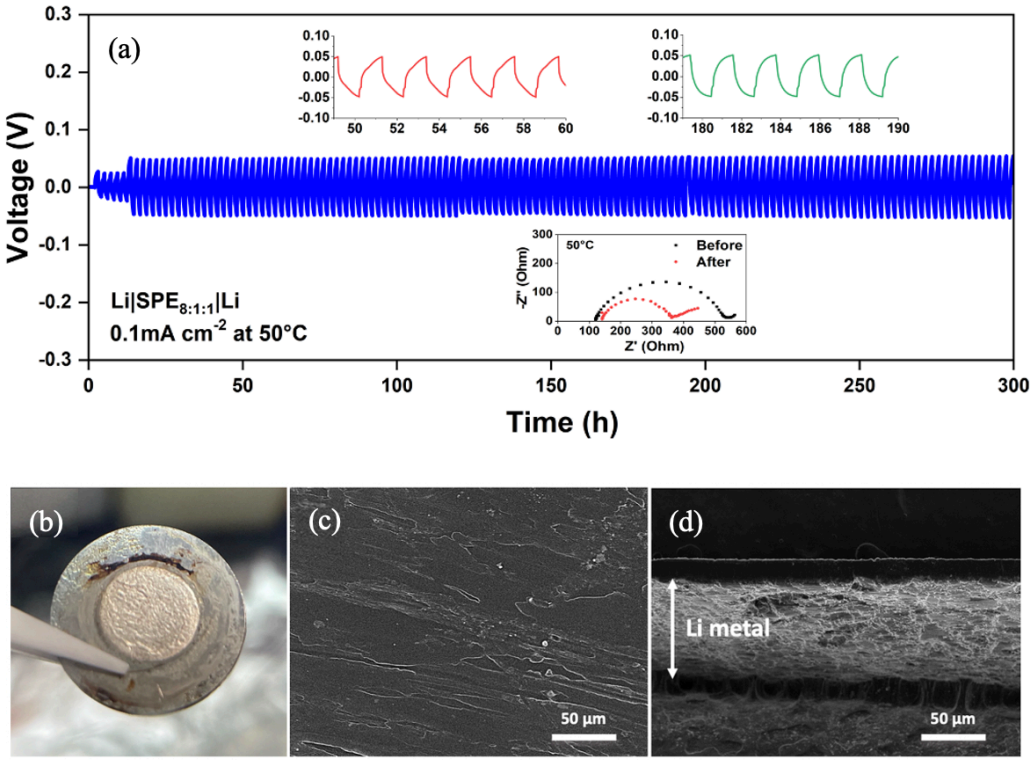

Figure 5 - 13. (a) Li||Li symmetric cell cycling of SPE8:1:1. (b-d) The surface image, surface morphology and cross-section SEM images of Li metal electrode (plated) after 150 cycles.

The interface stability between Li metal and the optimum $SPE_{8:1:1}$ was evaluated by Li plating-stripping cycling test (**Figure 5-13**). The symmetric Li|$SPE_{8:1:1}$|Li cell was cycled at constant current densities of 0.1 mA cm^{-2} for 1 hour polarisation at each step at 50 °C. As shown in **Fig. a**, stable and reversible

lithium plating–stripping was achieved over 150 cycles with minimal overpotential (50mV), and there was no sign of short circuit, indicating that $SPE_{8:1:1}$ possesses excellent compatibility with Li metal anode. The interfacial resistance decreased after 150 cycles (insert in **Fig. a**), indicating that the $SPE_{8:1:1}$ continually adjusted to enhance its contact with the lithium surface.

The surface image and morphology of Li metal after 150 cycles is shown in **Fig. b-d**. The SEM analysis of cycled cells reveals a smooth and dense Li metal surface, with no signs of Li dendrites or dead Li, indicating a uniform Li deposition process and the formation of a stable SEI layer. The cross-section SEM of the platted side displayed a uniform and dense interface, which confirmed the excellent mechanical and electrochemical properties of $SPE_{8:1:1}$ that allows it to accommodate volume changes of the Li anode, thereby sustaining facile and reversible Li plating–stripping.

These results demonstrate the role of high-concentration ionic liquids in promoting interfacial stability, as they form stable SEI layers that prevent Li dendrite formation and facilitate long-term cycling stability. The PiHCIL-SPE's ability to maintain stable Li cycling performance makes it a promising candidate for all-solid-state LMBs.

5.3.10 All solid-state LMB Performance

The best performed PiHCIL-SPE was further tested in all-solid-state LFP||Li and LMO||Li cells to assess its electrochemical performance in practical configurations.

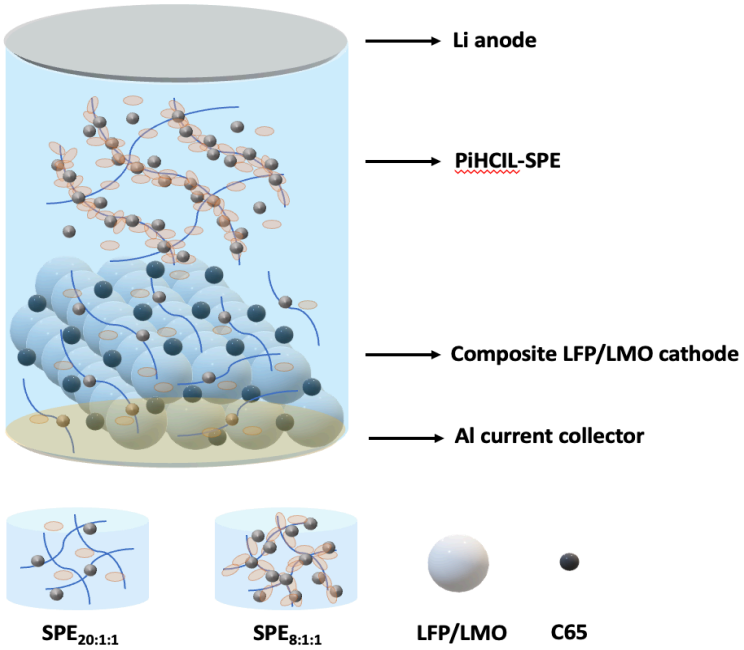

Figure 5 - 14. Schematic illustration of the assembled all-solid-state Li|$SPE_{8:1:1}$|c-LFP/c-LMO cell. Adapted from Zhang et al. ACS Appl. Mater. Interfaces 2024, 16, 41, 56095–56105.

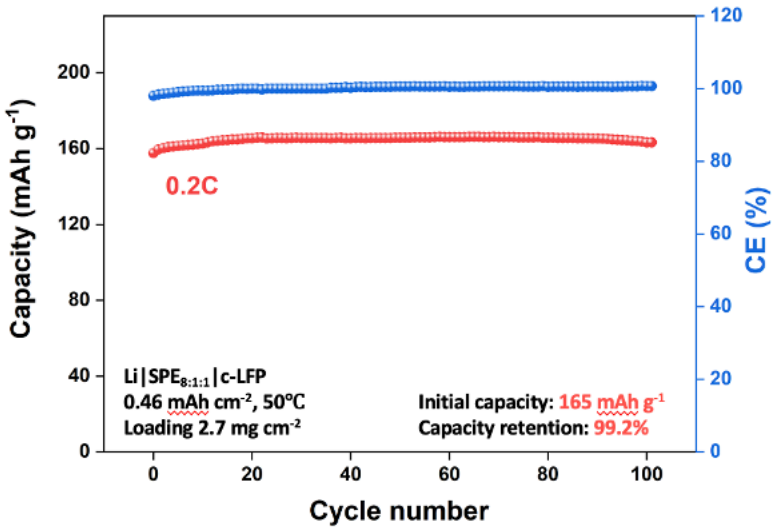

Figure 5 - 15. Cycling performance of Li|$SPE_{8:1:1}$|c-LFP (2.7 mg cm^{-2}) cell cycled at C/5 rate (or 0.2 C) between 2.5−4.0 V for 100 cycles.

Figure 5-14 schematically illustrates the prepared all-solid-state Li|$SPE_{8:1:1}$|c-LFP/c-LMO cell. Figure 5-15 presents the cycling performance of the Li|$SPE_{8:1:1}$|c-LFP cell, which was cycled at C/5 rate at 50 °C between 2.5 and 4 V. The c-LFP cathode was prepared using the designed SPE as the binder to maintain the Li percolation within the cathode structure (more details are mentioned in the experimental section). Thereby the LMB constructed here is all-solid-state avoiding any trace of liquid wetting and the cell delivered 160 mAh g^{-1} initial discharge capacity. The performance then increased to 165 mAh g^{-1} after 20 cycles and stabilized, demonstrating the self-adaptability of $SPE_{8:1:1}$ membrane over cycling. The cell achieved an exceptional 99.2% capacity retention over 100 cycles at C/5 rate, with near perfect coulombic efficiency (CE). Other works are summarized in **Table 2** which clearly outlines the novelty of our PiHCIL-$SPE_{8:1:1}$ membrane and thereby suggests an impressive performance in comparison with the existing literature using similar cathode active loading and applied current density.

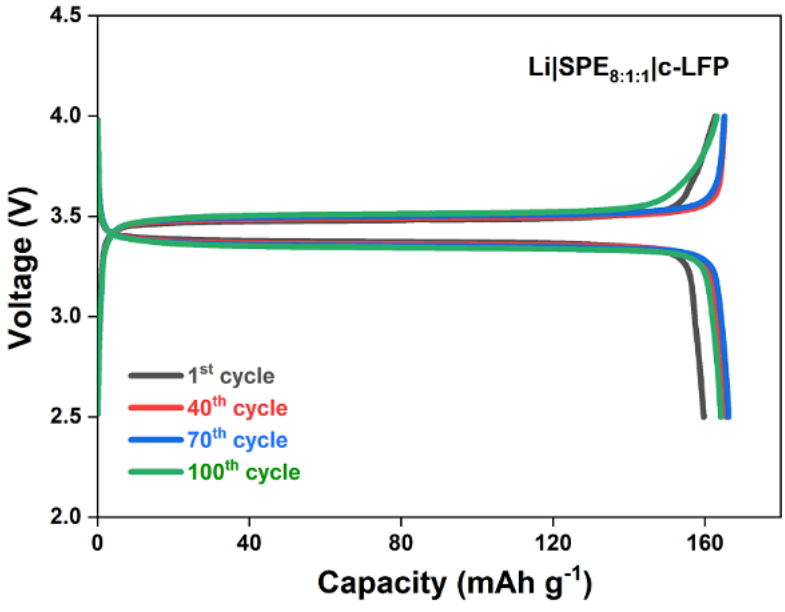

Figure 5 - 16. Charge-discharge profiles of different cycle numbers at C/5 rate. Adapted from Zhang et al. ACS Appl. Mater. Interfaces 2024, 16, 41, 56095–56105.

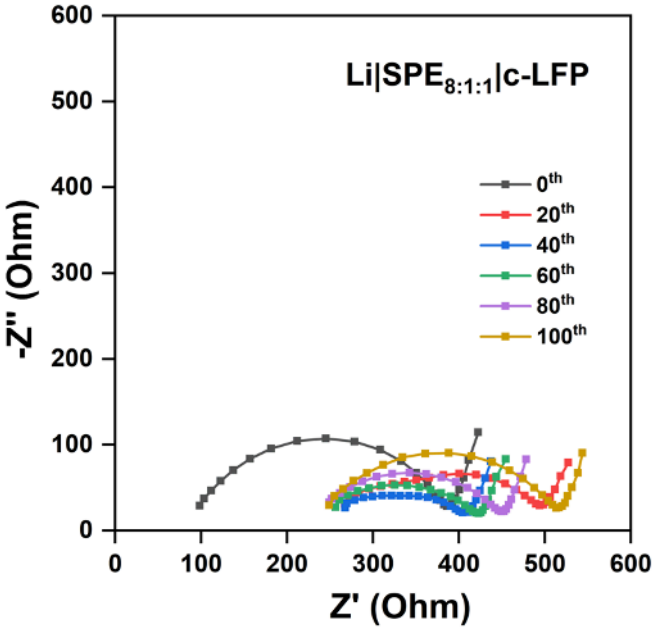

Figure 5 - 17. Impedance profiles of Li|$SPE_{8:1:1}$|c-LFP cell at different cycles at 0.2 C. Adapted from Zhang et al. ACS Appl. Mater. Interfaces 2024, 16, 41, 56095–56105.

Charge-discharge profiles at various cycle numbers are displayed in Figure 5-16. The polarization remains low (180 mV) after 100 cycles, demonstrating the high stability of $SPE_{8:1:1}$. AC impedance profiles (Figure 5-17) showed an initial increase due to SEI formation, and after 40 cycles, the impedance slowly increases due to interface stability.

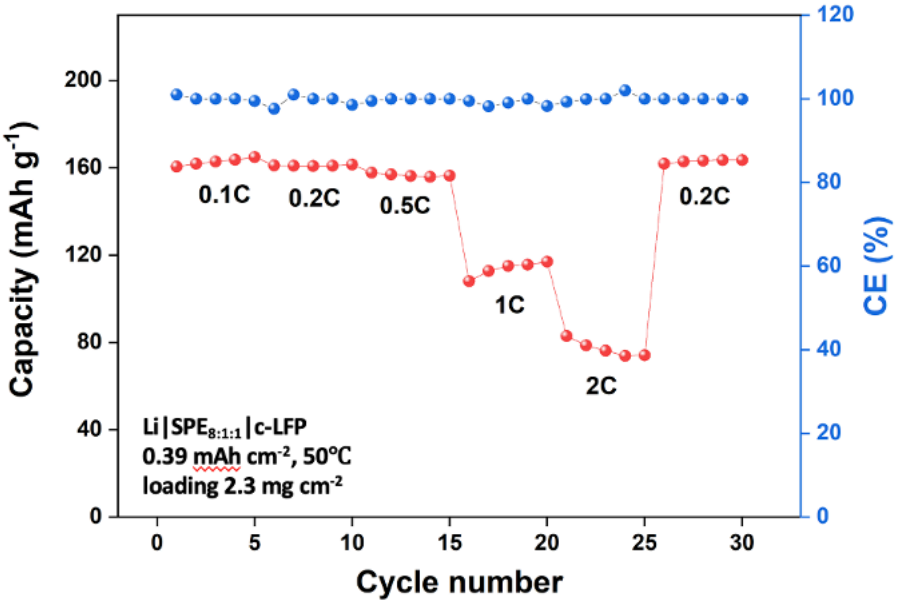

Figure 5 - 18. Rate performances of Li|$SPE_{8:1:1}$|c-LFP cell (2.3 mg cm^{-2}) at different C rates. Adapted from Zhang et al. ACS Appl. Mater. Interfaces 2024, 16, 41, 56095–56105.

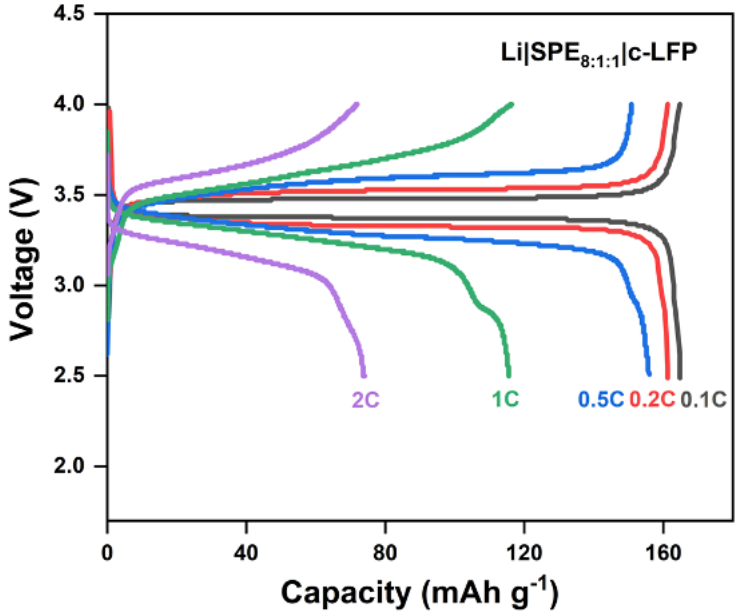

Figure 5 - 19. Charge-discharge profiles of Li|$SPE_{8:1:1}$|c-LFP cell at different C-rates. Adapted from Zhang et al. ACS Appl. Mater. Interfaces 2024, 16, 41, 56095–56105.

A rate capability test was conducted at C/10, C/5, C/2,1C, 2C and C/5 current rates (1C is 0.4 mA cm^{-2}) as shown in Figure 5-18. The Li|$SPE_{8:1:1}$|c-LFP cell showed 162, 159 and 155 mAh g^{-1} discharge capacities under C/10, C/5 and C/2 rate, respectively. It can maintain 47.3% discharge capacity when the current density is increased twentyfold from C/10 to 2C, indicating that the all-solid-state Li|$SPE_{8:1:1}$|c-LFP cell has an excellent tolerant to high current rate. The charge-discharge profiles at different C-rates are shown in Figure 5-19. The excellent rate performance indicated that $SPE_{8:1:1}$ have close contact with both Li and LFP electrodes to facilitate effective Li^+ transport and low interfacial resistance between the $SPE_{8:1:1}$ and cathode.[55]

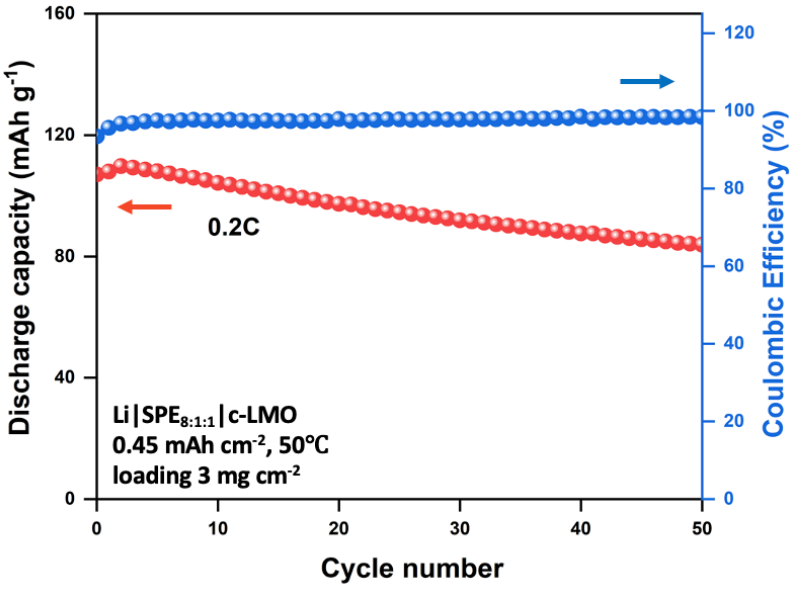

Figure 5 - 20. Cycling performance of Li|$SPE_{8:1:1}$|c-LMO (3 mg cm^{-2}) cell cycled at C/5 rate between 3−4.3 V for 50 cycles. Adapted from Zhang et al. ACS Appl. Mater. Interfaces 2024, 16, 41, 56095–56105.

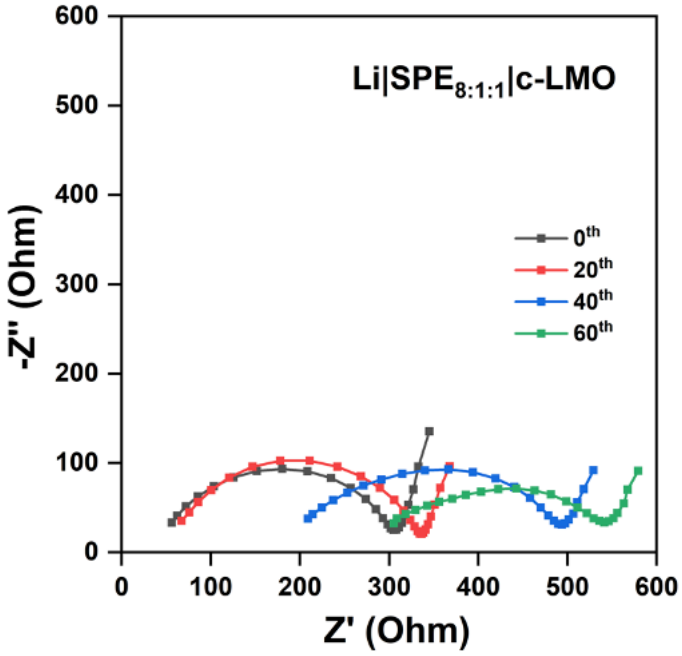

Figure 5 - 21. Impedance profiles of Li|$SPE_{8:1:1}$|c-LMO cell at different cycles at 0.2 C. Adapted from Zhang et al. ACS Appl. Mater. Interfaces 2024, 16, 41, 56095–56105.

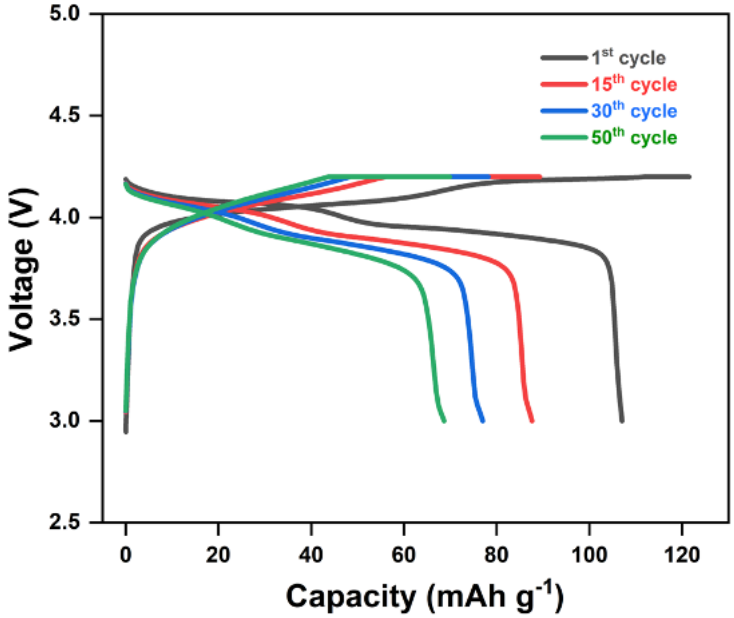

Figure 5 - 22. Charge-discharge profiles of Li|SPE$_{8:1:1}$|c-LMO cell at different cycles at 0.2 C. Adapted from Zhang et al. ACS Appl. Mater. Interfaces 2024, 16, 41, 56095–56105.

To assess the potential for wider applications of the prepared PiHCIL-SPEs working with high voltage materials, we assembled Li||c-LMO cells with a cathode loading of 3 mg cm^{-2} with SPE$_{8:1:1}$. Figure 5-20 illustrates the cycling performance of the Li|SPE$_{8:1:1}$|c-LMO cell at 0.2C in the voltage range between 3 and 4.3 V. The Li|SPE$_{8:1:1}$|c-LMO cell maintain 80% of its initial capacity after 50 cycles, demonstrating its resilience under more demanding conditions. The interfacial resistance (Figure 5-21) slowly increases through cycling. Figure 5-22 presents the charge–discharge profiles at different cycle numbers. The capacity decay maybe due to the dissolution of unstable manganese in LMO which is a common issue of high manganese active materials.

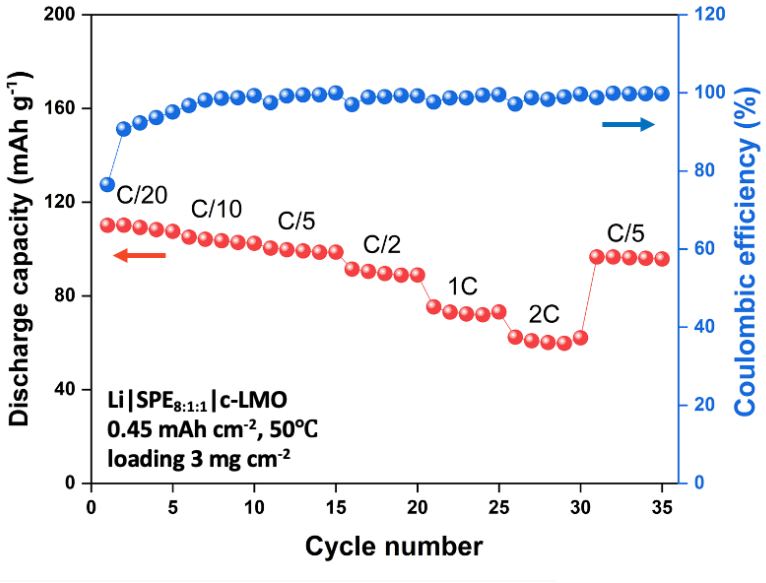

Figure 5 - 23. Rate performances of Li|$SPE_{8:1:1}$|c-LMO cell (3 mg cm^{-2}) at different C rates. Adapted from Zhang et al. ACS Appl. Mater. Interfaces 2024, 16, 41, 56095–56105.

The cell was further subjected to a rate capability test at various rates from C/20 to 2 C as show in **Figure 5-23.** The SPE shows satisfactory discharge capacity retention of 55% from C/20 to 2C, demonstrating superior tolerance to high current rate. The exceptional rate performance and cycling stability of the Li|$SPE_{8:1:1}$|c-LMO cell confirms the potential of the designed SPE to support high-energy-density and high-power applications, underscoring the advantages of integrating high salt concentration ionic liquids within PEO matrices for advanced solid-state LMBs.

Ref.	SPE System	All-Solid-State	Cathode (loading)	Initial Capacity	Temperature	Capacity Retention
2024 Du et al.[56]	PBO/PEO-LiTFSI	/	LFP (1.5mg cm^{-2})	158.7mAh g^{-1} (0.5C)	60°C	73% (2.5-4V, 300 cycles)
2024 Nguyen et al.[57]	P(EO-co-PO)-LiFSI	yes	LFP (3mg cm^{-2})	141 mAh g^{-1} (0.6C)	30°C	95% (2.5-4V, 200 cycles)
2023 Xiong et al.[48]	PEO-LiTFSI	yes	LCO (1.2mg cm^{-2})	131.5 mAh g^{-1} (0.1C)	60°C	82.6% (3-4.2V, 100 cycles)
2020 Homann et al.[35]	PEO/PEGDMA-LiTFSI	/	NMC622 (4mg cm^{-2})	140mAh g^{-1} (0.1C)	40°C	93% (3-4.3V, 50 cycles)
2020 Wang et al.[58]	PEO-LiFSI-N_{1222}FSI	yes	LFP (2mg cm^{-2})	158.8mAh g^{-1} (0.2C)	50°C	95.4% (2.5-4V, 120 cycles)
2019 Ji et al.[59]	PEO/TEGDME/PEGMEMA-LiTFSI	/	LFP (2mg cm^{-2})	160mAh g^{-1} (0.1C)	RT	93.7% (2.5-3.8V, 100 cycles)
2019 Choudhury et al.[60]	PEGDMA-Diglyme-$LiNO_3$	no	NMC622 (2mg cm^{-2})	100-155mAh g^{-1} (0.5C)	/	90% (250 cycles)

2019 Zhang et al.[61]	PEO/TEGDMA /TEGDME-LiTFSI	yes	LFP (1.3mg cm^{-2})	140mAh g^{-1} (0.1C)	RT	98.8% (2.5-4V, 100 cycles)
This work	**PEO-LiFSI-C_3mpryFSI**	**yes**	**c-LFP (2.7mg cm^{-2})**	**165mAh g^{-1} (0.2C)**	**50°C**	**99.2% (2.5-4V, 100 cycles)**

Table 2. Literature survey on performance of PEO-based SPE. Adapted from Zhang et al. ACS Appl. Mater. Interfaces 2024, 16, 41, 56095–56105.

5.4 Conclusion

A novel polymer-in-high-concentration ionic liquid (PiHCIL) solid polymer electrolyte (SPE) system was designed targeting enhanced ionic conductivity, electrochemical stability, and interfacial compatibility of PEO-based electrolytes for solid-state lithium metal batteries (LMBs). By leveraging a high-concentration ionic liquid (HCIL) environment, it was demonstrated how a targeted composition of PEO, LiFSI, and C3mpyrFSI can overcome the conventional limitations of PEO-based SPEs.

In particular, PiHCIL-SPEs with an EO:Li:IL molar ratio of 8:1:1 achieved a fully amorphous structure with significantly enhanced ionic conductivity of 5.6×10^{-4} S cm^{-1} at ambient temperature. This conductivity increase was attributed to the formation of interconnected ion clusters within the high-concentration ionic liquid environment, which improved Li^+ transport pathways in the polymer matrix. Additionally, the PiHCIL-SPE demonstrated an expanded electrochemical stability window of 5.1 V vs. Li^+/Li, significantly higher than traditional PEO-based electrolytes, supporting its applicability with high-voltage cathode materials.

The high-concentration ionic liquid environment also improved interfacial stability with lithium metal anodes. In Li||Li symmetric cells, the PiHCIL-SPE achieved stable and reversible lithium plating/stripping for over 150 cycles with minimal overpotential, indicating effective suppression of dendrite growth. Furthermore, all-solid-state LFP||Li and LMO||Li cells assembled with PiHCIL-SPE displayed excellent cycling performance, retaining over 80% of their initial capacity even under high-voltage conditions and fast cycling rates.

Thus, the PiHCIL approach is highlighted as a promising strategy for advancing PEO-based SPEs in high-energy-density, solid-state LMB applications. By combining the benefits of high ionic conductivity, increased electrochemical stability, and improved mechanical properties, the PiHCIL-SPE system addresses key challenges in solid-state electrolyte design, accounting for its potential application in next-generation energy storage technologies.

5.5 References

1. Janek, J. & Zeier, W. G. A solid future for battery development. *Nat. Energy* **1**, 16141 (2016).
2. Meyer, W. H. Polymer Electrolytes for Lithium-Ion Batteries. *Adv. Mater.* **10**, 439–448 (1998).
3. Song, Z. *et al.* A reflection on polymer electrolytes for solid-state lithium metal batteries. *Nat. Commun.* **14**, 4884 (2023).
4. Cheng, X., Pan, J., Zhao, Y., Liao, M. & Peng, H. Gel Polymer Electrolytes for Electrochemical Energy Storage. *Adv. Energy Mater.* **8**, 1702184 (2018).
5. Wang, X. *et al.* Gelled microporous polymer electrolyte with low liquid leakage for lithium-ion batteries. *J. Membr. Sci.* **454**, 298–304 (2014).
6. Qin, B. *et al.* Single-ion dominantly conducting polyborates towards high performance electrolytes in lithium batteries. *J. Mater. Chem. A* **3**, 7773–7779 (2015).
7. Fenton, D. E., Parker, J. M. & Wright, P. V. Complexes of alkali metal ions with poly(ethylene oxide). *Polymer* **14**, 589 (1973).
8. Armand, M. Polymer solid electrolytes - an overview. *Solid State Ion.* **9–10**, 745–754 (1983).
9. Xiao, S., Ren, L., Liu, W., Zhang, L. & Wang, Q. High-voltage polymer electrolytes: Challenges and progress. *Energy Storage Mater.* **63**, 102970 (2023).
10. Yusim, Y. *et al.* Evaluation and Improvement of the Stability of Poly(ethylene oxide)-based Solid-state Batteries with High-Voltage Cathodes. *Angew. Chem. Int. Ed.* **62**, e202218316 (2023).
11. Chen, L. *et al.* PEO/garnet composite electrolytes for solid-state lithium batteries: From “ceramic-in-polymer” to “polymer-in-ceramic”. *Nano Energy* **46**, 176–184 (2018).
12. Song, X. *et al.* Unraveling the Synergistic Coupling Mechanism of Li^+ Transport in an “Ionogel-in-Ceramic” Hybrid Solid Electrolyte for Rechargeable Lithium Metal Battery. *Adv. Funct. Mater.* **32**, 2108706 (2022).
13. Zhang, X. *et al.* Vertically Aligned and Continuous Nanoscale Ceramic–Polymer Interfaces in Composite Solid Polymer Electrolytes for Enhanced Ionic Conductivity. *Nano Lett.* **18**, 3829–3838 (2018).
14. Shin, J.-H., Henderson, W. A., Scaccia, S., Prosini, P. P. & Passerini, S. Solid-state Li/LiFePO4 polymer electrolyte batteries incorporating an ionic liquid cycled at 40°C. *J. Power Sources* **156**, 560–566 (2006).
15. Chen, Y. *et al.* Hyperbranched PEO-Based Hyperstar Solid Polymer Electrolytes with Simultaneous Improvement of Ion Transport and Mechanical Strength. *ACS Appl. Energy Mater.* **2**, 1608–1615 (2019).
16. Gomez, E. D. *et al.* Effect of Ion Distribution on Conductivity of Block Copolymer Electrolytes. *Nano Lett.* **9**, 1212–1216 (2009).
17. Zhang, H. *et al.* Single lithium-ion conducting solid polymer electrolytes: advances and perspectives. *Chem. Soc. Rev.* **46**, 797–815 (2017).

18. Bouchet, R. *et al.* Single-ion BAB triblock copolymers as highly efficient electrolytes for lithium-metal batteries. *Nat. Mater.* **12**, 452–457 (2013).
19. Porcarelli, L., Gerbaldi, C., Bella, F. & Nair, J. R. Super Soft All-Ethylene Oxide Polymer Electrolyte for Safe All-Solid Lithium Batteries. *Sci. Rep.* **6**, 19892 (2016).
20. Kim, G. T. *et al.* UV cross-linked, lithium-conducting ternary polymer electrolytes containing ionic liquids. *J. Power Sources* **195**, 6130–6137 (2010).
21. Armand, M., Endres, F., MacFarlane, D. R., Ohno, H. & Scrosati, B. Ionic-liquid materials for the electrochemical challenges of the future. *Nat. Mater.* **8**, 621–629 (2009).
22. Howlett, P. C., MacFarlane, D. R. & Hollenkamp, A. F. High Lithium Metal Cycling Efficiency in a Room-Temperature Ionic Liquid. *Electrochem. Solid-State Lett.* **7**, A97 (2004).
23. Yoon, H., Howlett, P. C., Best, A. S., Forsyth, M. & MacFarlane, D. R. Fast Charge/Discharge of Li Metal Batteries Using an Ionic Liquid Electrolyte. *J. Electrochem. Soc.* **160**, A1629–A1637 (2013).
24. Matsumoto, H. *et al.* Fast cycling of Li/$LiCoO_2$ cell with low-viscosity ionic liquids based on bis(fluorosulfonyl)imide [FSI]−. *J. Power Sources* **160**, 1308–1313 (2006).
25. Susan, Md. A. B. H., Kaneko, T., Noda, A. & Watanabe, M. Ion Gels Prepared by in Situ Radical Polymerization of Vinyl Monomers in an Ionic Liquid and Their Characterization as Polymer Electrolytes. *J. Am. Chem. Soc.* **127**, 4976–4983 (2005).
26. Suo, L. *et al.* "Water-in-salt" electrolyte enables high-voltage aqueous lithium-ion chemistries. *Science* **350**, 938–943 (2015).
27. Wang, J. *et al.* Superconcentrated electrolytes for a high-voltage lithium-ion battery. *Nat. Commun.* **7**, 12032 (2016).
28. Yoshida, K. *et al.* Oxidative-Stability Enhancement and Charge Transport Mechanism in Glyme–Lithium Salt Equimolar Complexes. *J. Am. Chem. Soc.* **133**, 13121–13129 (2011).
29. Yamada, Y. & Yamada, A. Review—Superconcentrated Electrolytes for Lithium Batteries. *J. Electrochem. Soc.* **162**, A2406–A2423 (2015).
30. Al-Masri, D., Yunis, R., Hollenkamp, A. F. & Pringle, J. M. Designing Solid-State Electrolytes through the Structural Modification of a High-Performing Ionic Liquid. *ChemElectroChem* **7**, 4118–4123 (2020).
31. Pal, U. *et al.* Enhanced ion transport in an ether aided super concentrated ionic liquid electrolyte for long-life practical lithium metal battery applications. *J. Mater. Chem. A* **8**, 18826–18839 (2020).
32. Pal, U. *et al.* Improved Li-Ion Transport by DME Chelation in a Novel Ionic Liquid-Based Hybrid Electrolyte for Li–S Battery Application. *J. Phys. Chem. C* **122**, 14373–14382 (2018).
33. Pal, U. *et al.* Interphase control for high performance lithium metal batteries using ether aided ionic liquid electrolyte. *Energy Environ. Sci.* **15**, 1907–1919 (2022).

34. Jin, L. *et al.* Structure and Transport Properties of a Plastic Crystal Ion Conductor: Diethyl(methyl)(isobutyl)phosphonium Hexafluorophosphate. *J. Am. Chem. Soc.* **134**, 9688–9697 (2012).
35. Homann, G., Stolz, L., Neuhaus, K., Winter, M. & Kasnatscheew, J. Effective Optimization of High Voltage Solid-State Lithium Batteries by Using Poly(ethylene oxide)-Based Polymer Electrolyte with Semi-Interpenetrating Network. *Adv. Funct. Mater.* **30**, 2006289 (2020).
36. Yang, J. *et al.* Crosslinked polymer-in-salt solid electrolyte with multiple ion transport paths for solid-state lithium metal batteries. *Energy Storage Mater.* **64**, 103088 (2024).
37. Gao, H., Grundish, N. S., Zhao, Y., Zhou, A. & Goodenough, J. B. Formation of Stable Interphase of Polymer-in-Salt Electrolyte in All-Solid-State Lithium Batteries. *Energy Mater. Adv.* **2021**, 2021/1932952 (2021).
38. Forsyth, M., Sun, J., Macfarlane, D. R. & Hill, A. J. Compositional dependence of free volume in PAN/LiCF3SO3 polymer-in-salt electrolytes and the effect on ionic conductivity. *J. Polym. Sci. Part B Polym. Phys.* **38**, 341–350 (2000).
39. Yoon, H., Best, A. S., Forsyth, M., MacFarlane, D. R. & Howlett, P. C. Physical properties of high Li-ion content N-propyl-N-methylpyrrolidinium bis(fluorosulfonyl)imide based ionic liquid electrolytes. *Phys. Chem. Chem. Phys.* **17**, 4656–4663 (2015).
40. Bar, N., Basak, P. & Tsur, Y. Vibrational and impedance spectroscopic analyses of semi-interpenetrating polymer networks as solid polymer electrolytes. *Phys. Chem. Chem. Phys.* **19**, 14615–14624 (2017).
41. Dissanayake, M. A. K. L. & Frech, R. Infrared Spectroscopic Study of the Phases and Phase Transitions in Poly(ethylene oxide) and Poly(ethylene oxide)-Lithium Trifluoromethanesulfonate Complexes. *Macromolecules* **28**, 5312–5319 (1995).
42. Dai, Y. *et al.* Lithium-7 NMR studies of concentrated LiI/PEO-based solid electrolytes. *Solid State Ion.* **106**, 25–32 (1998).
43. Wu, N. *et al.* Fast Li^+ Conduction Mechanism and Interfacial Chemistry of a NASICON/Polymer Composite Electrolyte. *J. Am. Chem. Soc.* **142**, 2497–2505 (2020).
44. Henderson, W. A. Crystallization Kinetics of Glyme−LiX and PEO−LiX Polymer Electrolytes. *Macromolecules* **40**, 4963–4971 (2007).
45. Kerner, M., Plylahan, N., Scheers, J. & Johansson, P. Thermal stability and decomposition of lithium bis(fluorosulfonyl)imide (LiFSI) salts. *RSC Adv.* **6**, 23327–23334 (2016).
46. Nguyen, H. T. T. *et al.* Facile Li^+ Transport in Interpenetrating O- and F-Containing Polymer Networks for Solid-State Lithium Batteries. *Adv. Funct. Mater.* **33**, 2213469 (2023).
47. Herbers, L. *et al.* The Influence of Polyethylene Oxide Degradation in Polymer-Based Electrolytes for NMC and Lithium Metal Batteries. *Adv. Energy Sustain. Res.* **4**, 2300153 (2023).

48. Xiong, Z. *et al.* 4.2V polymer all-solid-state lithium batteries enabled by high-concentration PEO solid electrolytes. *Energy Storage Mater.* **57**, 171–179 (2023).
49. Wu, H. *et al.* A Polymer-in-Salt Electrolyte with Enhanced Oxidative Stability for Lithium Metal Polymer Batteries. *ACS Appl. Mater. Interfaces* **13**, 31583–31593 (2021).
50. Johansson, P., Tegenfeldt, J. & Lindgren, J. Modelling amorphous lithium salt–PEO polymer electrolytes: ab initio calculations of lithium ion–tetra-, penta- and hexaglyme complexes. *Polymer* **40**, 4399–4406 (1999).
51. Molinari, N., Mailoa, J. P. & Kozinsky, B. Effect of Salt Concentration on Ion Clustering and Transport in Polymer Solid Electrolytes: A Molecular Dynamics Study of PEO–LiTFSI. *Chem. Mater.* **30**, 6298–6306 (2018).
52. Ratner, M. A. & Shriver, D. F. Ion transport in solvent-free polymers. *Chem. Rev.* **88**, 109–124 (1988).
53. Zhang, H. *et al.* Lithium bis(fluorosulfonyl)imide/poly(ethylene oxide) polymer electrolyte. *Electrochimica Acta* **133**, 529–538 (2014).
54. Itoh, T., Fujita, K., Uno, T. & Kubo, M. Polymer electrolytes based on vinyl ethers with various EO chain length and their polymer electrolytes cross-linked by electron beam irradiation. *Ionics* **23**, 257–264 (2017).
55. Tatara, R. *et al.* The Effect of Electrode-Electrolyte Interface on the Electrochemical Impedance Spectra for Positive Electrode in Li-Ion Battery. *J. Electrochem. Soc.* **166**, A5090–A5098 (2019).
56. Du, A. *et al.* Breaking the Trade-Off between Ionic Conductivity and Mechanical Strength in Solid Polymer Electrolytes for High-Performance Solid Lithium Batteries. *Adv. Energy Mater.* 2400808 (2024)
57. Nguyen, M. L., Nguyen, V.-C., Lee, Y.-L., Jan, J.-S. & Teng, H. Synergistic combination of ether-linkage and polymer-in-salt for electrolytes with facile Li+ conducting and high stability in solid-state lithium batteries. *Energy Storage Mater.* **65**, 103178 (2024).
58. Wang, W. *et al.* Solid polymer electrolytes based on the composite of PEO–LiFSI and organic ionic plastic crystal. *Chem. Phys. Lett.* **747**, 137335 (2020).
59. Ji, Y., Zhang, Y.-H., Shi, F.-N. & Zhang, L.-N. UV-derived double crosslinked PEO-based solid polymer electrolyte for room temperature. *J. Colloid Interface Sci.* **629**, 492–500 (2023).
60. Choudhury, S. *et al.* Stabilizing polymer electrolytes in high-voltage lithium batteries. *Nat. Commun.* **10**, 3091 (2019).
61. Zhang, Y. *et al.* Cross-linking network based on Poly(ethylene oxide): Solid polymer electrolyte for room temperature lithium battery. *J. Power Sources* **420**, 63–72 (2019).

Chapter 6

Conclusions and Future Work

6.1 Conclusions

To understand the effect of polymer crosslinking and high concentrated ionic liquid (HCIL) on the property and performance of PEO-based solid polymer electrolytes, soft UV-curing strategies were adopted and various EO:HCIL ratios were studied. The designed SPEs demonstrated high ambient temperature ionic conductivity, wide electrochemical stability and superior battery performance compared to common PEO-based SPEs reported in literature.

In this context, the key findings of this thesis are summarised with respect to the three main aims that were set in the Introduction (Chapter 1.6).

Aim 1: Conduct a comprehensive literature review on the crosslinking strategy as a powerful tool for developing high-performance SPEs for advanced lithium batteries.

Chapter 2 provides a comprehensive overview of different crosslinking strategies and discuss their impact on the properties and performance of SPEs. The study supplements existing research by addressing several key gaps. For example, it provides a comprehensive analysis of various crosslinking techniques used in SPEs and discussed their advantages and limitations. It further evaluates the impact of crosslinking on the physical and electrochemical properties of SPEs. Finally, it explores real-world applications of crosslinking employed by automobile industries and battery technology companies. By addressing these gaps, it provides a deeper understanding of the potential and limitations of crosslinking in SPE development.

Aim 2: Develop high-performance SPEs by combining a UV-crosslinked polymer matrix with a concentrated ionic liquid (CIL), addressing the key limitations of traditional PEO-based SPEs.

In Chapter 4, a novel crosslinked polymer-in-concentrated ionic liquid (PCIL) SPE was successfully designed, consisting of PEO, C_3mpyrFSI and LiFSI. The study found that the UV-crosslinking strategy synergistically reduces PEO

crystallinity while increasing the amount of encompassed lithium salt and IL, and improves PEO oxidative stability, therefore leading to enhanced electrochemical performance. The physical and electrochemical properties of both linear and crosslinked SPEs were explored and compared. The designed crosslinked SPEs exhibited a promisingly high oxidative stability of 4.9 V vs. Li^+/Li and high ambient temperature ionic conductivity of 4 $x10^{-4}$ S cm^{-1}. Stable and reversible lithium plating/stripping was demonstrated in symmetrical Li||Li cells over hundreds of hours. High loading solid-state LFP||Li cells showed favourable cycling with over 90% capacity retention at 0.1C over 100 cycles at 50°C. High voltage solid-state LMO||Li cells exhibited promising cycling with 93% capacity retention at 0.2 C rate over 50 cycles at 50°C. Both cathodes exploited a high areal capacity of 1 mAh cm^{-2}. Thus, the synergistic combination of crosslinking and concentrated ionic liquid electrolyte to form a robust SPE enables a new pathway for designing high-performing PEO-based SPEs for high energy density solid-state LMBs.

Aim 3: Optimizing PEO-in-high salt concentrated ionic liquid (HCIL) SPEs by varying the HCIL concentration. Study the effect of HCIL concentration on the physicochemical and electrochemical properties of the composite electrolyte.

In Chapter 5, the designed "polymer-in-high concentrated ionic liquid" (PiHCIL) solid electrolyte composed of PEO, C_3mpyrFSI ionic liquid and LiFSI was successfully optimized. The EO: [HCIL] ratio was widely varied and physical and electrochemical properties were explored. The Li-coordination and solvation structure was explored through FTIR spectroscopy and solid-state magic angle spinning (MAS) NMR. The optimized electrolyte (EO: [HCIL] ratio = 8:1) provided promisingly high oxidative stability of 5.1 V vs. Li^+/Li and high ambient temperature ionic conductivity of $5.6x10^{-4}$ S cm^{-1}. Li|Li symmetric cell tests showed very stable and reversible cycling of Li metal over 100 cycles and smooth, dendrite-free deposition morphology. All-solid-state cells using composite LFP cathode exhibited promising cycling with 99.2% capacity retention at C/5 rate over 100 cycles. Therefore, the novel approach of PiHCIL enables a new pathway to design high-performing SPEs for high-energy density all-solid-state LMBs.

6.2 Future Work

The promising results achieved in this study provide a strong foundation for further exploration and optimization of high concentration ionic liquid SPEs for solid-state lithium metal batteries.

- **Further optimization of crosslinking strategies**: Further refinement in crosslinking density and crosslinking method could benefit the long-term cycling stability. Investigating different photoinitiators and crosslinking agents may provide alternative routes to optimize the properties and performances of the SPEs.
- **Exploration of other polymer systems**: Given the successful SPE design with pure high molecular weight PEO. It would be plausible to try out other

more polymer systems such as polycarbonates or polyesters aiming to achieve more improvements in electrochemical performance.

- **Investigation of high voltage cathode compatibility**: The electrochemical stability of the designed PiHCIL electrolytes was demonstrated up to 5.1 V vs. Li^+/Li; however, compatibility with high-energy cathodes such as lithium nickel manganese cobalt oxides (NMC) or lithium-rich materials should be more deeply explored to further boost energy density. Understanding the interface will be also crucial for improving performance and longevity.
- **In-depth studies on ion transport mechanisms**: Although this work provided valuable insights into ion dynamics using NMR and FTIR spectroscopy, a deeper understanding of the specific ion transport pathways, including the role of ion clusters, could lead to more tailored electrolyte designs. Advanced modelling and simulations, combined with experimental studies, could help clarify these mechanisms.
- **Scaling and manufacturing**: Transitioning from lab-scale to practical, manufacturable SPEs is essential for commercial viability. Future work should focus on developing scalable production methods, such as roll-to-roll processes or inkjet printing, for the PiHCIL-SPE systems. Additionally, cost-effectiveness and environmental sustainability should be key considerations in selecting materials and manufacturing techniques.

By pursuing these avenues, the field of solid-state LMBs can move closer to the goal of creating commercially viable, safe, and high-performance energy storage systems for a wide range of applications.